MATHEMATICAL MODEL AND AUTOPILOT DESIGN OF A TWIN ENGINE JET PLANE

A THESIS SUBMITTED TO
THE GRADUATE SCHOOL OF NATURAL AND APPLIED SCIENCES
OF
MIDDLE EAST TECHNICAL UNIVERSITY

BY

HAZAL CANSU ATAK

IN PARTIAL FULFILLMENT OF THE REQUIREMENTS
FOR
THE DEGREE OF MASTER OF SCIENCE
IN
ELECTRICAL AND ELECTRONIC ENGINEERING

JANUARY 2020

Approval of the thesis:

MATHEMATICAL MODEL AND AUTOPILOT DESIGN OF A TWIN ENGINE JET PLANE

submitted by **HAZAL CANSU ATAK** in partial fulfillment of the requirements for the degree of **Master of Science** i**n Electrical and Electronic Engineering, Middle East Technical University** by,

Prof. Dr. Halil Kalıpçılar
Dean, Graduate School of **Natural and Applied Sciences**

Prof. Dr. İlkay Ulusoy
Head of the Department, **Electrical and Electronics Eng.**

Prof. Dr. Mehmet Kemal Leblebicioğlu
Supervisor, **Electrical and Electronics Eng., METU**

Examining Committee Members:

Prof. Dr. Ozan Tekinalp
Aerospace Eng., METU

Prof. Dr. Mehmet Kemal Leblebicioğlu
Electrical and Electronics Eng., METU

Prof. Dr. Klaus Werner Schmidt
Electrical and Electronics Eng., METU

Assoc. Prof. Dr. Afşar Saranlı
Electrical and Electronics Eng., METU

Assist. Prof. Dr. Yakup Özkazanç
Electrical and Electronics Eng., HU

Date: 17.01.2020

I hereby declare that all information in this document has been obtained and presented in accordance with academic rules and ethical conduct. I also declare that, as required by these rules and conduct, I have fully cited and referenced all material and results that are not original to this work.

Name, Last name: Hazal Cansu Atak

Signature:

ABSTRACT

MATHEMATICAL MODEL AND AUTOPILOT DESIGN OF A TWIN ENGINE JET PLANE

Atak, Hazal Cansu
Master of Science, Electrical and Electronic Engineering
Supervisor: Prof. Dr. Mehmet Kemal Leblebicioğlu

January 2020, 109 pages

Fighter aircrafts have very important place in military and aerospace industry. Lots of types of these aircrafts are used according to their primary missions like providing fire power from high above the ground and support for ground forces. Selecting the number of engines and their type are dependent to these missions. Turbojet, turbo prop and ramjet engines are most preferred types for these applications, and each has its own advantages and disadvantages. Turbojet engines have high performance as a means of propulsion and aircraft speed. Due to their small size and relatively small weights, it became convenient to use two turbojet engines.

In this thesis, mathematical model and autopilot design of a jet plane with two turbojet engines is studied and simulations are done by using MATLAB / Simulink. First, a mathematical model of a turbojet engine is developed with Mach number and throttle setting as inputs, thrust and mass fuel flow rate as outputs. Next a jet aircraft model with relatively larger load capacity (due to having larger wingspan), with respect to the similar planes in use like F-18 (hornet) and F-22 (raptor) has been designed and analyzed by XFLR5 program. At this stage, placement of turbojet engines is done in such a way that sufficient yaw moment is created on the plane when their thrusts differ. Then, a mathematical model of the plane is constructed with the base of aerodynamics block that is feed with the aerodynamic coefficients coming from XFLR5, equations of motion block and turbojet engine blocks. In this flight dynamic model, engines are controlled independently to perform yaw moment. Elevator, rudder, aileron and two throttles for each engine are considered as the control parameters of the flight dynamic model and an autopilot is designed by using suitable cascaded PID controllers. Different modes of the autopilot and guidance are also discussed as part of our study. This work ends with simulation studies which are expected to show the importance of the approach presented here.

Keywords: Turbojet, Six Degrees of Freedom Motion Model (6-DOF), Autopilot, Aerodynamic Analyses

ÖZ

ÇİFT MOTORLU BİR JET UÇAĞININ MATEMATİK MODELİ VE OTOPİLOT DİZAYNI

Atak, Hazal Cansu
Yüksek Lisans, Elektrik ve Elektronik Mühendisliği
Tez Yöneticisi: Prof. Dr. Mehmet Kemal Leblebicioğlu

Ocak 2020, 109 sayfa

Askeri ve havacılık uygulamalarında savaş uçaklarının önemli bir yeri vardır. Bu uçakların çeşitli türleri, hava sahası üstünlüğü sağlama ve yer bombardımanı görevleri gibi öncelikli işlevlerine göre kullanımdadır. Bu uygulamalarda tercih edilen motor türleri turbo jet, turbo prop ve ramjet motorlardır ve hepsinin kendisine özgü avantaj ve dezavantajları bulunur. İtki ve hız düşünüldüğünde turbo jet motorlar yüksek performanslı olarak değerlendirilir. Bu motorların aynı zamanda daha küçük boyutta ve daha hafif olması da uçakları iki motor kullanarak tasarlamayı elverişli hale gelmiştir.

Bu tez kapsamında, iki adet turbo jet motorlu bir jet uçağının matematik modeli ve otopilot tasarımı yapılmış ve benzetim çalışmaları MATLAB / Simulink ortamında geliştirilmiştir. İlk olarak, turbo jet motorun matematik modeli, Mach sayısı ve gaz ayarları girdi, itki ve yakıt kütle akış oranı çıktı olmak suratiyle oluşturulmuştur. Arkasından, F-18 (hornet) ve F-22 (raptor) gibi benzer uçaklardan farklı olarak, daha uzun kanat genişliği sayesinde daha fazla yük taşıyabilen bir uçak modeli XLR5 programında tasarlanmış ve analizleri yapılmıştır. Tasarım aşamasında, motorların yeri, sapma açısal kuvveti üretmesi hedeflenerek seçilmiştir ve motorlar kanatların altına x ekseninden hesaplanmış bir mesafede olacak şekilde yerleştirilmiştir.

Sonrasında, XFLR5 programında hesaplanmış aerodinamik katsayılarla beslenen aerodinamik bloğu, hareket denklemleri bloğu ve turbo jet motor blokları kullanılarak uçağın matematik modeli çıkartılmıştır. Bu uçuş dinamiği modelinde, motorların sapma açısal kuvveti yaratması için birbirlerinden bağımsız kontrol edilmiştir İrtifa dümeni, istikamet dümeni ve her bir motor için gaz komutları uçuş dinamiğinin control değişkenleridir ve kaskad PID kontrolcü yapısı kullanılaran otopilot tasarımı yapılmıştır. Sonuçları geliştirmek adına farklı otopilot modları ve güdüm incelenmiştir. Tez çalışması, önerilen yaklaşımın önemini gösterecek benzetim çalışmaları ile sonlandırılmıştır.

Anahtar Kelimeler: Turbo Jet, Altı Serbestlik Dereceli Hareket Modeli (6-DOF), Otopilot, Aerodinamik Analiz

Dedicated to my loving family

ACKNOWLEDGMENTS

I would first like to thank my advisor and mentor, Prof. Dr. Mehmet Kemal Leblebicioğlu, whose guidance and mentorship proved to be invaluable. There are not many professors who would spend so much extra time outside the classroom working side-by-side with their students.

Also, I would like to thank to my superiors in Roketsan, Erol Sertaç Sezgin and Demokan Demiray for understanding and providing all kinds of convenience.

I owe a deep sense of gratitude to my precious friends, Tuğçe Ceren Çeliker, Erkan Çeliker, Ceren Dümen, Berk Gökçe, Ataman Aydoğdu, Ali Can Özer, Deniz Tuğrul and Melis Aybar. Their prompt inspirations, timely suggestions with kindness, enthusiasm and dynamism have enabled me to complete my thesis.

Lastly, special thanks to my family; Fikret, Şengül and my lovely brother Ozan for their constant support throughout my education. It is a great treasure to know they are always there for me. Without their patience and understanding, this project could never have been realized.

TABLE OF CONTENTS

LIST OF TABLES

TABLES

LIST OF FIGURES

FIGURES

LIST OF ABBREVIATIONS

ABBREVIATIONS	
6-DOF	Six Degrees of Freedom
AR	Aspect Ratio
AOA	Angle of Attack
CFD	Computational Fluid Dynamics
DCM_{we}	Earth to Body Direct Cosine Matrix
MATLAB	Matrix Laboratory
NACA	National Advisory Committee for Aeronautics
PID	Proportional, Integral, Derivative
XFLR5	Free Analysis Tool for Airfoils, Wings and Planes

LIST OF SYMBOLS

SYMBOLS

a_0	Speed of Sound
b	Wingspan
c_p	Specific Heat at Constant Pressure
c_{pc}	Compressor Specific Heat at Constant Pressure
c_{pt}	Turbine Specific Heat at Constant Pressure
c_r	Root Chord
c_t	Tip Chord
f	Burner Fuel/Air Ratio
g	Newton's Constant
g_c	Acceleration of Gravity
h	Altitude
h_{PR}	Low Heating Value of Fuel
m	Weight of Plane
$\dot{m}_0$	Engine Mass Flow Rate
$\dot{m}_{0R}$	Reference Engine Mass Flow Rate
p	Roll Rate
q	Pitch Rate
r	Yaw Rate
u	X Axis Body Velocity Component
v	Y Axis Body Velocity Component

w	Z Axis Body Velocity Component
w_b	Angular Velocity in Body Axis
C_l	Rolling Moment Coefficient
C_m	Pitching Moment Coefficient
C_n	Yawing Moment Coefficient
C_{lp}	Roll Damping Coefficient
C_{lr}	Cross Derivative Due to Yaw
C_{mq}	Pitch Moment Coefficient
C_{np}	Cross Derivative Due to Roll
C_{nr}	Yaw Damping Coefficient
C_D	Drag Force Coefficient
C_L	Lift Force Coefficient
C_Y	Side Force Coefficient
D	Direction Cosine Matrix
F	Thrust
L	Rolling Moment
M	Pitching Moment
M_0	Initial Mach Number
M_9	Exit Mach Number
N	Yawing Moment
P_0	Initial Pressure
P_{0R}	Reference Initial Pressure

P_0/P_9	Ambient Pressure/Exhaust Pressure Ratio
P_{t9}/P_9	Total Pressure Ratio
R_c	Compressor Gas Constant
R_t	Turbine Gas Constant
S	Wing Reference Area
T	Engine Thrust
T_0	Initial Temperature
T_{t2}	Inlet Total Temperature
T_{t4}	Throttle Setting
T_{t4R}	Reference Throttle Setting
T_9/T_0	Exit Temperature Ratio
V_e	Linear Velocity
V_9	Exit Velocity
X	Axial Force
X_e	X Axis Position Vector
Y	Side Force
Y_e	Y Axis Position Vector
Z	Normal Force
Z_e	Z Axis Position Vector
α	Angle of Attack
β	Sideslip Angle
γ	Flight Path Angle

γ_c	Compressor Specific Heat
γ_t	Turbine Specific Heat
η_b	Burner Efficiency
η_c	Compressor Efficiency
π_b	Main Burner Total Pressure Ratio
π_c	Compressor Pressure Ratio
π_{cR}	Reference Compressor Pressure Ratio
π_d	Diffuser Pressure Ratio
π_n	Exit Nozzle Total Pressure Ratio
π_r	Rotor Pressure Ratio
π_{rR}	Reference Rotor Pressure Ratio
π_t	Turbine Pressure Ratio
π_{dR}	Reference Diffuser Pressure Ratio
ρ	Air Density
τ_c	Compressor Temperature Ratio
τ_{cR}	Reference Compressor Temperature Ratio
τ_r	Rotor Temperature Ratio
τ_t	Turbine Temperature Ratio
τ_λ	Enthalpy Ratio
φ	Bank / Roll Angle
θ	Pitch Angle
ψ	Heading / Yaw Angle

CHAPTER 1

INTRODUCTION

1.1 Motivation

Fighter aircrafts have highly importance role in the defense industry and technological improvements in this area is outstanding. Most of the developed countries allocate remarkable amount of money to lead and follow this industry. It is also an exciting concept in engineering because every stage of design requires and contains multidisciplinary know-how. In this thesis, I wanted to build a mathematical model for an unmanned jet plane. In Roketsan, where I am currently working, projects of missiles with jet engine go on and knowledge about jet engines is insufficient. Designing an unmanned jet plane (aircraft) with twin turbojet engines will create a base for these projects.

1.2 Aim

Aim of this thesis is developing a 6-DOF mathematical model and autopilot design of a twin-engine jet plane with additive features. With the advantage that turbojet engines have less weight than other engines like turboprop and ramjet, larger and heavier wing design will be used to get more load capacity. Also, using the difference between thrust values of each engine, creating yaw moment in addition to the one that is created by rudder movement will be the other improvement of this work. This is sort of thrust vector control and it will enable the plane to make more agile maneuvers and have good stall characteristics.

1.3 Approach

The mathematical model will be analyzed with both longitudinal and lateral aspects. The control parameters are determined as aileron, rudder and elevator motions in addition to the turbojet engines that are controlled independently. To simulate the physical challenge of the aileron, rudder and elevator movement, two second order nonlinear actuator models will be used for each controller. Mathematical model will consist of thrust, aerodynamics and equations of motion blocks. Both static and dynamic coefficients of the plane will be calculated by an XFLR5 analyses. Exported coefficients will be stored in 2-D look-up table for longitudinal axis and 3-D look-up table for lateral axis and used to calculate aerodynamic forces and moments. Next, the model is constructed in MATLAB / Simulink and autopilot loops will be added one by one for each controller including inner and outer loops. PID blocks will be tuned with simulation of the model. These autopilot systems will be feed by flight management system that will be the part which create the reference tracking values for all three axes position and velocity. Guidance mechanism will assign the attitude of reference tracking values according to the desired position and velocity changes.

1.4 Organization of the Thesis

In this work, Chapter 2 describes the geometry of aircraft, airfoil specifications that are used in different parts of the aircraft and calculation of both longitudinal and lateral aerodynamic derivatives. In Chapter 3, mathematical model of designed turbojet engine, reference design parameters and results for thrust computation for specified inputs are demonstrated. Mathematical model of the aircraft with the aspect of 6-DOF equations of motion is proposed in Chapter 4. Chapter 5 deals with the autopilot designs and tuning processes for designed aircraft. Chapter 6 presents guidance and flight management system and simulation results for two different target point. Chapter 7 concludes this study by examining the results of the designed system.

CHAPTER 2

MODELING OF AERODYNAMIC CHARACTERISTICS

The first step of mathematically modeling of aircraft is to specify control and stability derivatives. Flying characteristics of the aircraft are constructed with these derivatives and the design of the control surfaces and autopilot system depends on them [1]. In order to achieve this goal, two different approach can be used. First, with the geometry and inertial properties of the aircraft; simulation tools can be used to obtain the derivatives. Second, in order to evaluate the control and stability derivatives precisely, flight testing can be an usuful technique. However, this method is considerably time consuming and costly therefore in this work, first approach is taken and XFLR5 flight analysis software is used to determine stability and control derivatives.

2.1 Defining the Geometry of the Aircraft

Preliminary design consists of a plane with maximum weight (m), engine thrust per each turbojet engine (T) and wing area (S) [2]. The conceptual design of components; wing, horizontal tail and vertical tail are made with respect to the requirements of the plane such that it should has more load capacity and maneuverability than the similar ones in the industry. In the Table 2.1, basic specifications of six aircrafts from different countries that are used in similar mission in the industry (or military) are given.

Table 2.1 Specifications of Similar Aircrafts

	MG-31	**SU-35**	**SU-57**	**F-22 Raptor**	**J-20**	**F/A-18E/F**
Length	22.69 m	21.9 m	22 m	18.92 m	23 m	18.31 m
Wing Span	13.46 m	15.3 m	14.2 m	13.56 m	14 m	13.62 m
Height	6.15 m	5.9 m	6 m	5 m	6 m	4.88 m
Weight(empty)	21.8 t	18.4 t	18.5 t	14.36 t	Unknown	13.86 t
Engines	2 x PNPP Aviadvigatel D-30F6 turbofans	2 x Saturn 117S (AL-41F1S)	Unknown	2 x Pratt & Whitney F119-P-100 turbofans	Unknown	2 x General Electric F414-GE-400 turbofans
Maximum Speed	3 000 km/h	2 390 km/h	2 600 km/h	2 500 km/h	2 700 km/h	1 915 km/h
Thrust (dry / with afterburning)	2 x 93.19 / 152.06 kN	2 x 86.3 / 142 kN	Unknown /175 kN	2 x Unknown / 155.69 kN	Unknown	2 x Unknown / 97.86 kN

Design and analysis of the aircraft are conducted in XFLR5, which is a free aerodynamic analysis program for airfoils, wings and planes.

2.1.1 Airfoil Selection

Airfoils that are preferred in similar aircraft were examined in order to select the most suited airfoil to achieve all requirements of this study. In NACA database, one can find hundreds of airfoil types and their aerodynamic software packages (CFD) [3]. As a wing airfoil, the 6-series NACA airfoils are studied because these series is the newest version of the designs and their design enables to maintain laminar flow over a large part of the chord while they have the lower C_d compared to the older 4- or 5-digit airfoils [4]. After examining the two most widely used 6-series NACA airfoils, NACA 64-210 and NACA 65-210; it was predicted that chosing an airfoil with a lower lift-drag ratio for the design which would have wings wider than its counterparts would be beneficial for the longitudinal balance of the aircraft. Hence, NACA 64-210 was chosen to be used in wings and its structure is given in Figure 2.1.

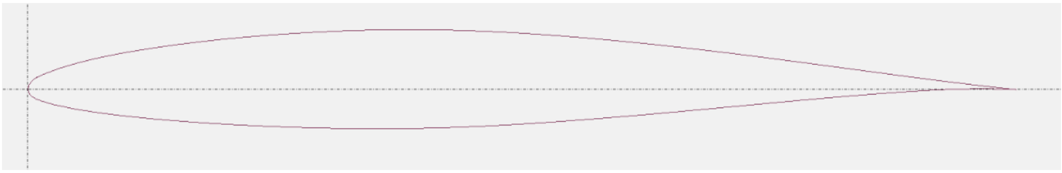

Figure 2.1. NACA 64-210 airfoil structure

. The reasons behind this preference are listed below:

- The maximum lift coefficient (C_L) of NACA 64-210 is approximately 10% above in comparison to NACA 65-210.
- The minimum profile-drag coefficient (C_D) of the NACA 64-210 is slightly higher (about 0.0004) than that of the NACA 65-210.
- The maximum lift-drag ratio is correspondingly lower than that of the NACA 65-210 [5].

On most aircrafts, the airfoil of tail is thinner than that of wing [6]. Therefore, a thinner version of the NACA 64-210, namely NACA Neutral is designed to use in tail design and its structure can be found in Figure 2.2.

Figure 2.2. NACA Neutral airfoil structure

For longitudinal and lateral analyses, two types of these airfoils are derived to model control surfaces deflection, i.e., elevator, rudder and aileron with different tip edge flap angles. Whereas -10˚ tip edge flap versions are named as up, the ones with 10˚ tip edge flap are named as down. In Figures 2.3, 2.4, 2.5 and 2.6, the structures of these airfoils and in Table 2.2, summarization of the specifications of all airfoils can be found.

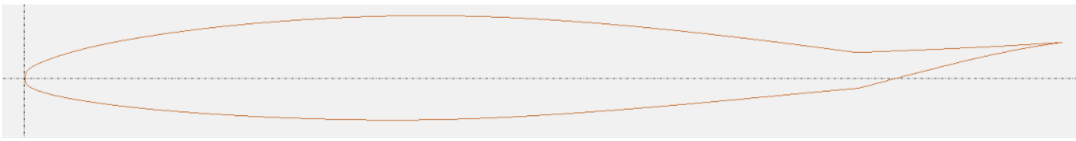

Figure 2.3. NACA 64-210 up airfoil structure

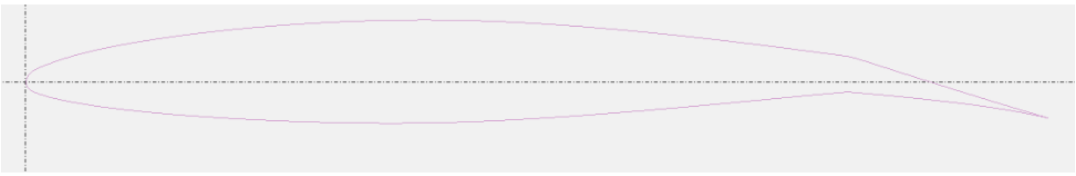

Figure 2.4. NACA 64-210 down airfoil structure

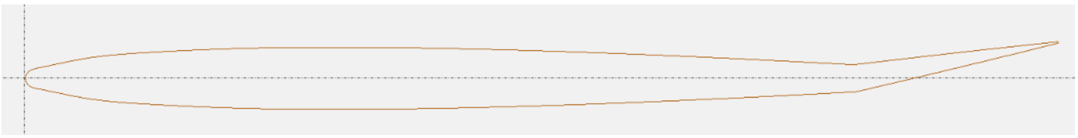

Figure 2.5. NACA up airfoil structure

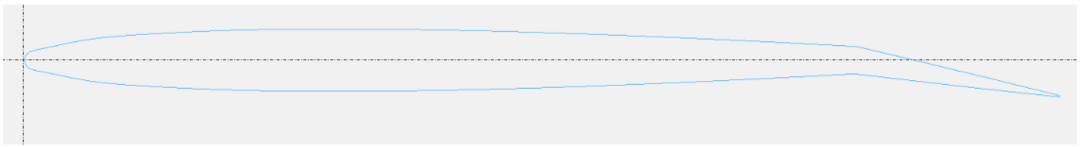

Figure 2.6. NACA down airfoil structure

Table 2.2 Specifications of Airfoils

Name	Thickness	Tip Edge Flap (˚)
NACA 64-210	9.99	0
NACA 64-210 Up	9.99	-10
NACA 64-210 Down	9.99	10
NACA Neutral	6	0
NACA Up	6	-10
NACA Down	6	10

2.1.2 Wing Design

The most critical part of the aircraft design is the wing section. A wing should produce enough lift to carry out the entire mission requirement and have enough strength to carry fuel, payload and engine [7]. The first consideration when designing the wing is to get maximum lift force (L) while minimizing drag force (D) and nose-down pitching moment (M). A monoplane, mid wing and fixed wing with fixed shape was selected. Single wing is chosen because with the same total area, single wing has longer wingspan than the planes with two wings [8]. With the help of developing technology in years, manufacturing longer wings are not a problem anymore. Therefore, single fixed wing type is determined in this work. The reason for selecting mid wing is that having less interference drag compared to low or high wing.

After choosing the suitable airfoil, other specifications of the wing; i.e., wing planform area (S), wingspan (b), aspect ratio (AR), taper ratio, dihedral angle and incidence angle are determined.

Planform area is the result of choices of wingspan and airfoil type and it is 27 m^2 in this design. Aspect ratio is the ratio between the wingspan (b) and the wing Mean Aerodynamic Chord $\bar{C}$. Therefore; it is a result of wingspan and chord. Since high AR means high wing lift curve slope, high AR is needed [9]. The ratio between the tip chord (Ct) and the root chord (Cr) is called taper ratio. It has effects on lift distribution, wing weight, lateral control and lateral stability.

Dihedral angle is chosen as 0˚ because there is no need to change lateral stability with this parameter. Wing incidence is the angle between fuselage center line and the wing chord line at root [10]. The most preffered values for wing incidence angle is between. The typical number for wing incidence for majority of aircraft is between 0˚ to 4˚ [11]. However; after 2˚ the simulation results gave the enormous lift-to-drag ratios, which makes the simulation goes outside the flight envelope. Therefore, incidence angle is selected as 2˚ because with the help of the wing incidence angle, the wing can generate more lift coefficient. All these parameters are given in Table 2.3. The 3D view of the wing is shown in Figure 2.7.

Table 2.3 Specifications of the Wing

Wing Properties	Wing
Wingspan	16 m
Wing Area	27 m^2
Mean Aerodynamic Chord	2.33 m
Aspect Ratio	9.48
Taper Ratio	2
Dihedral Angle	0
Incidence Angle	2˚

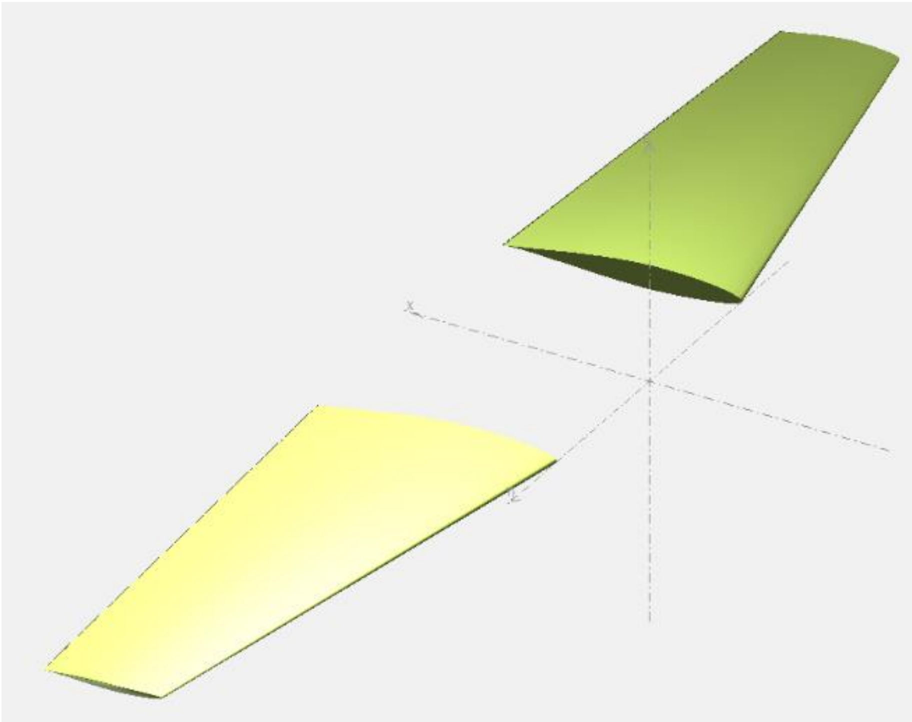

Figure 2.7. 3D view of the wing

2.1.3 Tail Design

Aft tail and one aft vertical tail are used in the tail design section of the aircraft. Because the airfoil of the tail should be thinner then the one for wing [6]; the airfoil type for both tails is NACA Neutral. Specifications of the horizontal and vertical tails are given in Table 2.4. 3D views of horizontal and vertical tails can be found in Figure 2.8 and 2.9, respectively.

Table 2.4 Specifications of Horizontal and Vertical Tails

Tail Properties	Horizontal Tail	Vertical Tail
Wingspan	8.34 m	6.24 m
Wing Area	16.68 m^2	6.49 m^2
Mean Aerodynamic Chord	2.17 m	2.25 m
Aspect Ratio	4.17	3
Taper Ratio	3	2.92

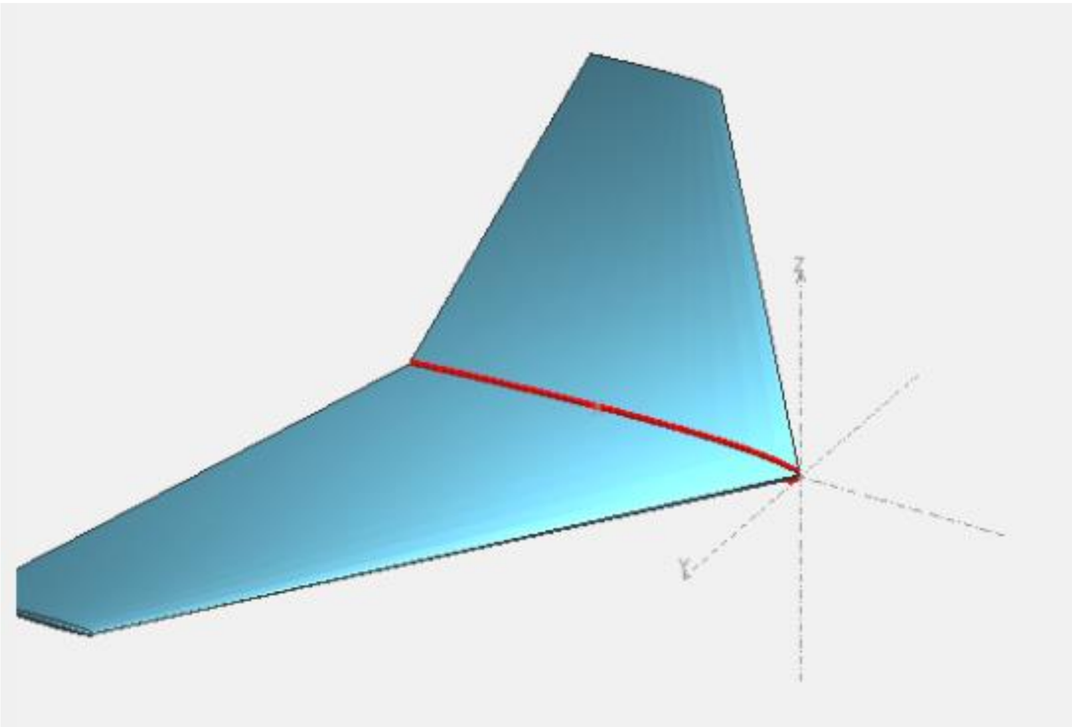

Figure 2.8. 3D view of the horizontal tail

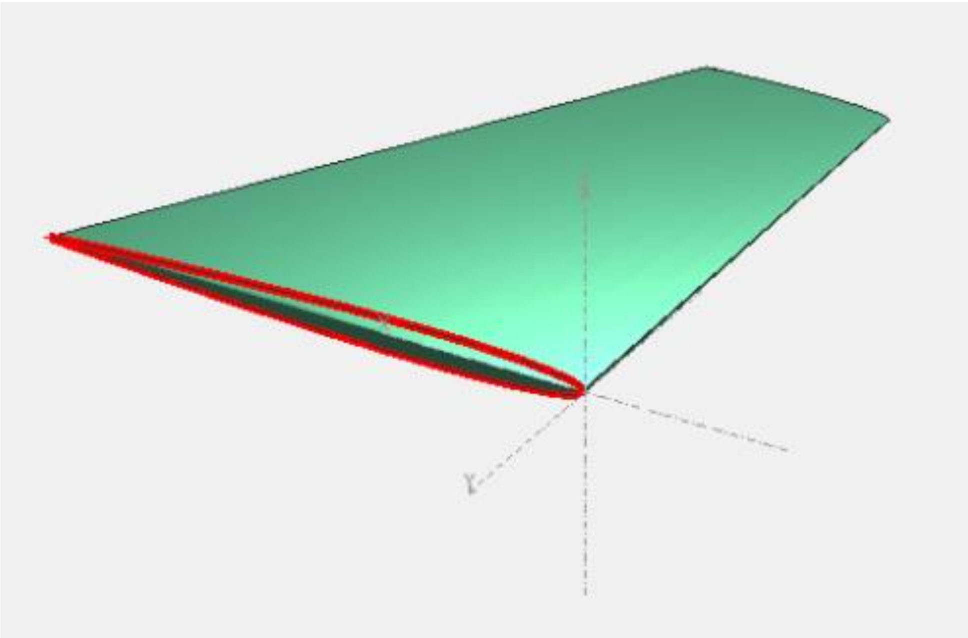

Figure 2.9. 3D view of the vertical tail

2.1.4 Weight Distribution and Final Model of the Aircraft

After the wing and tails are designed, masses for body, avionics and turbojet engines are added. In Table 2.5, mass components are given.

Table 2.5 Mass Distribution of the Aircraft

	Mass (kg)
Horizontal Tail	1000
Vertical Tail	800
Wing	3000
Jet Engines	2x1500
Bombs and Avionics	15200

Turbojet masses are added such that they are placed under the wings. This allocation is chosen because by controlling the turbojet engines separately, thrust vector control is aimed. The distance from the center of gravity creates higher yaw moment. In Figure 2.10, mass distribution, allocations and center of gravity point can be found. In Figure 2.11, 3D view of the overall plane is shown.

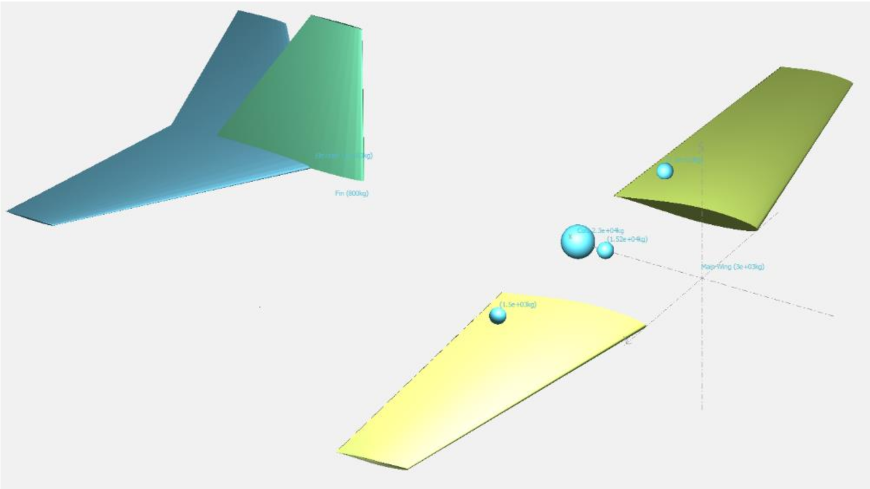

Figure 2.10. Mass distribution and their allocation of the aircraft

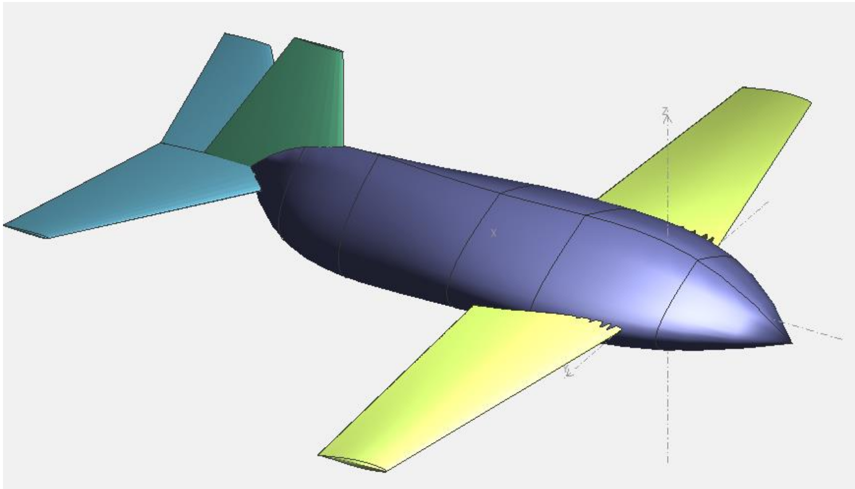

Figure 2.11. 3D view of the overall design

2.2 Modeling the Deflections of Control Surfaces

In order to calculate the longitudinal and lateral derivatives, models that include the deflections of control surfaces are created.

2.2.1 Model of the Deflections of Longitudinal Control Surface

Elevator is the control surface of the aircraft in longitudinal axis. Elevator deflections are created by using two more aircrafts in addition to main aircraft. These two aircrafts are designed with up and down horizontal tail deflection while the wing and vertical tail designs remain the same. These tail differences are made by using appropriate up and down airfoil designs.

In order to model positive elevator deflection, airfoil shape is changed to NACA Up airfoil, which has -10˚ tip edge flap. The horizontal tail structure is illustrated in Figure 2.11.

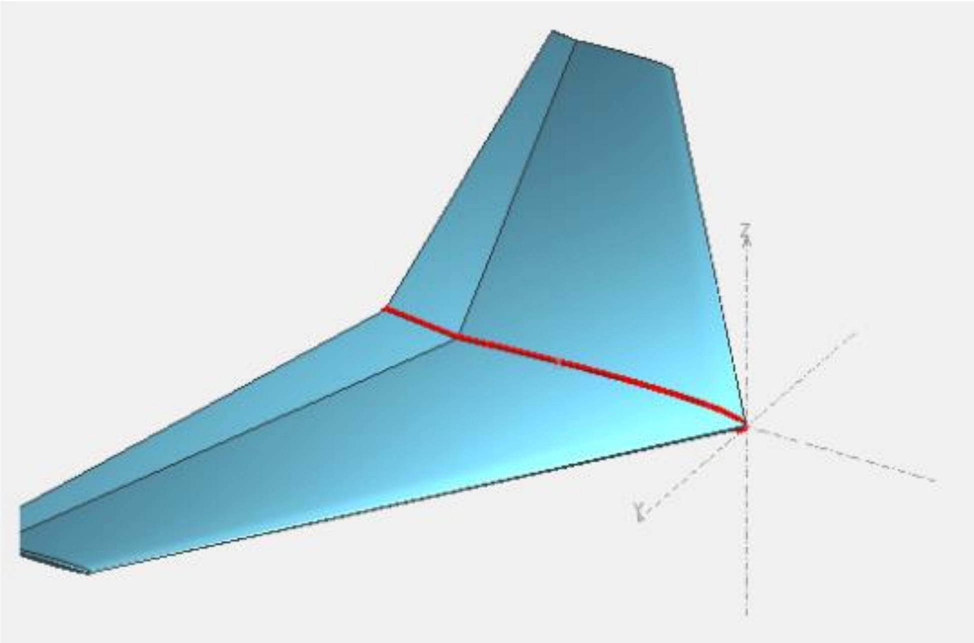

Figure 2.12. Positive elevator deflection

The effects of positive elevator deflection are listed below:

- The elevator goes positive values,
- Nose goes up,
- Positive pitching moment is produced,
- Pitch angle (θ) increases,
- Aircraft starts to pull up.

In order to model negative elevator deflection, the airfoil of horizontal tail is changed to NACA Down which has +10˚ tip edge flap. Figure 2.12 shows the horizontal tail with NACA Down.

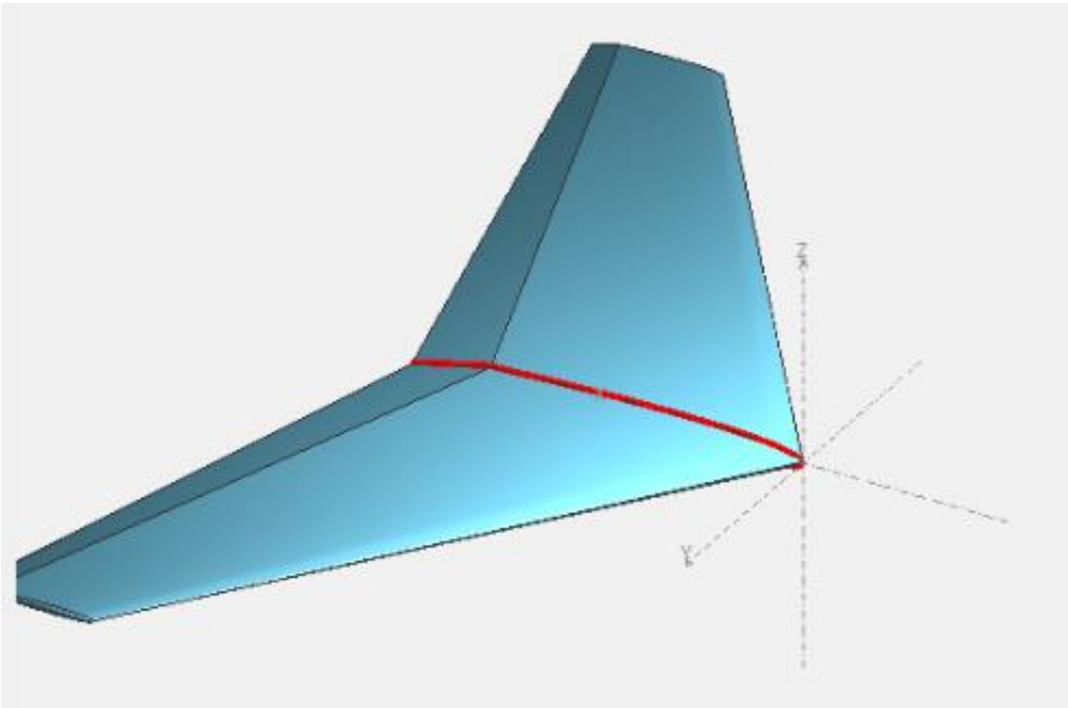

Figure 2.13. Negative elevator deflection

With the negative elevator deflection:

- The elevator goes negative values,
- Nose goes down,
- Negative pitching moment is produced,
- Pitch angle (θ) decreases,
- Aircraft starts to pull down.

2.2.2 Model of the Deflections of Lateral Control Surfaces

There are two lateral control surfaces in the aircraft, namely rudder and aileron. In order to model these control surfaces deflections, four more aircrafts are design with the combination of the deflections of the rudder and the aileron.

Deflections in rudder control surface are modeled by using NACA Up and NACA Down airfoils in vertical tail. Positive rudder deflection is created by changing the airfoil of the vertical tail to NACA Up. In Figure 2.13, vertical tail with NACA Up can be found.

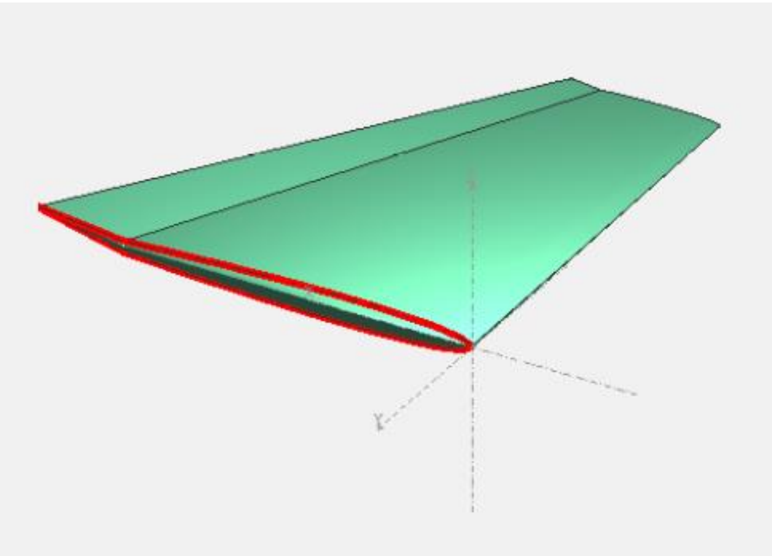

Figure 2.14. Positive rudder deflection

With the positive rudder deflection:

- The rudder goes positive values,
- Positive yawing moment is produced,
- Yaw angle (ψ) increases,
- Aircraft starts to turn right.

In order to model negative rudder deflection, the airfoil of vertical tail is changed to NACA Down which has +10˚ tip edge flap. Figure 2.14 shows the vertical tail with NACA Down.

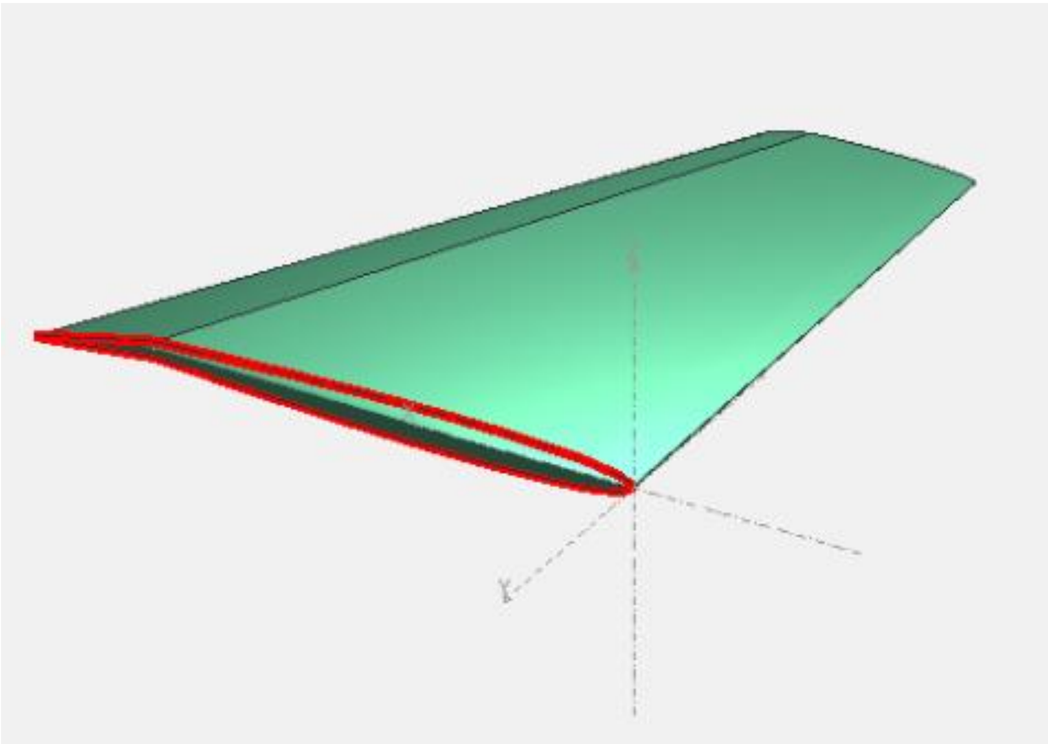

Figure 2.15. Negative rudder deflection

The effects of negative rudder deflection:

- The rudder goes negative values,
- Negative yawing moment is produced,
- Yaw angle (ψ) decreases,
- Aircraft starts to turn left.

Aileron deflection is modeled by using cross airfoils in the right and left wings. Positive aileron deflection is generated by using NACA 64-210 Up airfoil in the right wing and NACA 64-210 Down airfoil in the left wing. Figure 2.15 shows the positive aileron deflection.

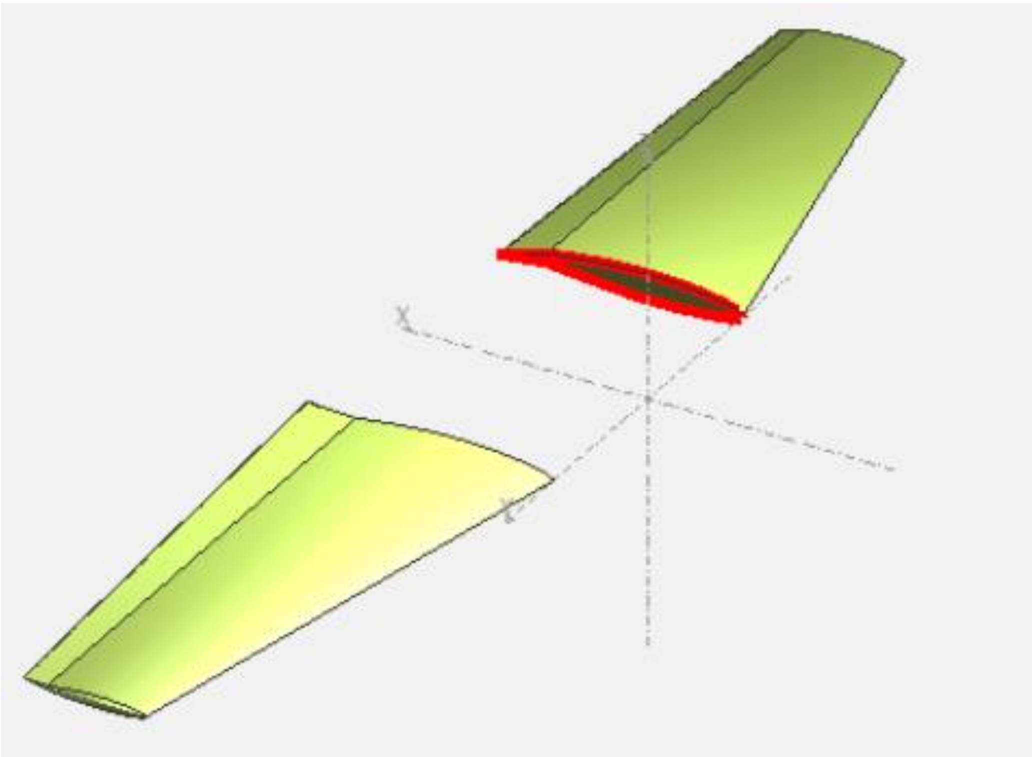

Figure 2.16. Positive aileron deflection

With the positive aileron deflection:

- The aileron goes positive values,
- Positive rolling moment is produced,
- Roll angle (φ) increases,
- Aircraft starts to bank towards to right.

As expected, the version that NACA 64-210 Down airfoil in the right wing and NACA 64-210 Up airfoil in the left wing is applied to model negative aileron deflection. The wing with negative aileron deflection is given in Figure 2.16.

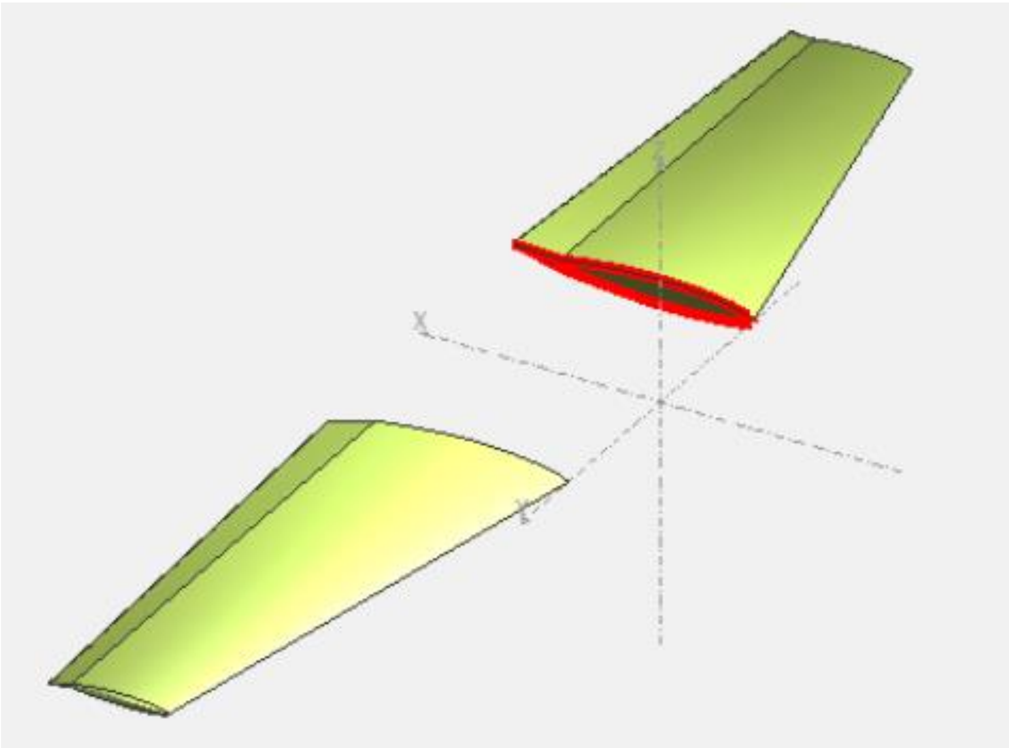

Figure 2.17. Negative aileron deflection

The effects of negative aileron deflection:

- The aileron goes negative values,
- Negative rolling moment is produced,
- Roll angle (φ) decreases,
- Aircraft starts to bank towards to left.

2.3 Analysis of Aerodynamic Characteristics of the Aircraft

Aerodynamic characteristics of the plane is one of the key parts of the flight dynamics model. Aerodynamic forces and moments, in particular; aerodynamic coefficients are the fundamental parts of mathematical model of the plane. Both longitudinal and lateral analyses are made to get dynamic coefficients. In addition, for static coefficients, stability analysis is conducted.

In longitudinal analysis conducted on neutral aircraft, lift force coefficient (C_L), drag force coefficient (C_D) and pitching moment coefficient (C_m) are found. Analysis is performed at the conditions that are listed below:

- At 400 m/s fixed airspeed,
- Varying angle of attack (α), from -10˚ to +10˚,
- Sideslip angle (β) is set to zero.

This procedure is repeated for the other two models which have longitudinal control surface deflections. Table 2.6 shows the results of longitudinal analysis with the change of angle of attack and elevator deflection for lift force coefficients. Drag force coefficients and pitching moment coefficients are obtained with a similar approach.

Table 2.6 Results of Longitudinal Analysis for Lift Force Coefficient

	Resultant C_L	Elevator Deflection		
		-10	0	10
Angle of Attack (°)	-10	-0,18913	-0,28138	-0,37014
	-9	-0,15219	-0,24347	-0,33198
	-8	-0,11512	-0,2054	-0,29361
	-7	-0,07796	-0,16719	-0,25506
	-6	-0,04074	-0,12887	-0,21636
	-5	-0,00349	-0,09048	-0,17755
	-4	0,033765	-0,05204	-0,13864
	-3	0,070995	-0,01358	-0,09967
	-2	0,108171	0,024866	-0,06067
	-1	0,145262	0,063273	-0,02166
	0	0,18224	0,101609	0,017315
	1	0,219075	0,139847	0,056237
	2	0,255739	0,177956	0,095073
	3	0,292205	0,215908	0,133796
	4	0,328443	0,253676	0,172375
	5	0,364427	0,29123	0,210783
	6	0,40013	0,328544	0,248991
	7	0,435526	0,36559	0,286973
	8	0,470588	0,402342	0,3247
	9	0,505292	0,438773	0,362147
	10	0,539613	0,47486	0,399288

Side force coefficient (C_Y), rolling moment coefficient (C_l) and yawing moment coefficient (C_n) are found with lateral analysis. This study is conducted at the conditions below:

- At 400 m/s fixed airspeed,
- Changing sideslip angle (β), -10˚ to +10˚,
- Angle of attack (α) is set to zero.

Lateral dynamic derivatives are calculated for first neutral aircraft, then for the other four models which are positive rudder & positive aileron, positive rudder & negative aileron, negative rudder & positive aileron and lastly negative rudder & negative aileron with the deflections of lateral control surfaces. The results of lateral analysis with the change of sideslip angle, rudder and aileron deflection for side force coefficient are given in Table 2.7, where aileron deflection is 0 due to it is not possible to illustrate the results in 3D view. Rolling moment coefficients and yawing moment coefficients are obtained with a similar approach.

Table 2.7 Results of Lateral Analysis for Side Force Coefficient

	Resultant C_Y	Rudder Deflection (Aileron Deflection= 0)		
		-10	0	10
Sideslip Angle (°)	-10	0,699928	0,465152	0,201196
	-9	0,649776	0,414548	0,151724
	-8	0,59954	0,362336	0,102376
	-7	0,557116	0,317552	0,058624
	-6	0,517316	0,27662	0,018868
	-5	0,474432	0,23282	-0,02283
	-4	0,426296	0,183108	-0,07007
	-3	0,381384	0,135268	-0,1177
	-2	0,339892	0,0927	-0,15996
	-1	0,296012	0,049036	-0,20226
	0	0,248524	0	-0,24733
	1	0,203448	-0,04529	-0,29482
	2	0,161148	-0,08896	-0,33869
	3	0,11888	-0,13154	-0,38019
	4	0,071248	-0,17939	-0,4251
	5	0,024004	-0,2291	-0,47324
	6	-0,01769	-0,2729	-0,51613
	7	-0,05745	-0,31384	-0,55593
	8	-0,10121	-0,35863	-0,59836
	9	-0,15055	-0,41084	-0,64859
	10	-0,2	-0,46144	-0,69874

Finally, stability analysis is defined in XFLR5 to calculate static coefficients of the aircraft. This analysis gives the C_{mq}, C_{lp}, C_{ln}, C_{np} and C_{nr}.

CHAPTER 3

MATHEMATICAL MODEL OF TURBOJET ENGINE

Before the starting to create a mathematical model of a turbojet engine, design constants, inputs and outputs should be specified. Reference values are taken according to the reference values of common turbojet engines, including the circumstances of work, reliability and inner structure. Input limits are taken according to the results of analyses that are conducted in Chapter 2, with the requirements of the designed aircraft.

3.1 History and Overview of Turbojet Engine

At the beginning of the 20th century, there were internal combustion and steam engines in the industry. However, the engines that have this mechanism were too heavy to be used in aircraft industry. Works on air-breathing jet propulsion started in the late 1930s. It is a special type of internal combustion energy engine. It produces its net output power which is proportional to the rate of change in the kinetic energy of the engine's working fluid [12]. This new propulsion system had considerably better power/weight ratio and resultant overall efficiency enabled this type of engines to be used in flight applications.

In the same time period, there were several patent applications for air-breathing engines by various scientists from different countries. However, no jet engines were constructed in that period because they had not enough flight speed capacity [13]. The first patented turbojet engine that is produced was composed of an axial-flow compressor, a radial compressor stage, a combustor, an axial-flow turbine driving the compressor and an exhaust nozzle and designed by Frank Whittle.

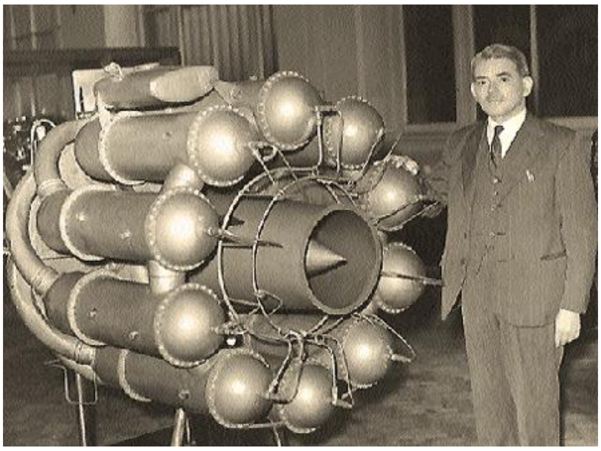

Figure 3.1. Turbojet engine with its inventor, Frank Whittle

Most advantages of turbojet engines are:

- Turbojet engine is 2 to 3 times efficient than best propeller piston engines of equal thrust power because of having a very efficient ratio of net power output to engine weight.
- The combustion chambers could be made small enough to fit in the engine and could have a wide operational range from start to high altitude and from low to high flight speed.
- Their vibration attitudes are more reliable due to having fewer moving parts and moving toward one direction.

These features contribute to have high-speed flight and good maneuverability.

3.2 Modeling the Turbojet Engine

3.2.1 Determining of the Parametric Cycle Analysis

Turbojet engine system consists of lots of subsystems such as compressor, turbine, nozzle and others. Understanding the concept of the relations between these inner parts and transition of basic parameters like temperature and pressure is highly important. The effects of these variables to the engine performance and parametric cycle of the engine are the key knowledge to build the mathematical model.

In this analysis, main burner exit temperature (throttle setting), T_{t4}, and initial flight conditions, i.e., Mach number, M_0, temperature, T_0 and pressure, P_0 are determined as design inputs and they are independent from engine performance. The outputs of jet engine; thrust and fuel consumption are called specific thrust and thrust specific fuel consumption, when the design inputs are used for calculation with certain combination. This special combination of design inputs is called design point or reference point.

When we think of that an aircraft with turbojet engine, the performance of the plane changes with throttle setting directly and initial flight conditions indirectly.

Mathematical model assumptions are listed below:

- At the primary exit nozzle, low-pressure turbine entrance nozzle and high-pressure turbine entrance nozzle, the flow is restrained.
- The main burner and primary exit nozzle total pressure ratios (π_b and π_n) are taken as their reference values along the whole analysis.
- Also, the combustor and burner efficiencies (η_c and η_b) are taken as their reference values along the analysis.
- Cooling of turbine and dropping of oil are neglected.
- There is no power transition from the turbine to the drive subsystems.

• In both downstream and upstream of the main burner, gases are accepted as calorically perfect [14].

The expression unity plus fuel/air ratio is taken as constant.

3.2.2 Performance Analysis of the Turbojet Engine

The throttle setting (T_{t4}), initial Mach number (M_0), temperature (T_0), pressure (P_0) and ambient pressure/exhaust pressure ratio (P_0/ P_9) are the independent variables that are used in analytical expressions for component performance [15]. Engine mass flow rate ($\dot{m}_0$), exit Mach number (M_9), compressor temperature ratio (τ_c), compressor pressure ratio (π_c), burner fuel/air ratio (f) and exit temperature ratio (T_9/T_0) are the other variables in this analysis but they are dependent.

The thrust equation of this engine is:

$$\frac{F}{\dot{m}_0} = \frac{a_0}{g_c}\left[(1+f)\frac{V_9}{a_0} - M_0 + (1+f)\frac{R_t}{R_c}\frac{T_9/T_0}{V_9/A_0}\frac{1-P_0/P_9}{\gamma_c}\right] \tag{3-1}$$

where;

$$\frac{T_9}{T_0} = \frac{T_{t4}\tau_t}{(P_{t9}/P_9)^{(\gamma_t-1)/\gamma_t}}\frac{c_{pc}}{c_{pt}}$$

$$\frac{P_{t9}}{P_9} = \frac{P_0}{P_9}\pi_r\pi_d\pi_c\pi_b\pi_t\pi_n$$

$$\frac{V_9}{a_0} = M_9\sqrt{\frac{\gamma_t R_t T_9}{\gamma_c R_c T_0}} \tag{3-2}$$

$$M_9 = \sqrt{\frac{2}{\gamma_t - 1}\left[\left(\frac{P_{t9}}{P_9}\right)^{(\gamma_t-1)/\gamma_t} - 1\right]}$$

The thrust specific fuel consumption equation is:

$$S = \frac{f}{F/\dot{m}_0} \tag{3-3}$$

where fuel air ratio, f:

$$f = \frac{\tau_\lambda - \tau_r \tau_c}{h_{PR}\eta_b/\left(c_p T_0\right) - \tau_\lambda} \tag{3-4}$$

The compressor pressure ratio, τ_c:

$$\tau_c = 1 + (\tau_{cR} - 1)\frac{T_{t4}/T_{t2}}{(T_{t4}/T_{t2})_R} \tag{3-5}$$

The compressor pressure ratio is correlated to its temperature ratio with its efficiency:

$$\pi_c = [1 + \eta_c(\tau_c - 1)]^{\gamma_c/(\gamma_c - 1)} \tag{3-6}$$

Engine mass flow rate can be obtained with the pressure ratios of the components and the reference values:

$$\dot{m}_0 = \dot{m}_{0R}\frac{P_0\pi_r\pi_d\pi_c}{(P_0\pi_r\pi_d\pi_c)_R}\sqrt{\frac{T_{t4R}}{T_{t4}}} \tag{3-7}$$

The other equations related to gas, diffuser and flight parameters are shown below:

$$R_c = \frac{\gamma_c - 1}{\gamma_c} c_{pc}$$

$$R_t = \frac{\gamma_t - 1}{\gamma_t} c_{pt}$$

$$a_0 = \sqrt{\gamma_c R_c g_c T_0}$$

$$V_0 = a_0 M_0$$

$$\tau_r = 1 + \frac{\gamma_c - 1}{2} {M_0}^2$$

$$\pi_r = \tau^{\gamma_c/(\gamma_c - 1)}$$

$$\eta_r = 1 \qquad \text{for } M_0 \leq 1 \tag{3-8}$$

$$\eta_r = 1 - 0.075(M_0 - 1)^{1.35} \qquad \text{for } M_0 > 1$$

$$\pi_d = \pi_{d\,max} \eta_r$$

$$T_{t2} = T_0 \tau_r$$

$$\tau_\lambda = \frac{c_{pt} T_{t4}}{c_{pc} T_0}$$

$$F = \dot{m}_0 \left(\frac{F}{\dot{m}_0} \right)$$

Mathematical model of a turbojet engine is constructed according to the equations above in MATLAB / Simulink. The reference values for the components are taken from a simple turbojet engine and component limits are considered while choosing the suitable jet engine model.

3.2.3 Results of the Turbojet Engine Simulation

Once the mathematical model of the turbojet engine is implemented in MATLAB / Simulink, according the flight conditions that are aimed to simulate, thrust analysis of the turbojet engine is conducted. With the reference Mach number, 0.8 and throttle setting, 1800 K; the behavior of the jet engine is studied. In Figure 3.2, at the Mach number 0.6, thrust values correspond to eight different throttle settings (1200 K, 1400 K, 1600 K, 1800 K, 2000 K, 2200 K, 2400 K, 2600 K) are shown.

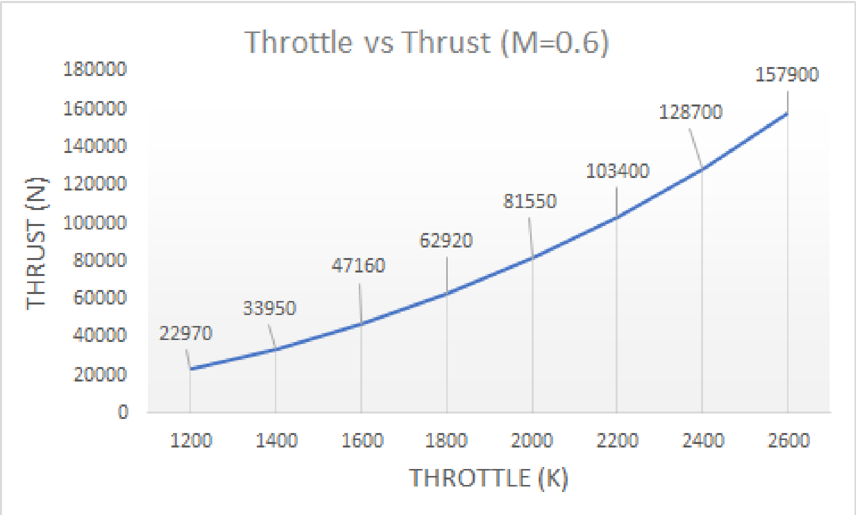

Figure 3.2. Resultant thrust with changing throttle settings at *M = 0.6*

In Table 3.1, the resultant thrust values are given for seven different Mach number (0.6, 0.8, 1, 1.2, 1.4, 1.6, 1.8) with eight different throttle settings (1200 K, 1400 K, 1600 K, 1800 K, 2000 K, 2200 K, 2400 K, 2600 K).

Table 3.1 Resultant Thrust with the Change of Mach Number and Throttle Settings

Throttle Setting (K)		Mach Number						
		0.6	0.8	1	1.2	1.4	1.6	1.8
	1200	22970	23970	26180	29440	33560	38660	44760
	1400	33950	35380	38390	42820	48460	55500	64050
	1600	47160	49070	52980	58710	65990	75110	86260
	1800	62920	65360	70270	77420	86490	97850	111800
	2000	81550	84560	90570	99270	110300	124100	140900
	2200	103400	107000	114200	124600	137700	154100	174100
	2400	128700	133000	141500	153800	169100	188300	211700
	2600	157900	163000	172900	187100	204900	227000	254000

CHAPTER 4

MATHEMATICAL MODEL OF THE JET PLANE

The equations of motion of the aircraft are observed using the laws kinetic and kinematic to constuct the mathematical model of the aircraft in MATLAB / Simulink. Determining the equations that explain the motion of the aircraft is the key of modeling the aircraft.

4.1 Reference Frames

Inertial reference frame is the essential part of any dynamics problem. In this study, inertial frame is chosen as earth-fixed reference frame.

4.1.1 Earth Frame

Determining the aircraft motion with the earth fixed reference frame is preferable in general. In order to defining earth frame, a reference point o_0 on the surface of the earth is the origin of a right-handed orthogonal system of axes (o_0 x_0 y_0 z_0) where, o_0x_0 points to the north, o_0y_0 points to the east and o_0z_0 points vertically down along the gravity vector [16]. To show the aircraft translational and rotational kinematics, earth frame is suitable because taking this frame as inertial is possible with certain assumptions. The notation {e} refers to this frame.

4.1.2 Body Frame

A right-handed orthogonal axis system fixed in the aircraft and constricted to carry with it is useful in modeling an aircraft. Body frame is fixed in the aircraft and the (ox_bz_b) plane represents the plane of symmetry of the aircraft. In body frame, the origin and the axes remain fixed relative to the aircraft, therefore it is common to use this frame to define certain aircraft attitudes. This means that the relative orientation of the earth and body frames describes the aircraft attitude. In order to indicate roll, pitch and yaw axes, the forces acting upon an aircraft that are measured from the center of gravity are calculated with respect to the body axis of the aircraft [17]. Also, in some applications like thrust vectoring, the direction of the thrust force is set to the body frame. This frame is denoted by {b}.

4.1.3 Wind Frame

It is convenient defining an aircraft fixed axis such that the ox axis is parallel to the total velocity vector, V_0. This axis is named as wind axis and it relates the direction of wind flow and flight with the aircraft movement [18]. In order to explain the aerodynamic forces and moments acting on an aircraft, the wind frame is suitable. The {w} notation is used to denote this frame. The reference frames of an aircraft are given in Figure 4.1.

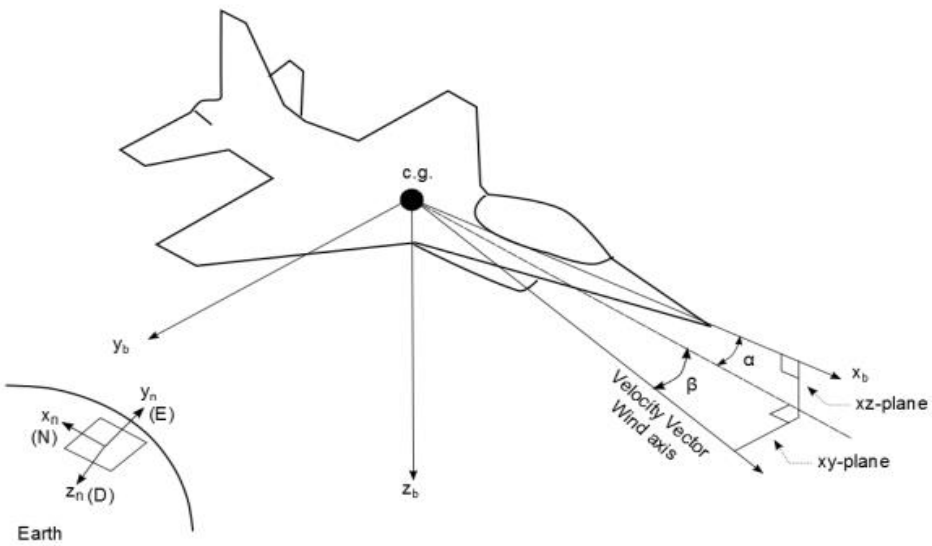

Figure 4.1. Aircraft reference frames

4.2 Transformation Matrices

In this study, earth frame is chosen as inertial frame and whereas some linear quantities are in body frame, some of them are in wind frame. Therefore, it is needed to define transformation matrices to transform motion variables from one system of axes to another. If (ox_3, oy_3, oz_3) represent components of a linear quantity in the frame ($ox_3y_3z_3$) and (ox_0, oy_0, oz_0) represent components of the same linear quantity transformed into the frame of ($ox_0y_0z_0$), the transformation matrix may be shown that [19]:

$$\begin{bmatrix} ox_3 \\ oy_3 \\ oz_3 \end{bmatrix} = \mathbf{D} \begin{bmatrix} ox_0 \\ oy_0 \\ oz_0 \end{bmatrix}$$

where the direction cosine matrix D is given by,

$$\mathbf{D} = \begin{bmatrix} cos\theta cos\psi & cos\theta sin\psi & -sin\theta \\ sin\varphi sin\theta cos\psi - cos\varphi sin\psi & sin\varphi sin\theta sin\psi + cos\varphi cos\psi & sin\varphi cos\theta \\ cos\varphi sin\theta cos\psi + sin\varphi sin\psi & cos\varphi sin\theta sin\psi - sin\varphi cos\psi & cos\varphi cos\theta \end{bmatrix}$$

4.3 Rigid Body Equations of Motion

The application of Newton's laws of motion to an aircraft in flight, manage to define a set of nonlinear differential equations for the determining of the aircraft's response and attitude with time.

The motion of a rigid body in 3D is governed by its mass (m) and inertia tensor (I), including aerodynamic loads, gravitational forces, inertial forces and moments [20].

In order to explain the nonlinear dynamics of motion, a dynamic relationship is defined as follows:

$$\dot{x} = f(x, u, t)$$

where x: state variables, u: input variables, t: time [21]. There are 12 state variables in formulation of the equations of motions for flight dynamics, six of them for aircraft velocity and the rest six variables for aircraft position.

The vector of aircraft velocity:

$$[\nu] = \begin{bmatrix} u \\ v \\ w \\ p \\ q \\ r \end{bmatrix} = \begin{bmatrix} velocity\ in\ forward\ direction \\ velocity\ in\ transverse\ direction \\ velocity\ in\ vertical\ direction \\ rate\ of\ roll\ motion \\ rate\ of\ pitch\ motion \\ rate\ of\ yaw\ motion \end{bmatrix}$$

where;

$$V_T = \sqrt{u^2 + v^2 + w^2} \tag{4-1}$$

The vector of aircraft position:

$$[\eta] = \begin{bmatrix} X_e \\ Y_e \\ Z_e \\ \varphi \\ \theta \\ \psi \end{bmatrix} = \begin{bmatrix} earth\ fixed\ x - axis \\ earth\ fixed\ y - axis \\ earth\ fixed\ z - axis \\ angle\ of\ roll \\ angle\ of\ pitch \\ angle\ of\ yaw \end{bmatrix}$$

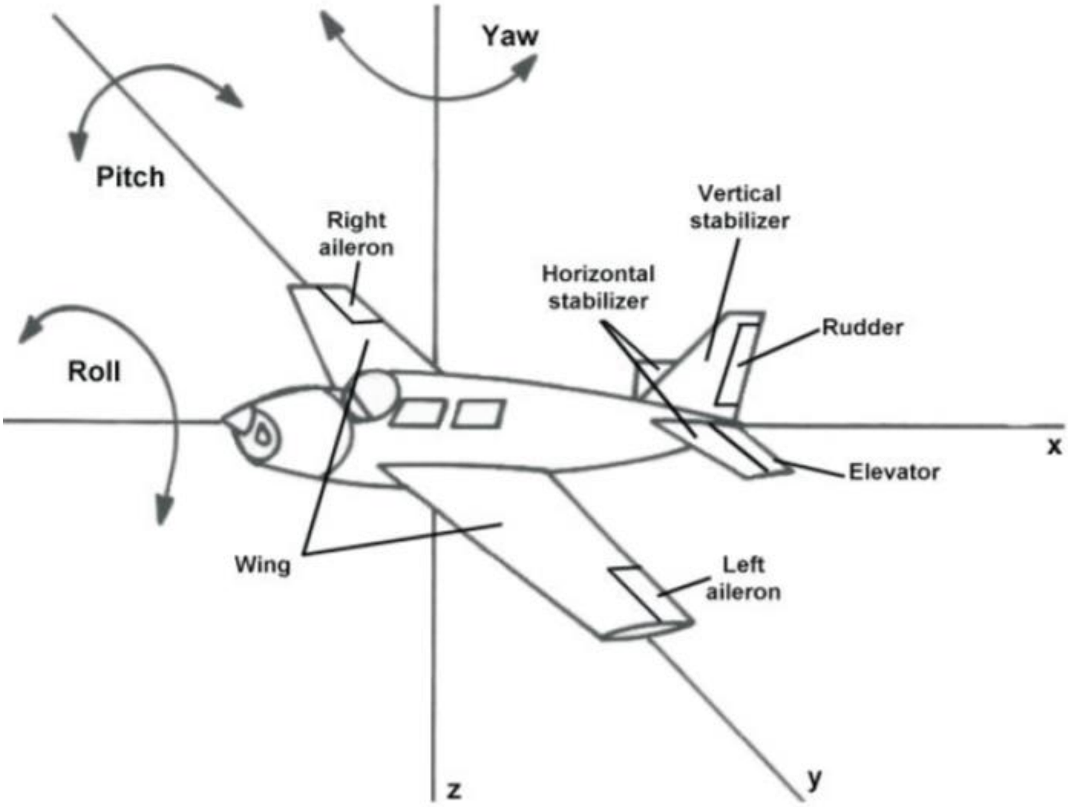

Figure 4.2. Control surfaces and roll, pitch and yaw angle in an aircraft

Table 4.1 shows the state variables in dynamics and kinematics separation [22].

Table 4.1 State Variables in Equations of Motion

	Dynamics	Kinematics
Translation	u	X_e
Translation	v	Y_e
Translation	w	Z_e
Rotation	p	φ
Rotation	q	θ
Rotation	r	ψ

The net forces and moments acting on the aircraft are the input variables for the motion of an aircraft. There are three force components corresponding to each axis, namely; axial force (X), side force (Y) and normal force (Z). Also, there are three moments corresponding to each axis, namely rolling moment (L), pitching moment (M) and yawing moment (N) [19].

The vector of forces and moments are:

$$[\tau] = \begin{bmatrix} X \\ Y \\ Z \\ L \\ M \\ N \end{bmatrix} = \begin{bmatrix} force\ in\ longitudinal\ direction \\ force\ in\ transverse\ direction \\ force\ in\ vertical\ direction \\ moment\ in\ rolling \\ moment\ in\ pitching \\ moment\ in\ yawing \end{bmatrix}$$

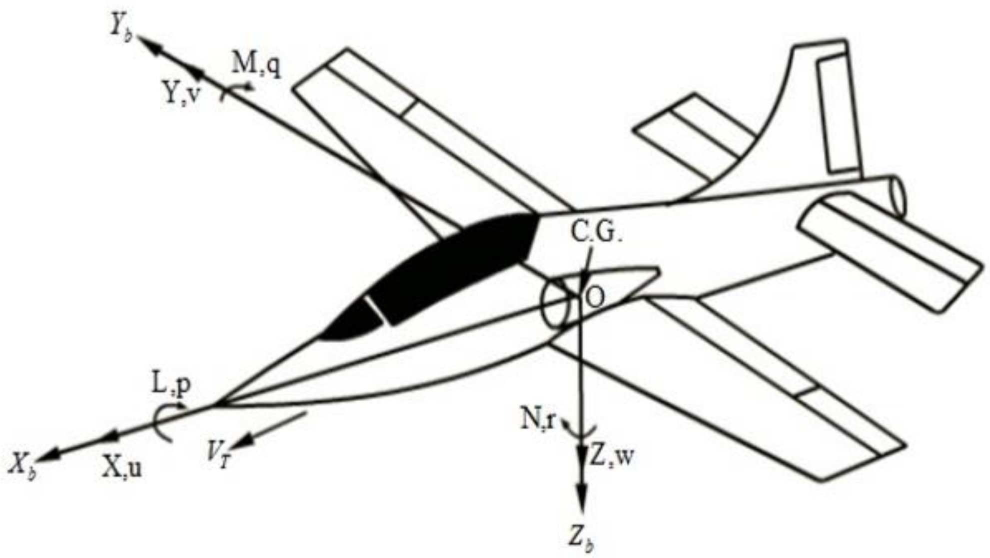

Figure 4.3. The forces and moments acting on an aircraft

With the principles of Newton's Second Law, the state variables that exist due to translational dynamics can be evaluated: the summation of all external forces (F) acting on a rigid body is equal to the time rate of change of the linear momentum (mV) of the body:

$$\sum F = \frac{d}{dt}(mV) \tag{4-2}$$

The mass is assumed to be constant:

$$F = m\frac{d}{dt}V \tag{4-3}$$

Moment relations are defined as follows; the summation of the external moments (M) acting on a rigid body is equal to the time rate of change of the angular momentum (H), which can be explained by Euler's formula:

$$\sum M = \frac{d}{dt}\int H \tag{4-4}$$

Equations of motion can be expressed in terms of state and input variables:

$$\begin{bmatrix} X \\ Y \\ Z \end{bmatrix} = m\begin{bmatrix} \dot{u} + qw - rv \\ \dot{v} + ru - pw \\ \dot{w} + pv - qu \end{bmatrix}$$

$$\begin{bmatrix} L \\ M \\ N \end{bmatrix} = \begin{bmatrix} I_x\dot{p} - \left(I_y - I_z\right)qr - I_{xz}(pr + \dot{r}) \\ I_y\dot{q} + (I_x - I_z)pr + I_{xz}(p^2 - r^2) \\ I_z\dot{r} - \left(I_x - I_y\right)pq + I_{xz}(qr - \dot{p}) \end{bmatrix} \tag{4-5}$$

$$\begin{bmatrix} \dot{\varphi} \\ \dot{\theta} \\ \dot{\psi} \end{bmatrix} = \begin{bmatrix} 1 & \sin\varphi\tan\theta & \cos\varphi\tan\theta \\ 0 & \cos\varphi & -\sin\varphi \\ 0 & \sin\varphi\sec\theta & \cos\varphi\sec\theta \end{bmatrix}\begin{bmatrix} p \\ q \\ r \end{bmatrix}$$

$$\begin{bmatrix} \frac{dx}{dt} \\ \frac{dy}{dt} \\ \frac{dz}{dt} \end{bmatrix}$$
$$= \begin{bmatrix} \cos\theta\cos\psi & \sin\varphi\sin\theta\cos\psi - \cos\varphi\sin\psi & \cos\psi\sin\theta\cos\psi + \sin\varphi\sin\psi \\ \cos\theta\sin\psi & \sin\varphi\sin\theta\sin\psi + \cos\varphi\cos\psi & \cos\varphi\sin\theta\sin\psi - \sin\varphi\cos\psi \\ -\sin\theta & \sin\varphi\cos\theta & \cos\varphi\cos\theta \end{bmatrix} \begin{bmatrix} u \\ v \\ w \end{bmatrix}$$

4.4 Aerodynamic Forces and Moments

Aerodynamic forces and moments are created with the aerodynamic characteristics of the aircraft. They are obtained as follows [21]:

$$\begin{bmatrix} X_{aero} \\ Y_{aero} \\ Z_{aero} \end{bmatrix} = \frac{S * u^2 * \rho}{2} \begin{bmatrix} -C_D \\ C_Y \\ -C_L \end{bmatrix}$$

(4-6)

$$\begin{bmatrix} L_{aero} \\ M_{aero} \\ N_{aero} \end{bmatrix} = \frac{S * u^2 * \rho}{2} \begin{bmatrix} C_l * b \\ C_m * c \\ C_n * b \end{bmatrix}$$

Density of the air (ρ) are calculated from altitude (h) with the formulas below:

$$T = 15.04 - 0.00649h$$

$$P = 101.29 \left[\frac{T + 273.1}{288.08}\right]^{5.256} \qquad (4\text{-}7)$$

$$\rho = \frac{P}{0.2869(T + 273.1)}$$

4.5 Gravitational Forces and Moments

The gravitational force acting on the aircraft acts through the center of gravity of the aircraft. The gravitational force has components acting along the body axis and it is an external force that must be into consideration in modeling the aircraft. Hence, in order to calculate the gravitational forces, the aircraft weight into the disturbed body axis is solved. The resultant equations are given as follows:

$$\begin{bmatrix} X_{g_e} \\ Y_{g_e} \\ Z_{g_e} \end{bmatrix} = \begin{bmatrix} -mgsin\theta \\ mgcos\theta\varphi \\ mgcos\theta cos\varphi \end{bmatrix} \tag{4-8}$$

Gravitational force creates zero moment about any of axes due to the body frame is fixed to the center of gravity of the aircraft; therefore:

$$L_g = M_g = N_g = 0 \tag{4-9}$$

4.6 Thrust Forces and Moments

In order to include external energy to the system, thrust is essential to contribute required maneuvers to the aircraft. The thrust force make possible to cover larger disturbances [22]. Besides, thrust force brings lots of advantages even in the case of small disruptions from the nominal trajectory, such as smaller actuator performances is needed, and it is more accessible to convergence to the nominal path [21]. The thrust force due to the turbojet engines have only a component in X axis because the engines are placed parallel to the x-y plane of the aircraft. Since the engines are controlled separately and allocated under the wings with a distance 3 m, they can create yawing moment. If the thrust forces of turbojet engines are donated as $F_{1_{Thrust}}$ and $F_{2_{Thrust}}$, the propulsive forces and moments are given as follows:

$$\begin{bmatrix} X_{Thrust} \\ Y_{Thrust} \\ Z_{Thrust} \end{bmatrix} = \begin{bmatrix} F_{1_{Thrust}} + F_{2_{Thrust}} \\ 0 \\ 0 \end{bmatrix}$$

$$\begin{bmatrix} L_{Thrust} \\ M_{Thrust} \\ N_{Thrust} \end{bmatrix} = \begin{bmatrix} 0 \\ 0 \\ (F_{1_{Thrust}}) * (3) + (F_{2_{Thrust}}) * (-3) \end{bmatrix} \tag{4-10}$$

4.7 Stability Analyses of the Model

4.7.1 Linearization and Trimming of the Model

To understand the stability of the designed model, four separate linearization analyses are conducted with four different trim points. In this study; altitude, velocity, angle of attack and sideslip angle are choosen as trim values.

$$\begin{bmatrix} h_{trim} \\ v_{trim} \\ \alpha_{trim} \\ \beta_{trim} \end{bmatrix} = \begin{bmatrix} 1000\ m \\ 400\ m/s \\ 0^{\circ} \\ 0^{\circ} \end{bmatrix}$$

The stability analyses have been made in longitudinally and laterally. The poles that are in the left side of the s-plane indicate that the system is stable [23].

Analysis 1:

Transfer function of linearization between elevator and altitude; at the altitude trim point and poles and zeros of the system is shown below:

$$H(s) = \frac{-0.88s^3 - 474.3s^2 + 685.4s - 21.95}{s^5 + 539.6s^4 + 642.8s^3 + 9.217s^2 + 1.121s + 0.0003653} \tag{4-11}$$

$$\begin{bmatrix} p_1 \\ p_2 \\ p_3 \\ p_4 \\ p_5 \end{bmatrix} = 100 * \begin{bmatrix} -5.3836 \\ -0.0118 \\ -0.0001 + 0.0004i \\ -0.0001 - 0.0004i \\ 0 \end{bmatrix}$$

$$\begin{bmatrix} z_1 \\ z_2 \\ z_3 \end{bmatrix} = \begin{bmatrix} -540.4491 \\ -1.4084 \\ -0.0328 \end{bmatrix}$$

Analysis 2:

Transfer function of linearization between elevator and valocity; at the velocity trim point and poles and zeros of the system is shown below:

$$H(s) = \frac{-0.3756s^4 - 202.9s^3 - 766.6s^2 - 17.64s - 0.4525}{s^5 + 539.6s^4 + 642.8s^3 + 9.217s^2 + 1.121s + 0.0003653}$$

$$\begin{bmatrix} p_1 \\ p_2 \\ p_3 \\ p_4 \\ p_5 \end{bmatrix} = 100 * \begin{bmatrix} -5.3836 \\ -0.0118 \\ -0.0001 + 0.0004i \\ -0.0001 - 0.0004i \\ 0 \end{bmatrix} \tag{4-12}$$

$$\begin{bmatrix} z_1 \\ z_2 \\ z_3 \\ z_4 \end{bmatrix} = 100 * \begin{bmatrix} -5.3625 \\ -0.0378 \\ -0.0001 + 0.0002i \\ -0.0001 - 0.0002i \end{bmatrix}$$

Analysis 3:

Transfer function of linearization between elevator and pitch angle; at the angle of attack trim point and poles and zeros of the system is shown below:

$$H(s) = \frac{248s^3 + 104.4s^2 - 2.492s + 0.0001388}{s^5 + 539.6s^4 + 642.8s^3 + 9.217s^2 + 1.121s + 0.0003653}$$

$$\begin{bmatrix} p_1 \\ p_2 \\ p_3 \\ p_4 \\ p_5 \end{bmatrix} = 100 * \begin{bmatrix} -5.3836 \\ -0.0118 \\ -0.0001 + 0.0004i \\ -0.0001 - 0.0004i \\ 0 \end{bmatrix} \tag{4-13}$$

$$\begin{bmatrix} z_1 \\ z_2 \\ z_3 \end{bmatrix} = \begin{bmatrix} -0.4435 \\ -0.0226 \\ -0.0001 \end{bmatrix}$$

Analysis 4:

Transfer function of linearization between rudder and yaw angle; at the sideslip angle trim point and poles and zeros of the system is shown below:

$$H(s) = \frac{s^3 + 0.0476s^2 + 4.75e^{-6}s}{s^5 + 0.003s^4 + 0.0005366s^3 + 8.55e^{-7}s^2 + 1.495e^{-10}s}$$

$$\begin{bmatrix} p_1 \\ p_2 \\ p_3 \\ p_4 \\ p_5 \end{bmatrix} = \begin{bmatrix} -0.0007 + 0.231i \\ -0.0007 - 0.231i \\ -0.0014 \\ -0.0002 \\ 0 \end{bmatrix} \tag{4-14}$$

$$\begin{bmatrix} z_1 \\ z_2 \\ z_3 \end{bmatrix} = \begin{bmatrix} -0.0475 \\ -0.0001 \\ 0 \end{bmatrix}$$

4.7.2 Open Loop Responses of the Model

Before the autopilot design, the open loop responses of the system are observed. For five different control inputs of the system, i.e., elevator, rudder, aileron, total thrust and moment difference, step inputs are used to examine the attitude of the model.

Simulation 1: Elevator Deflection

The attitude of the model is observed under 10° elevator deflection in the circumstances that rudder and aileron deflections are zero, there is no moment difference and an average total thrust which is 70000 N. As expected, altitude and pitch angle increased with higher slope while velocity decreased [23]. The reason behind the increases of the altitude and pitch angle with 0° elevator deflection is that aircraft has 2° incidence angle [24]. In Figures 4.4, 4.5, 4.6, 4.7 and 4.8; system responses can be observed.

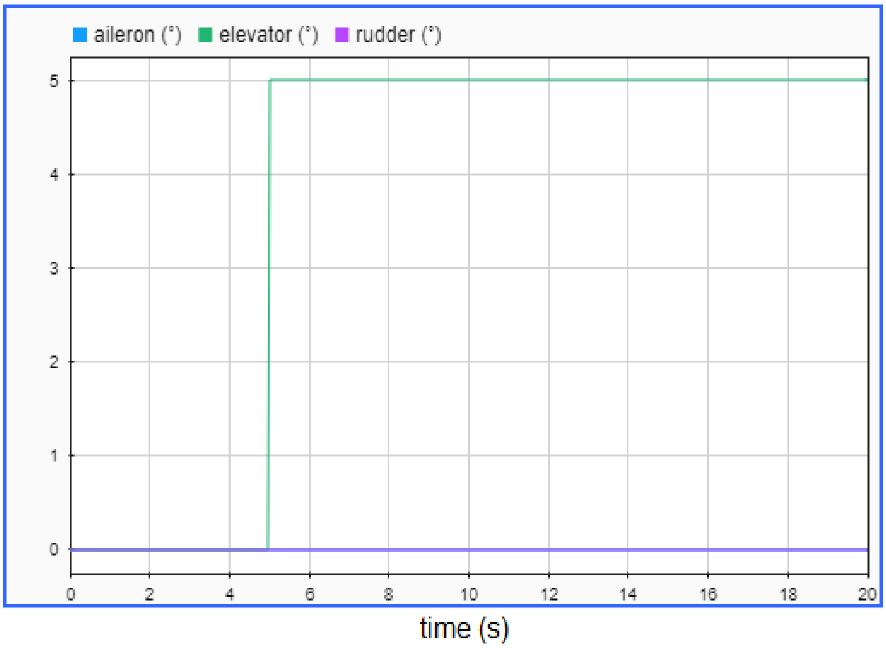

Figure 4.4. Control surfaces of the aircraft in simulation 1

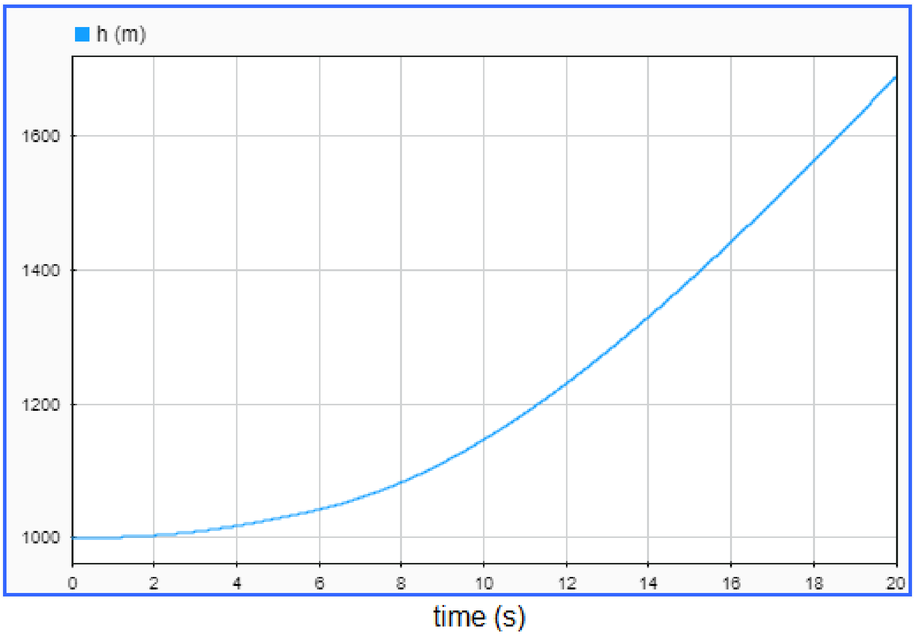

Figure 4.5. Altitude of the aircraft simulation 1

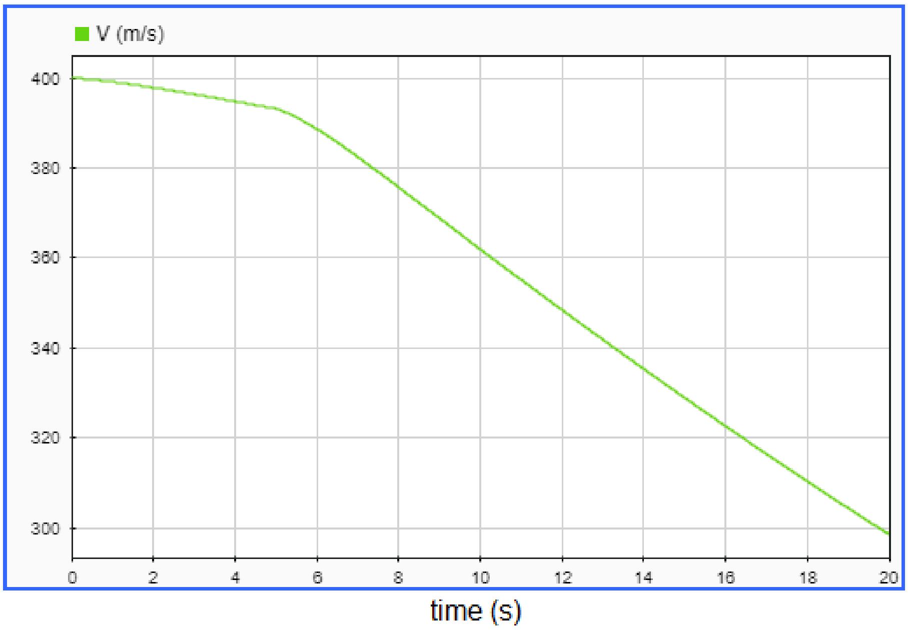

Figure 4.6. Velocity of the aircraft simulation 1

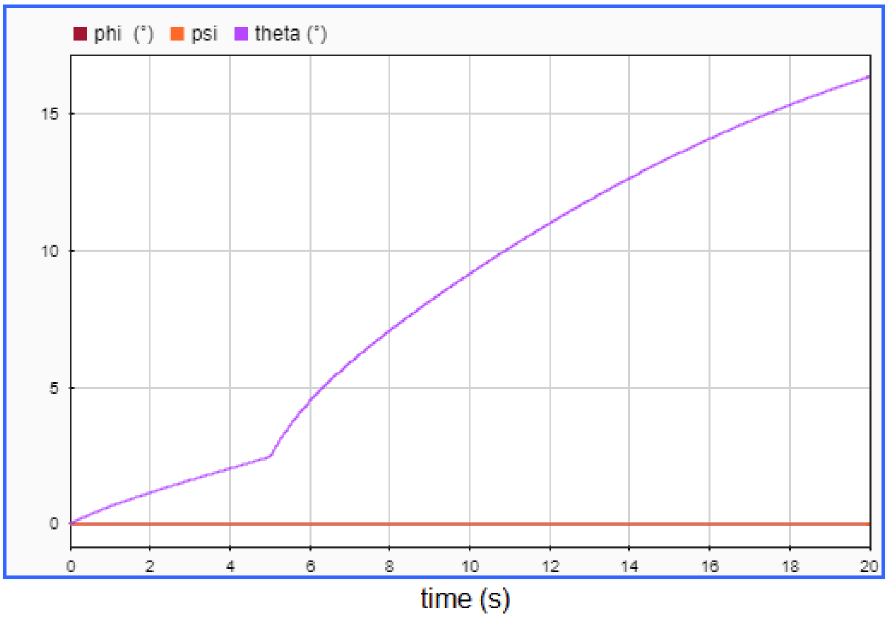

Figure 4.7. Euler angles of the aircraft in simulation 1

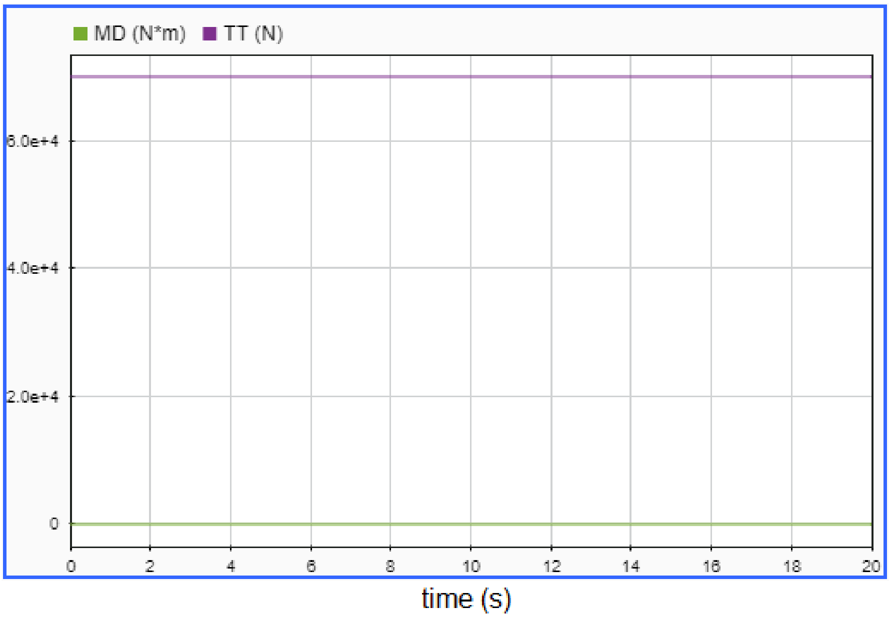

Figure 4.8. Total thrust and moment difference of the aircraft in simulation 1

Simulation 2: Rudder Deflection

The attitude of the model is observed under 10° rudder deflection in the circumstances that elevator and aileron deflections are zero, there is no moment difference and an average total thrust which is 70000 N. As expected, rudder deflection creates positive heading and bank angle [25]. Also, altitude and pitch angle increased because of incidence angle and velocity decreased. In Figures 4.9, 4.10, 4.11, 4.12 and 4.13; system responses can be found.

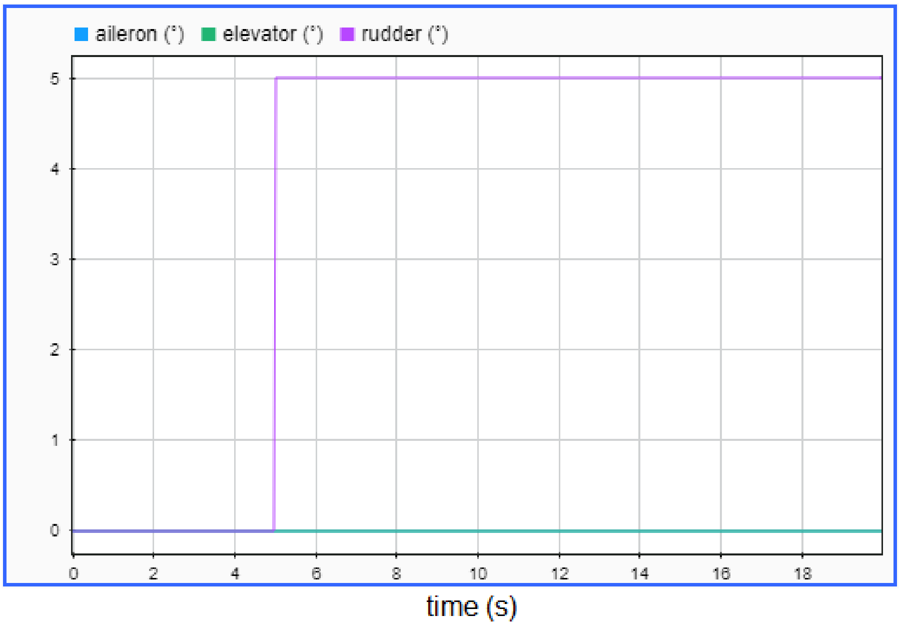

Figure 4.9. Control surfaces of the aircraft in simulation 2

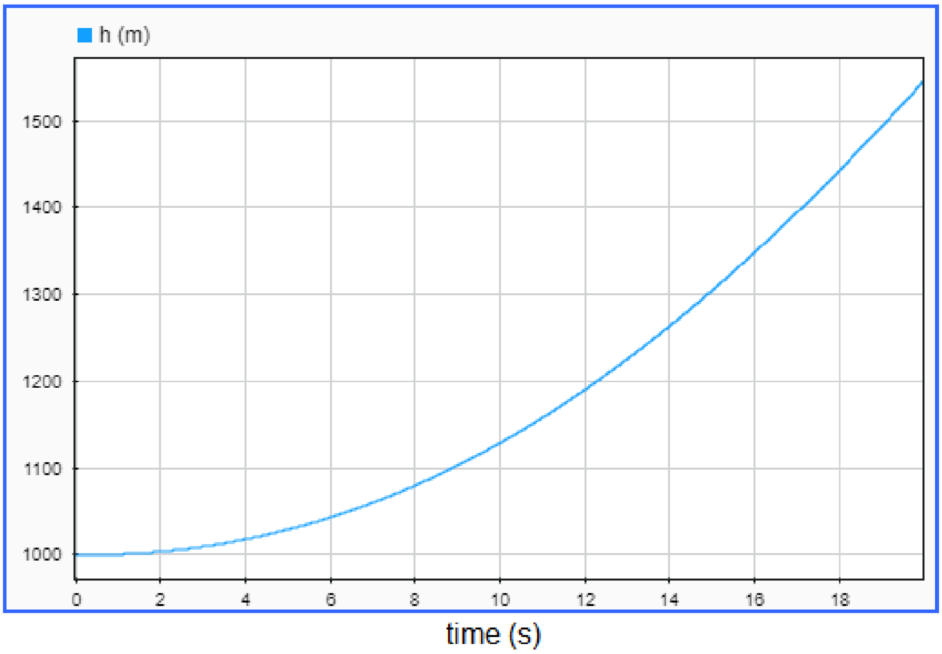

Figure 4.10. Altitude of the aircraft in simulation 2

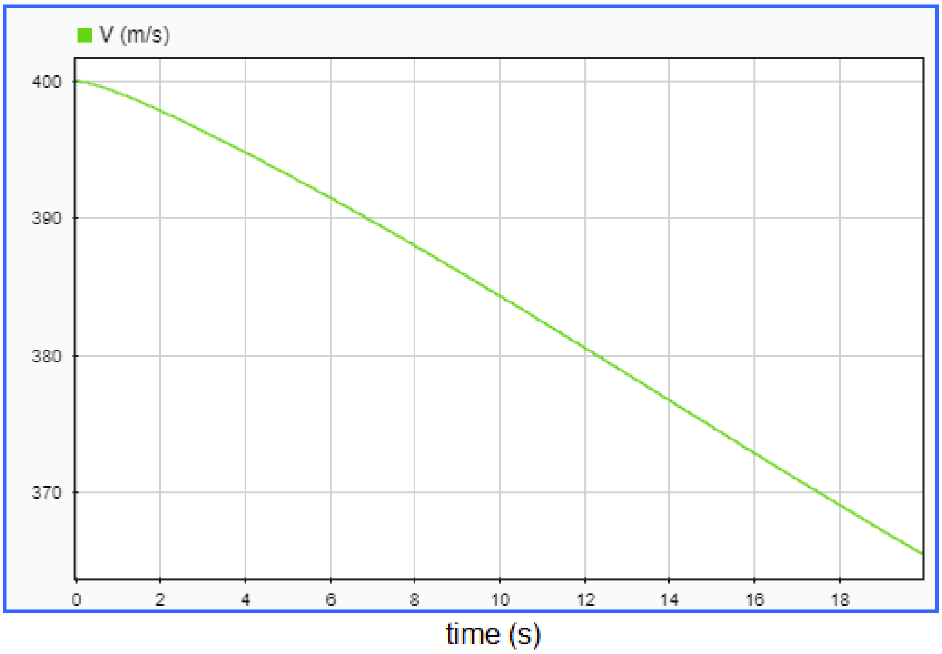

Figure 4.11. Velocity of the aircraft in simulation 2

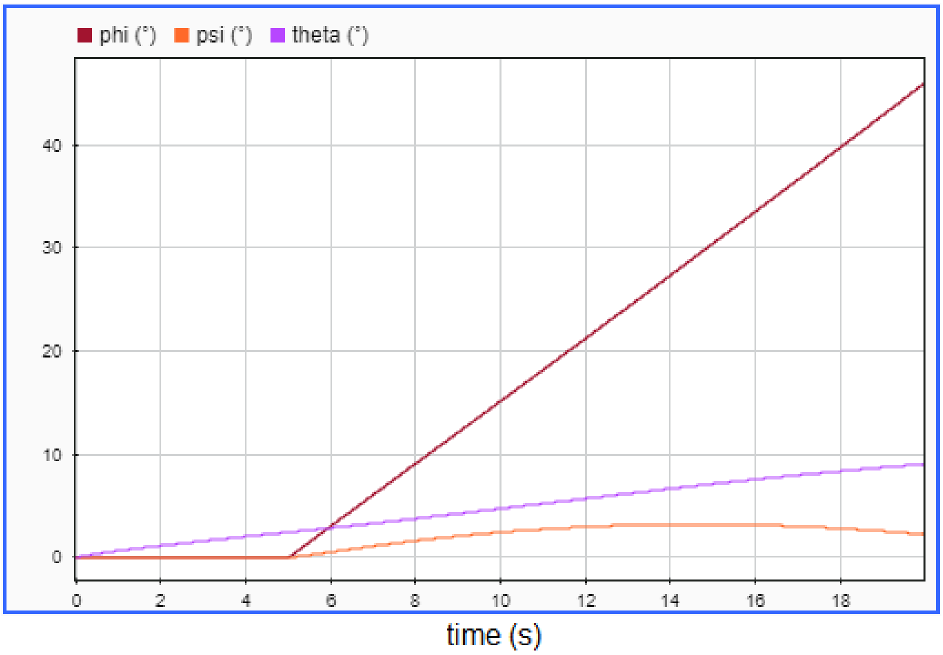

Figure 4.12. Euler angles of the aircraft in simulation 2

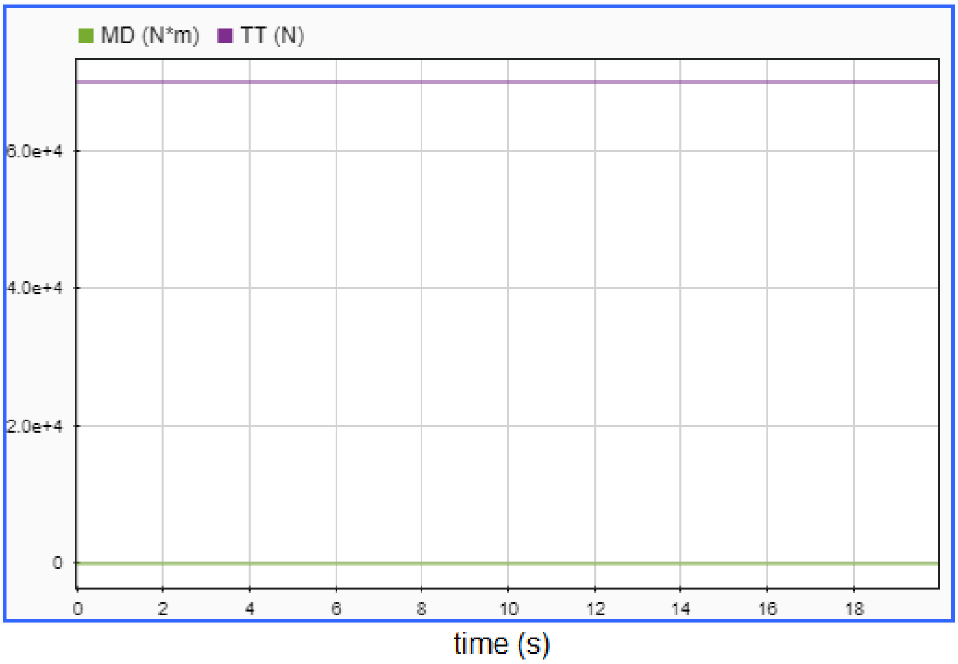

Figure 4.13. Total thrust and moment difference of the aircraft in simulation 2

Simulation 3: Aileron Deflection

The attitude of the model is observed under 10˚ aileron deflection in the circumstances that elevator and rudder deflections are zero, there is no moment difference and an average total thrust which is 70000 N. It is observed that bank angle and heading angle increases with the positive aileron deflection [26]. Altitude and pitch angle increased because of incidence angle and velocity decreased. In Figures 4.14, 4.15, 4.16, 4.17 and 4.18; system responses are shown.

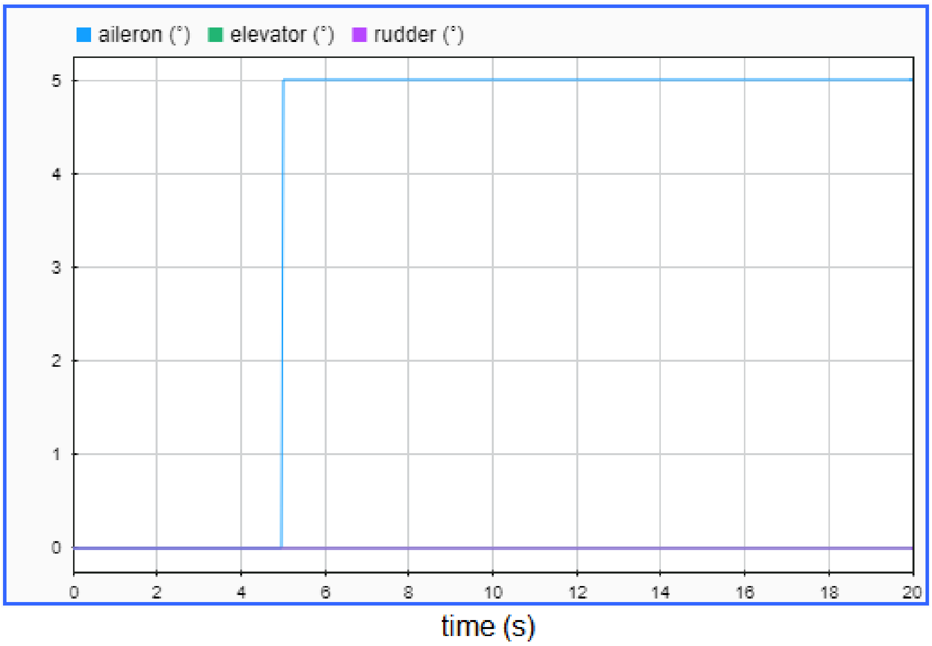

Figure 4.14. Control surfaces of the aircraft in simulation 3

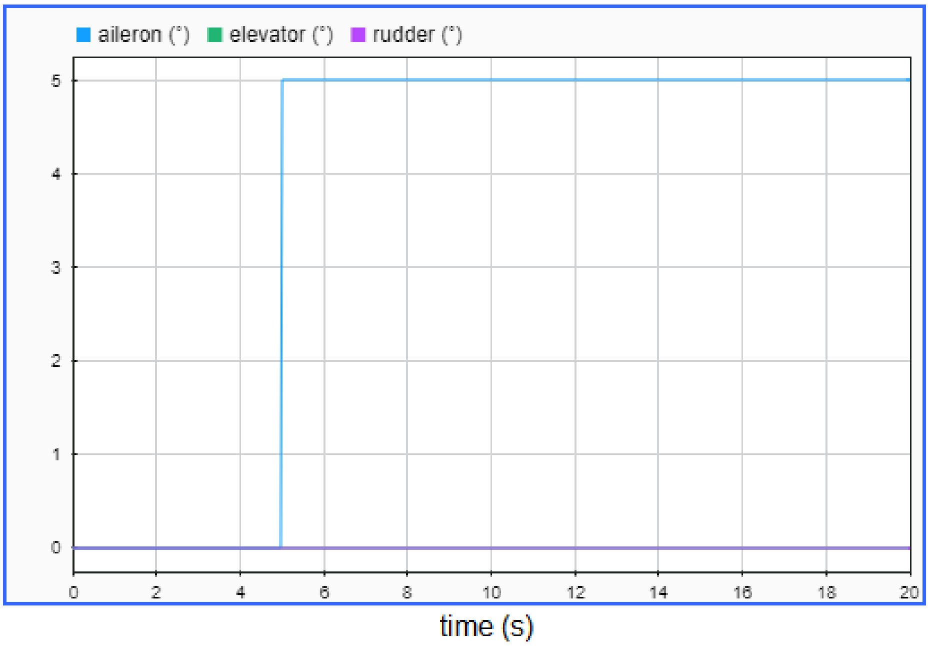

Figure 4.15. Altitude of the aircraft in simulation 3

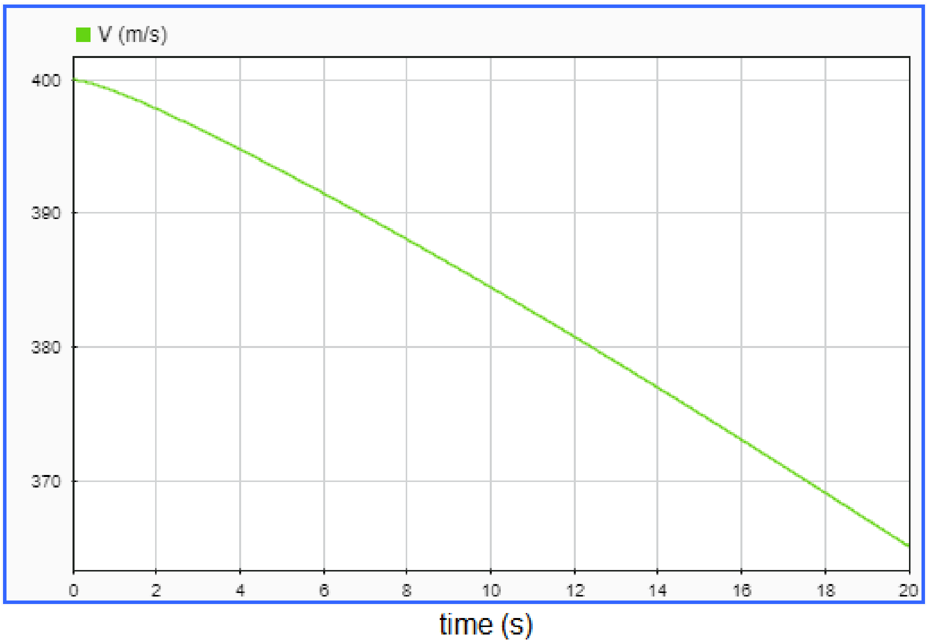

Figure 4.16. Velocity of the aircraft in simulation 3

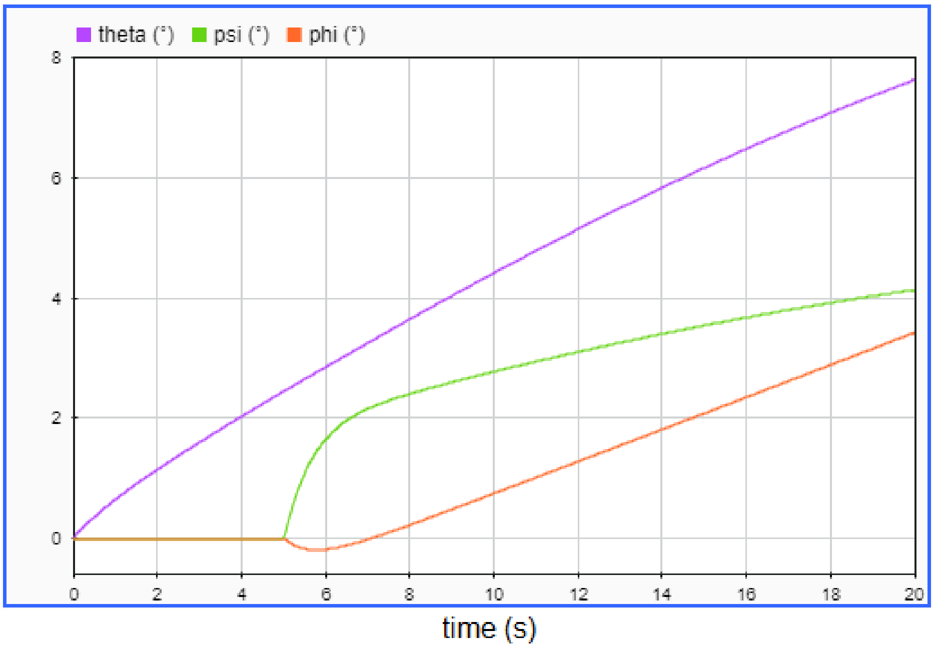

Figure 4.17. Euler angles of the aircraft in simulation 3

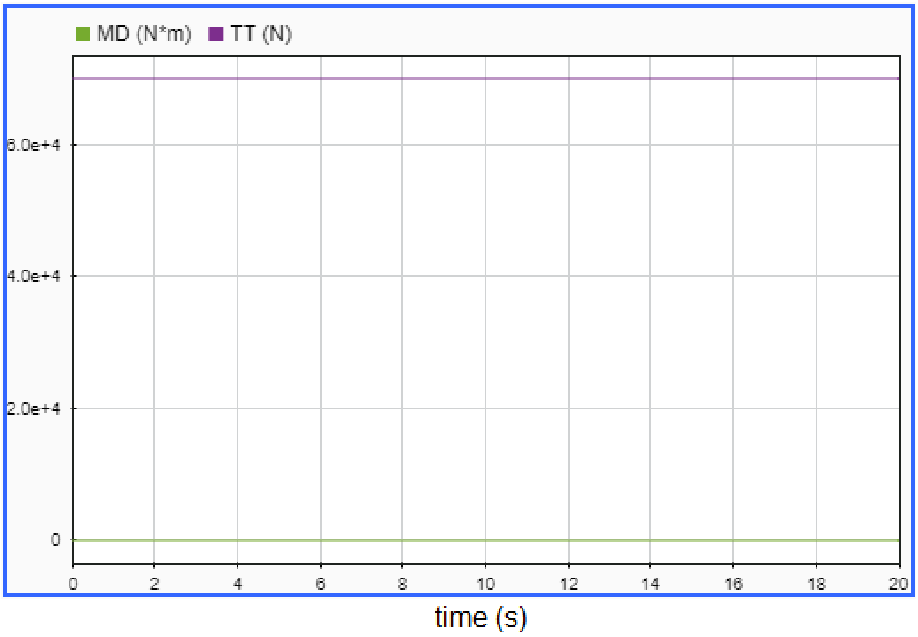

Figure 4.18. Total thrust and moment difference of the aircraft in simulation 3

Simulation 4: Existing of Moment Difference

The attitude of the model is observed under 100 Nm moment difference in the circumstances that elevator, rudder and aileron deflections are zero and an average total thrust which is 70000 N. It is observed that bank angle and heading angle increases with the positive moment difference [27]. Altitude and pitch angle increased because of incidence angle and velocity decreased. In Figures 4.19, 4.20, 4.21, 4.22, 4.23 and 4.24; system responses are illustrated.

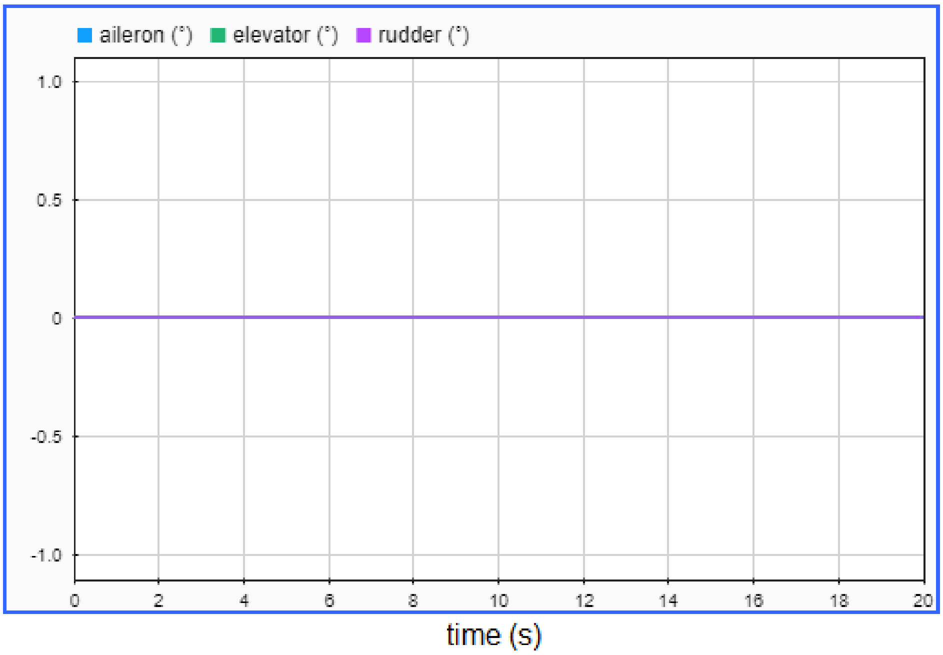

Figure 4.19. Control surfaces of the aircraft in simulation 4

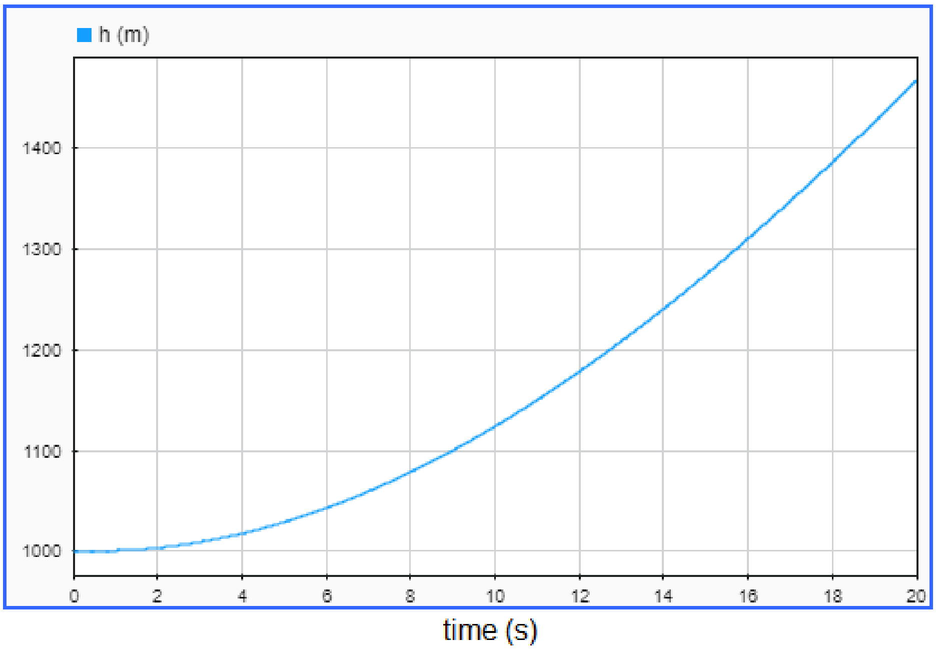

Figure 4.20. Altitude of the aircraft in simulation 4

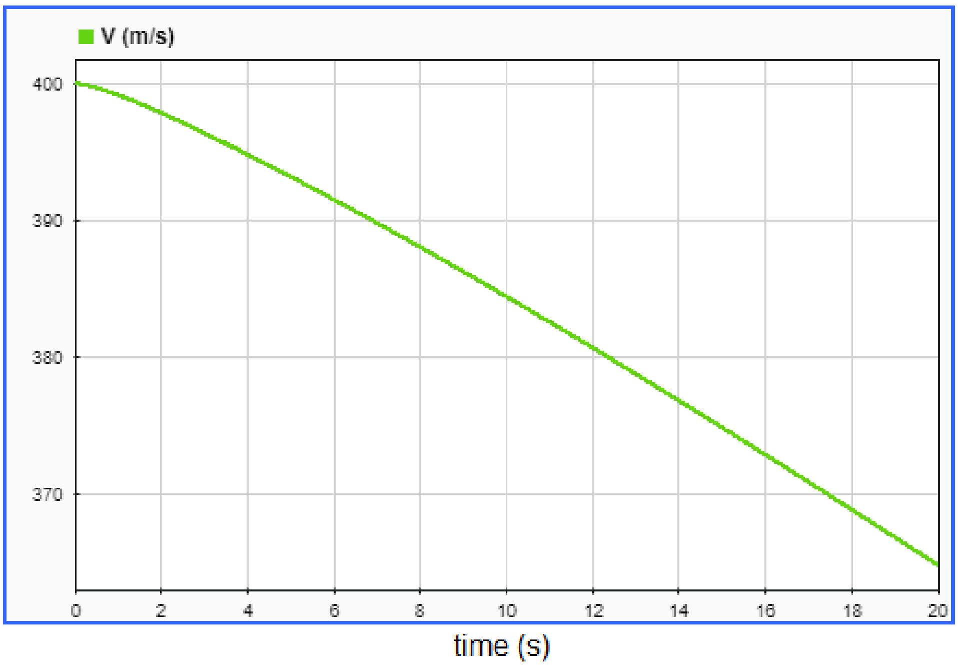

Figure 4.21. Velocity of the aircraft in simulation 4

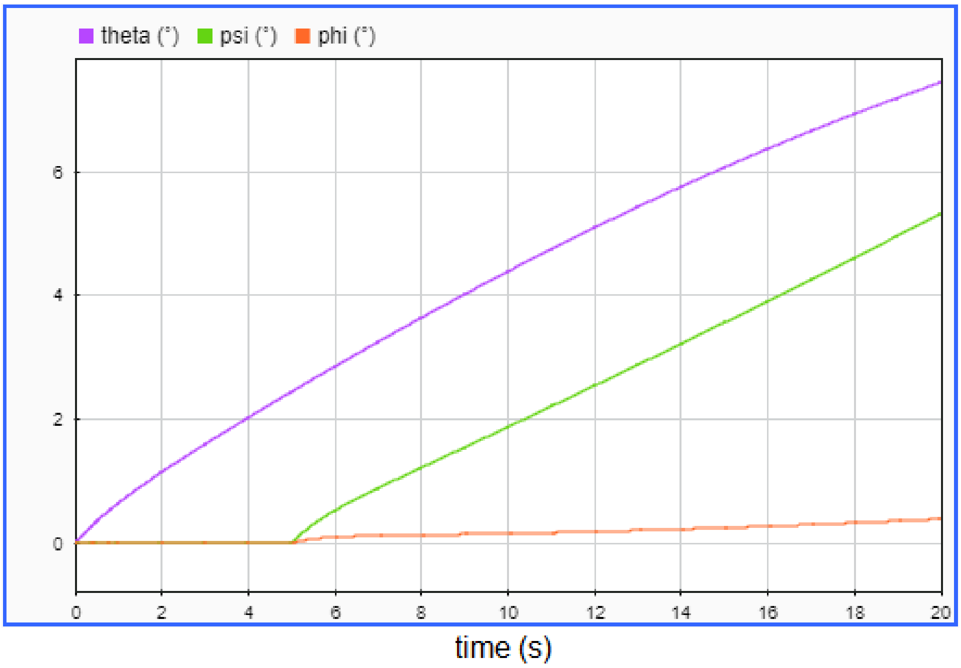

Figure 4.22. Euler angles of the aircraft in simulation 4

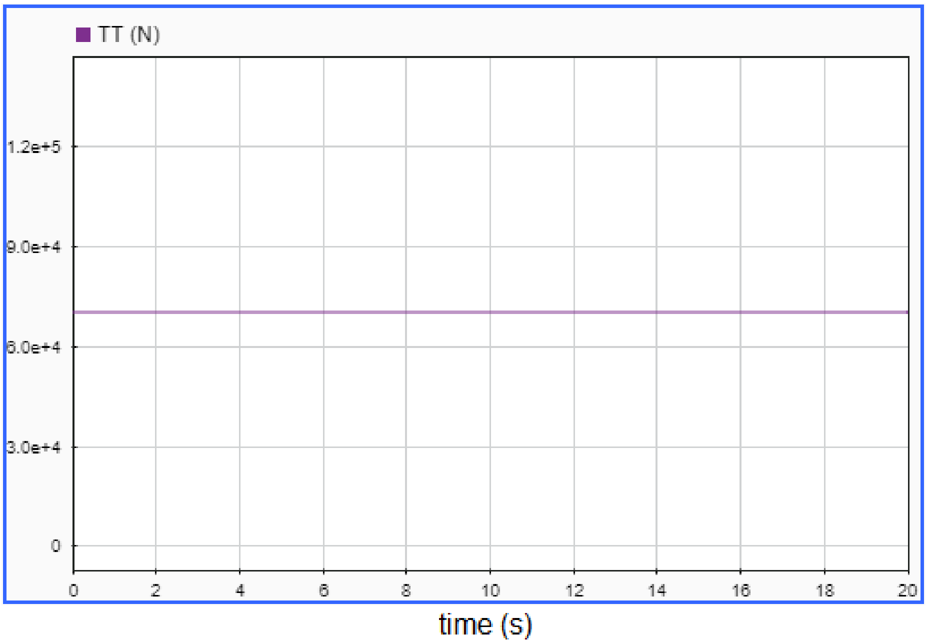

Figure 4.23. Total thrust of the aircraft in simulation 4

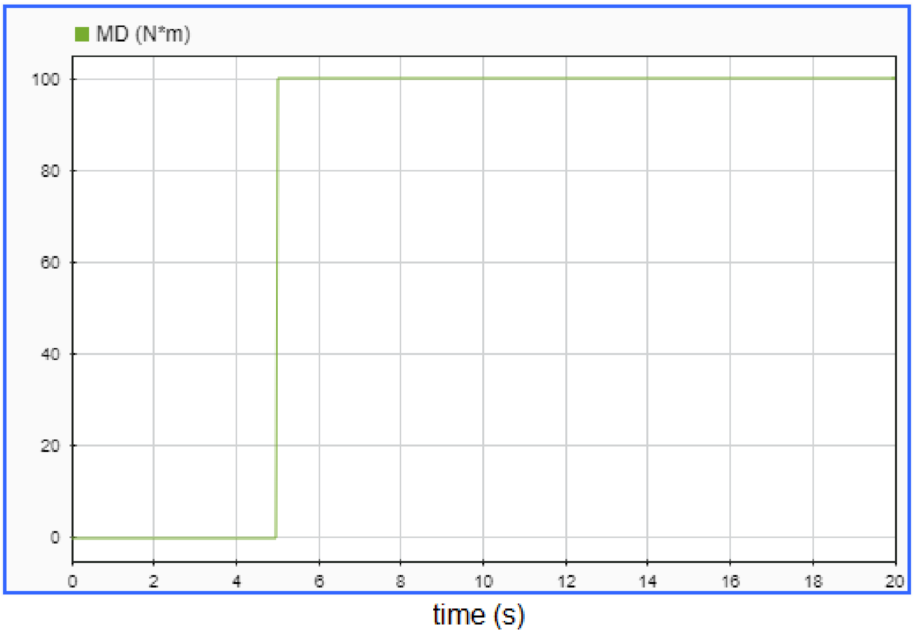

Figure 4.24. Moment difference of the aircraft in simulation 4

Simulation 5: Increase of Total Thrust

The attitude of the model is observed under 200000 N total thrust in the circumstances that elevator, rudder and aileron deflections are zero and there is no moment difference. It is observed that velocity increases, altitude and pitch angle increased with higher slope and bank angle and heading angle stayed constant at zero. In Figures 4.25, 4.26, 4.27, 4.28, 4.29 and 4.30; system responses can be found.

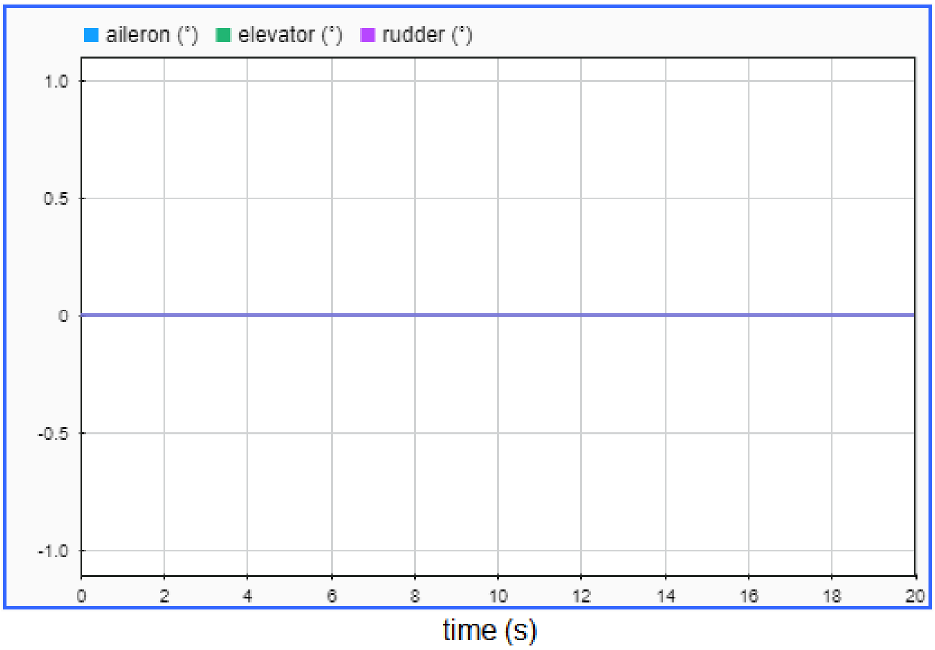

Figure 4.25. Control surfaces of the aircraft in simulation 5

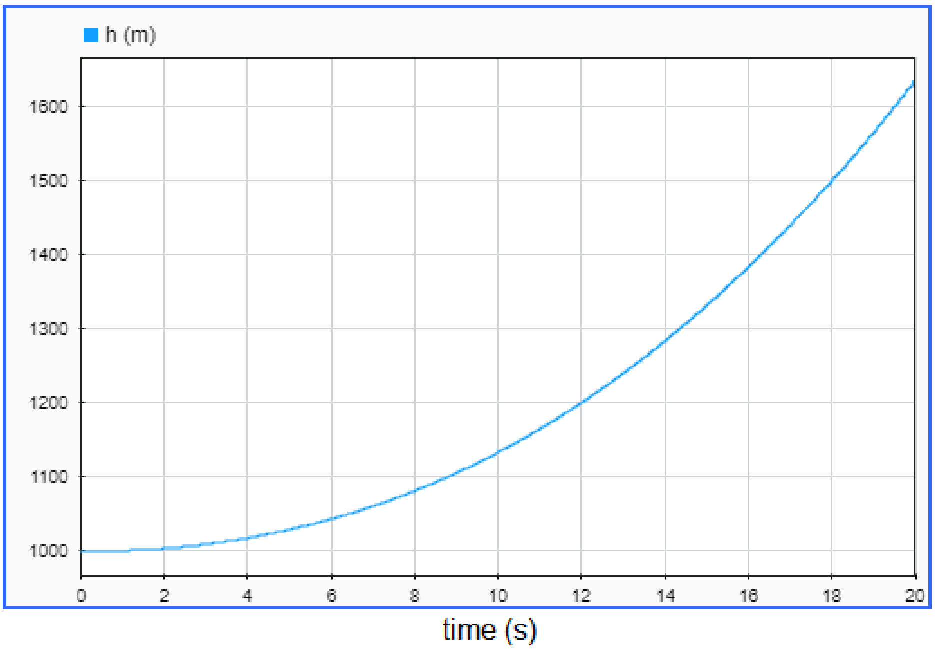

Figure 4.26. Altitude of the aircraft in simulation 5

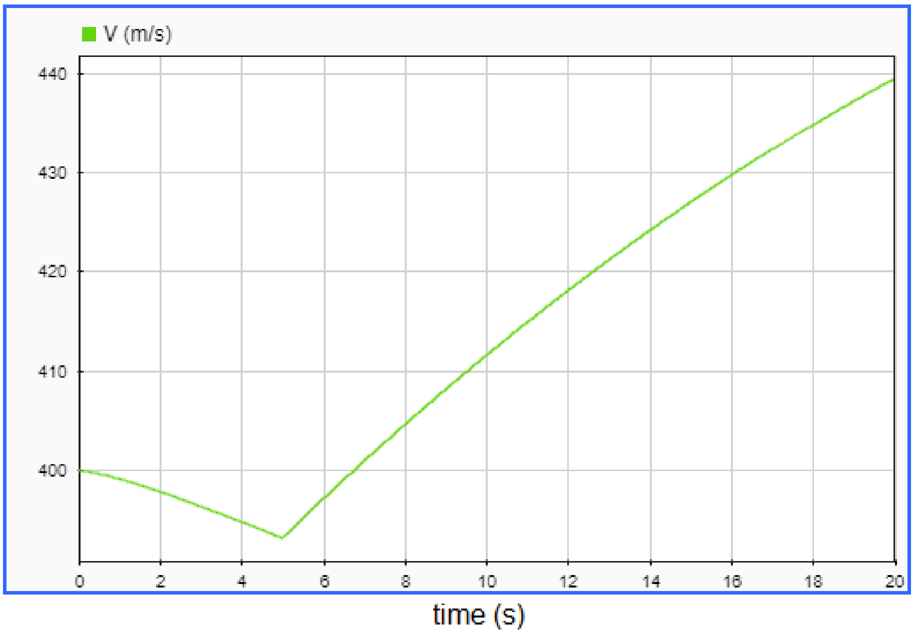

Figure 4.27. Velocity of the aircraft in simulation 5

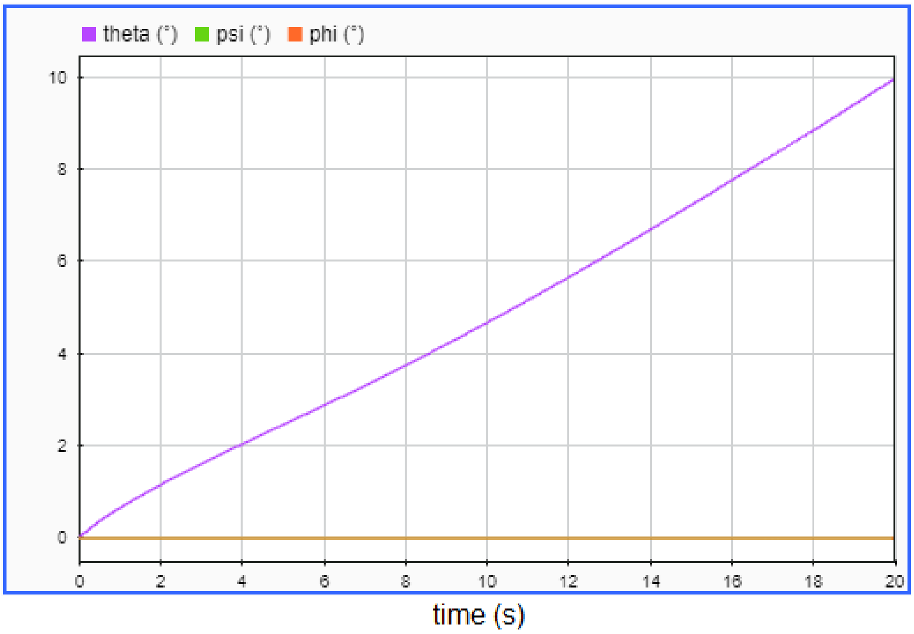

Figure 4.28. Euler angles of the aircraft in simulation 5

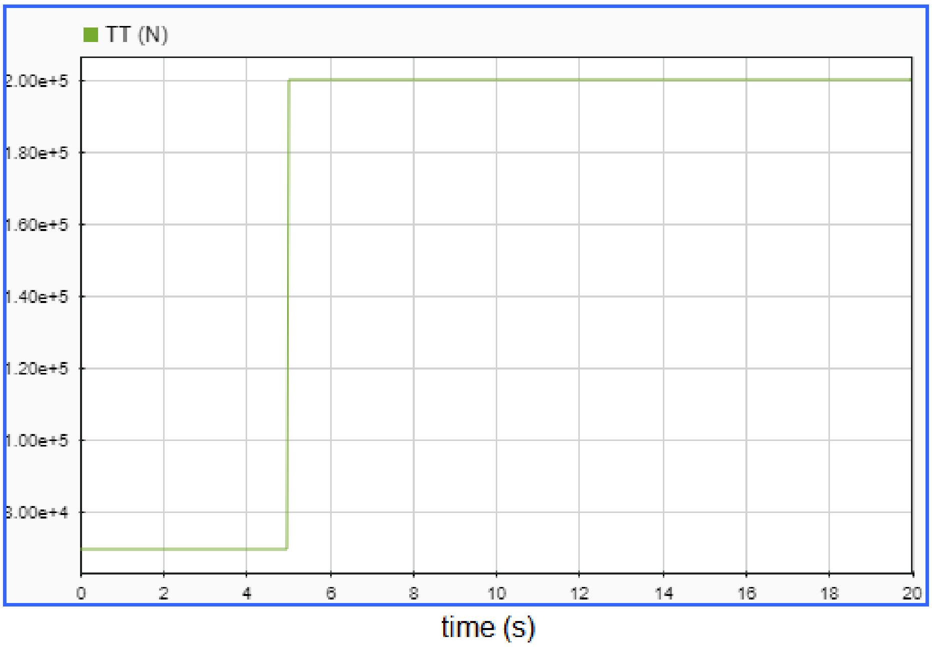

Figure 4.29. Total thrust of the aircraft in simulation 5

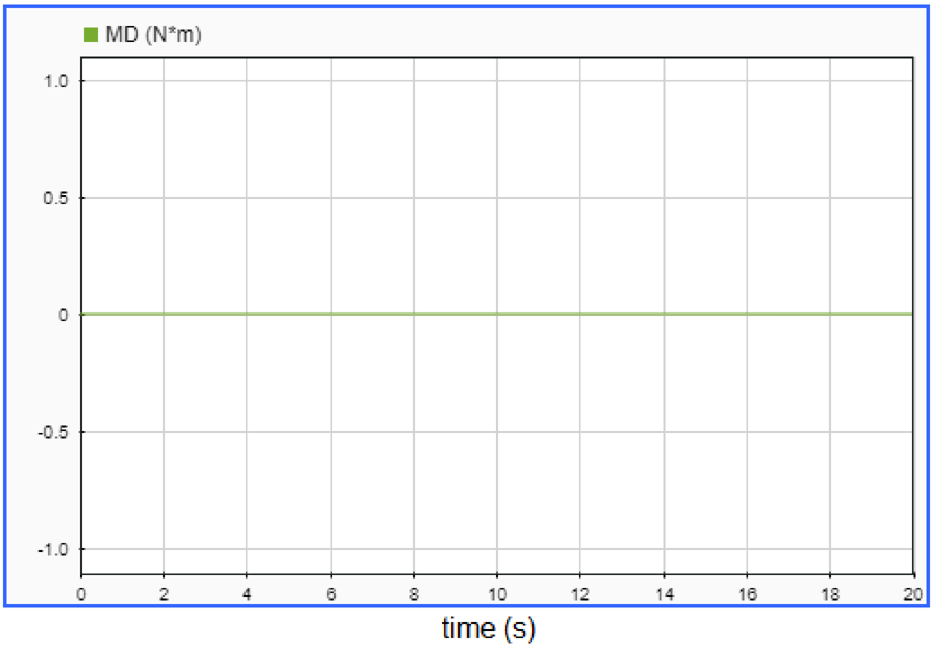

Figure 4.30. Moment difference of the aircraft in simulation 5

CHAPTER 5

AUTOPILOT DESIGN OF THE JET PLANE

In design applications, in order to stabilize a system, reduce interruptions, be less fragile to parameter variations, track reference more accurately, contribute stability to uncertanties; closed-loop control systems are used [28]. Modern techniques are complicated and hard to implement in real world, the conventional PID method and the combination of two or more PID controllers are still most preferable controllers. Besides, the fact that the design of PID controllers is cost-effective and simple with satisfactory high performance makes them the most attractive and the most frequently used method [29]. Hence, cascade control system structure based on PID control is proposed due to the these advanteges in autopilot design part of this work.

In a cascade control system; there are two loops; primary loop or the outer loop and secondary loop or the inner loop. The controller in the secondary loop is called as the secondary controller or slave controller while the controller in the primary loop is defined as the primary controller or the master controller [28]. The control signal of the primary controller is the input of the secondary controller or the set point of it. In tuning process, design constraints are listed below:

- Rise time: The rise time refers to the time required for the response of the system to reach from a low value to a high value. Typically, these values are 10% and 90% of the steady-state value respectively.
- Settling Time: The settling time refers to the time taken for the response to reach and remains in a specified error band. The tolerable error band is usually (2-5) % of the steady-state value.
- Peak overshoot: The peak overshoot refers to the ratio of first peak value measured from steady-state value to the steady-state value [28].

5.1 Autopilot Designs in Longitudinal Axis

5.1.1 Altitude Control

In altitude autopilot, the pitch angle of the jet plane is used as input for inner loop controller and altitude of the aircraft is used for outer loop controller. The control surface in longitudinal axis of the aircraft, i.e., elevator is controlled with the output of this structure. Elevator deflection is limited to -40˚ to +40˚ with a nonlinear second order actuator to build the relationship between the desired deflection angle and the realized deflection angle.

PI controller is chosen for the inner loop controller, and PD controller is chosen for the outer loop controller. In this design, cascade control is appropriate because secondary loop has a faster dynamic response and the rejection of the disturbance in the secondary output reduces the steady state output error in the primary loop [30]. For both controller; design constraints and parameters, i.e., rise time, settling time and overshoot ratio are given in Table 5.1.

Table 5.1 Design Parameters for Altitude Autopilot

Design Constraints / Parameters	Rise Time (s)	Settling Time (s)	Overshoot (%)
Inner Loop	0.5 / 0.0899	3 / 0.728	30 / 8.43
Outer Loop	2 / 0.62	6 / 1.59	5 / 1.52

In Figures 5.1, 5.2 and 5.3; the step response of inner loop, controller effort of inner loop and the step response of outer loop are given. In tuning, controller effort is taken consideration as well as design constraints.

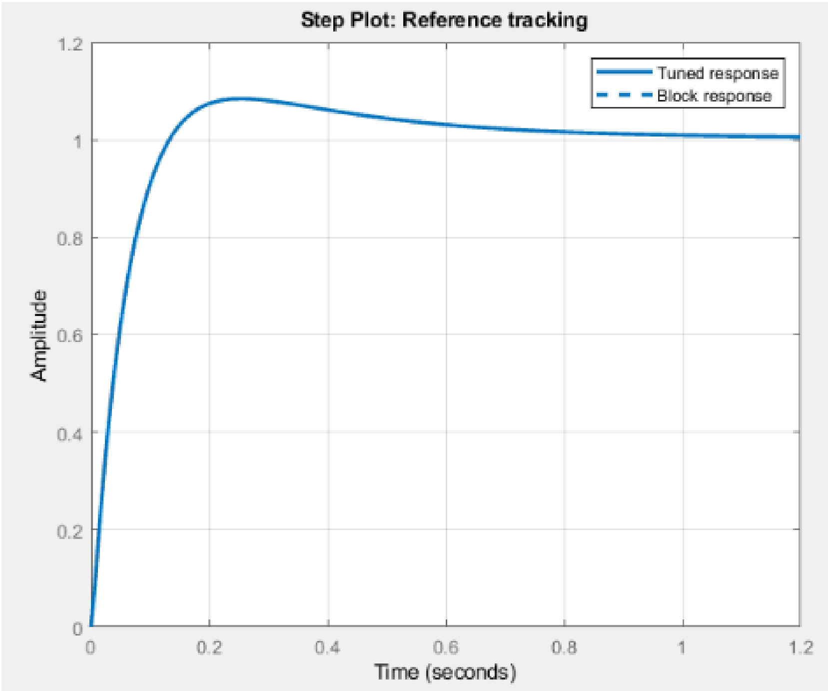

Figure 5.1. Step response of pitch angle

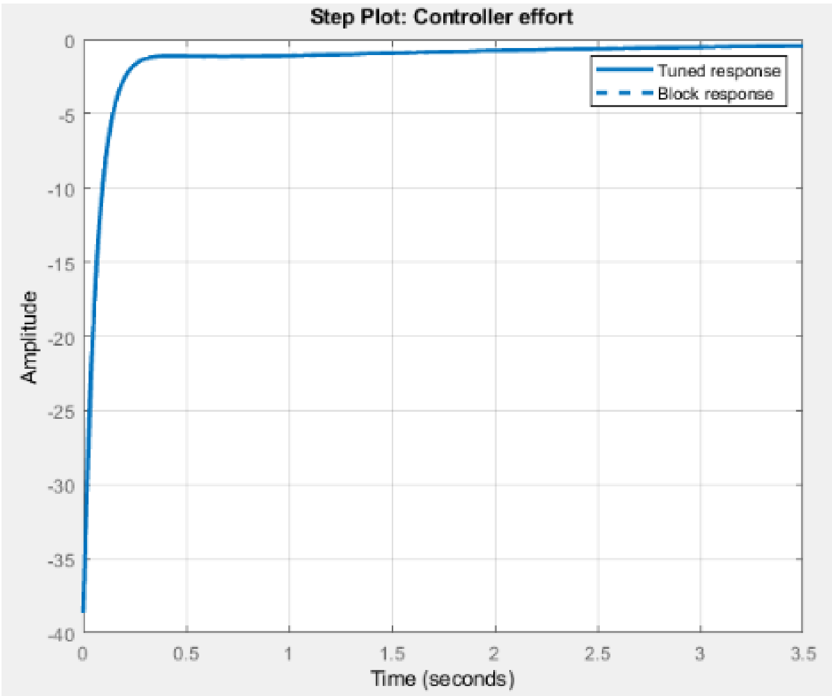

Figure 5.2. Controller effort for elevator

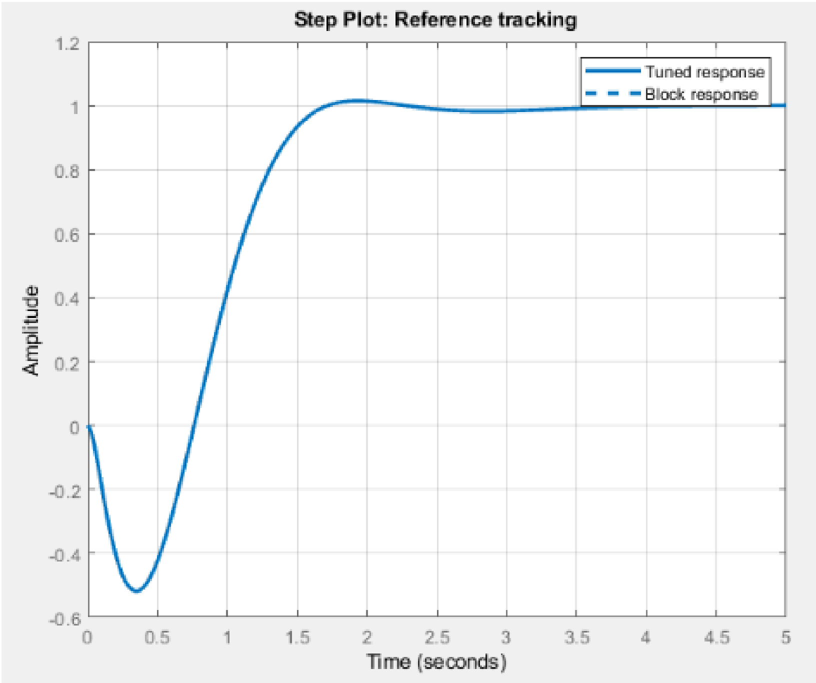

Figure 5.3. Step response of altitude

Resultant structure of the altitude autopilot is shown below.

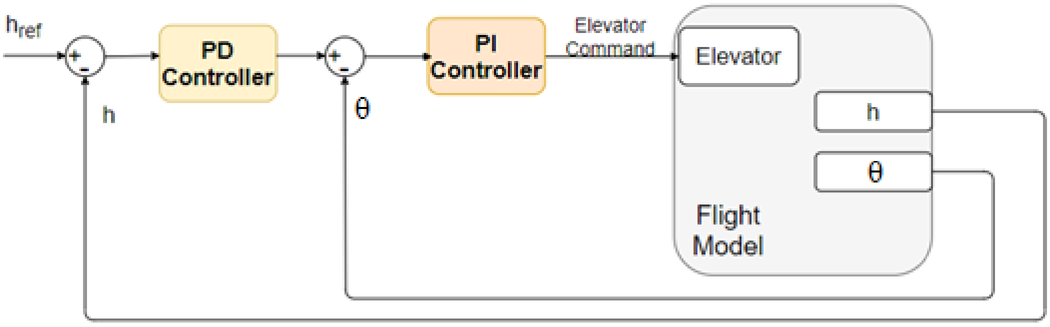

Figure 5.4. Altitude autopilot structure

5.1.2 Velocity Control

In velocity autopilot, the scalar value of the velocity of the aircraft is used as input of the PI controller. Total thrust that produced with two turbojet engines is controlled with the output of this structure [31]. Total thrust is limited to 200 N to 500000 N according to the designed turbojet engine's performances [32]. The design constraints and parameters, i.e., rise time, settling time and overshoot ratio of this controller are given in Table 5.2.

Table 5.2 Design Parameters for Velocity Autopilot

Design Constraints / Parameters	Rise Time (s)	Settling Time (s)	Overshoot (%)
	2 / 0.222	6 / 1.71	5 / 2.46

In Figures 5.5 and 5.6, step response of the controller and its controller effort are given.

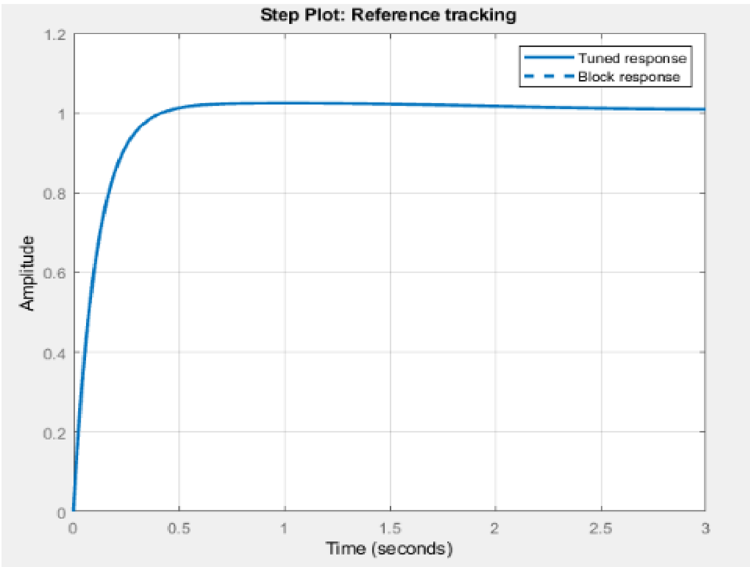

Figure 5.5. Step response of velocity

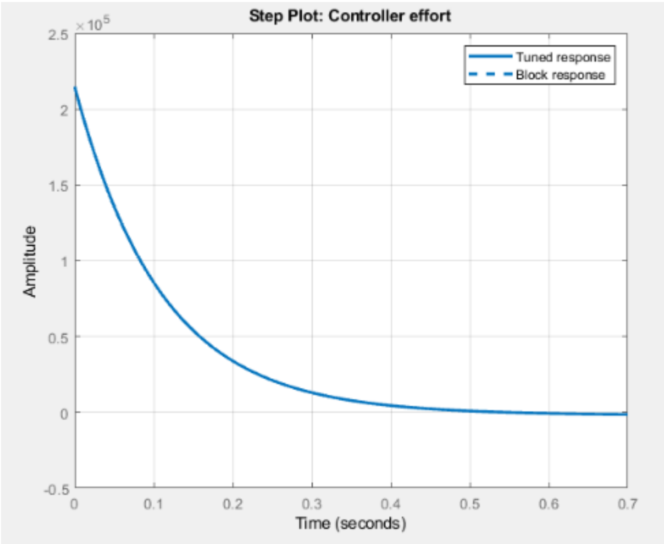

Figure 5.6. Controller effort for total thrust

Resultant structure of the velocity autopilot is shown in Figure 5.7.

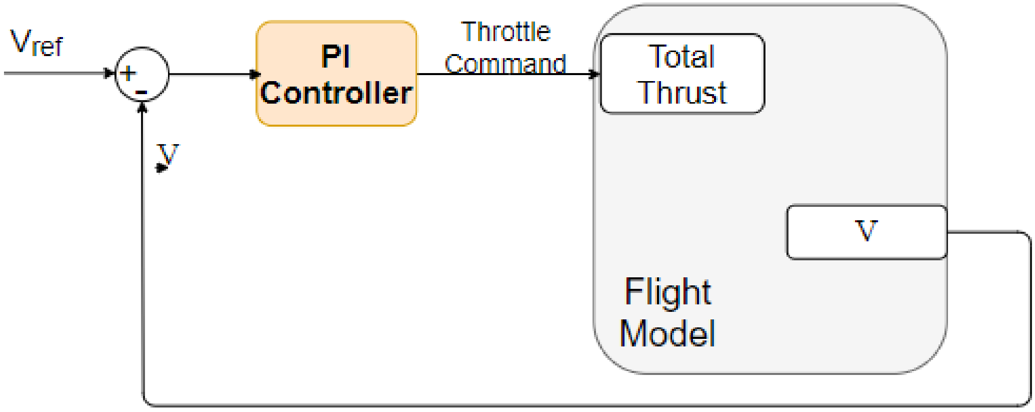

Figure 5.7. Velocity autopilot structure

5.2 Autopilot Designs in Lateral Axis

5.2.1 Agile Heading Angle Maneuver Control

In agile heading angle maneuver control autopilot, the yaw rate of the jet plane is used as input for inner loop controller and yaw angle is used for outer loop controller [32]. The moment difference that produced with two turbojet engines is controlled with the output of this structure. Moment difference is limited to – 5000 kNm to 5000 kNm according to the designed turbojet engine's performances [33]. PI controller is chosen for the in inner loop controller and P controller is chosen for outer loop controller [34]. For both controller; design constraints and parameters, i.e., rise time, settling time and overshoot ratio are given in Table 5.3.

Table 5.3 Design Parameters for Agile Heading Angle Maneuver Autopilot

Design Constraints / Parameters	Rise Time (s)	Settling Time (s)	Overshoot (%)
Inner Loop	0.5 / 0.0586	3 / 0.981	30 / 4.17
Outer Loop	2 / 0.0516	6 / 0.217	5 / 1.04

In Figures 5.8, 5.9 and 5.10, the step response of inner loop, controller effort of inner loop and the step response of outer loop are given, respectively. In tuning, controller effort is taken into consideration in addition to the design constraints [35].

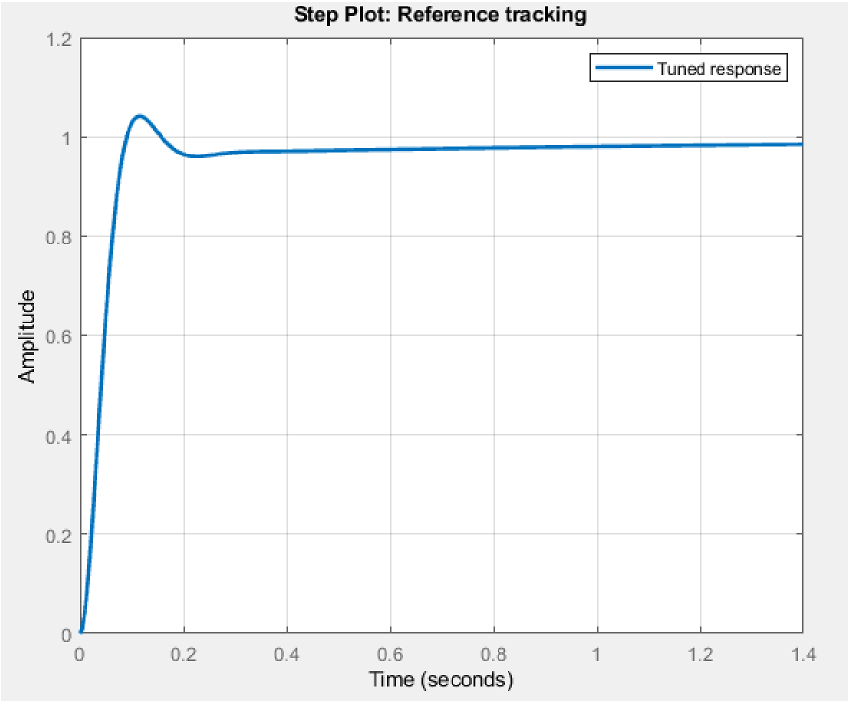

Figure 5.8. Step response of yaw rate

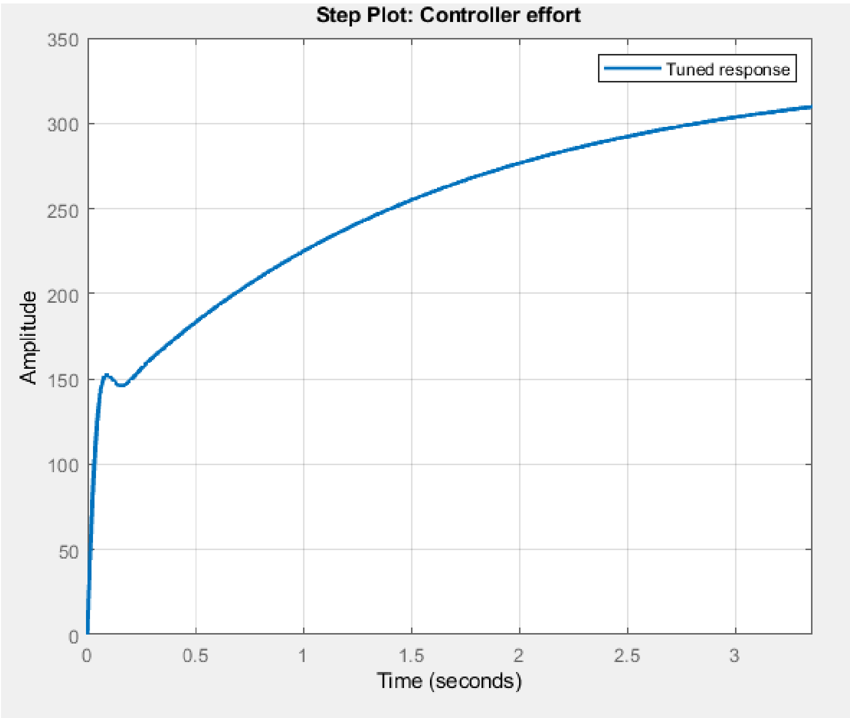

Figure 5.9. Controller effort for moment difference

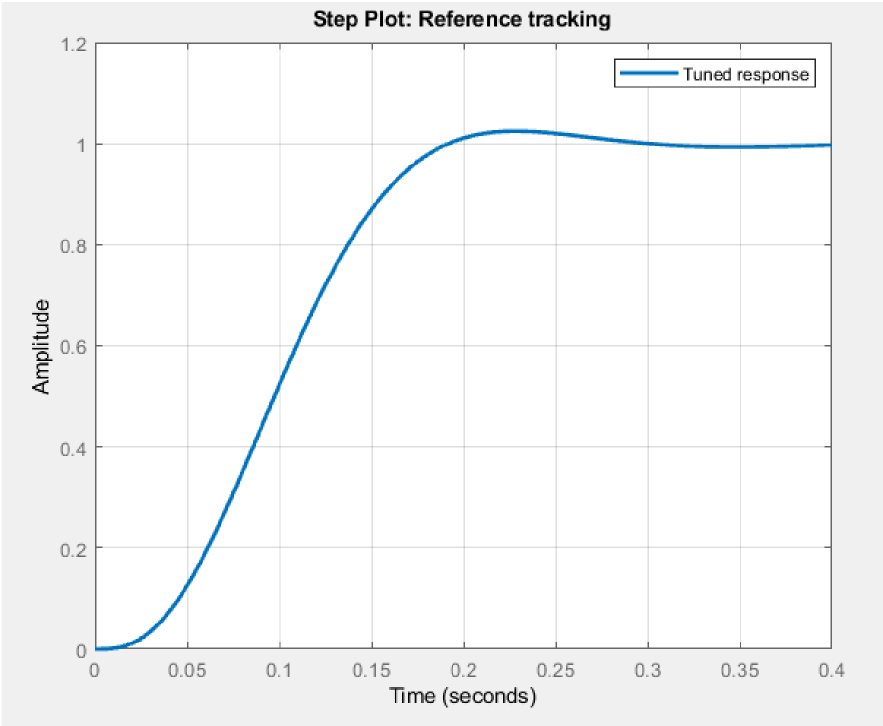

Figure 5.10. Step response of yaw angle

Resultant structure of the agile yaw angle maneuver autopilot is shown below.

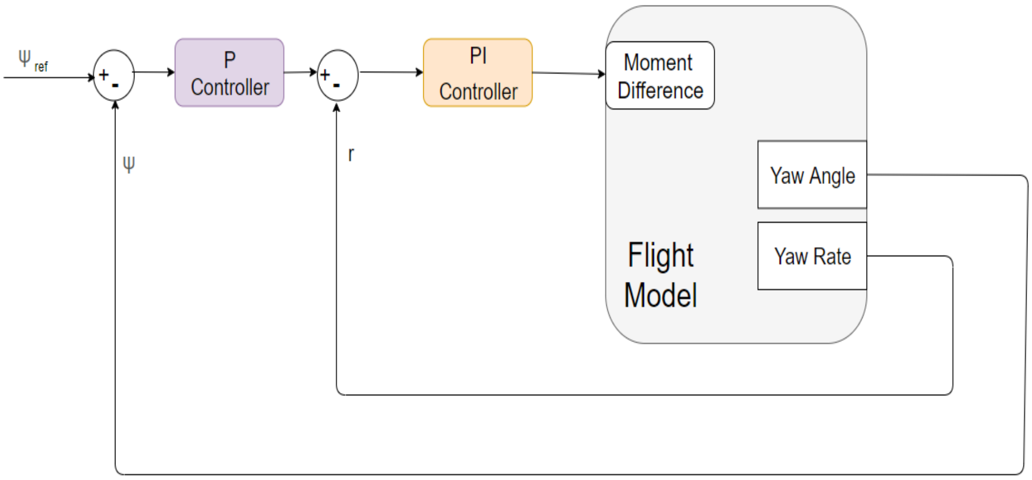

Figure 5.11. Agile heading angle maneuver autopilot structure

5.2.2 Heading and Bank Angles Control

In heading angle autopilot, the yaw angle of the aircraft is used as input of the PID controller [36]. The control surface in lateral axis of the aircraft, i.e., rudder is controlled with the output of this structure. Rudder movement is limited to -40˚ to +40˚ with a nonlinear second order actuator to build the relationship between the desired deflection angle and the realized deflection angle [37]. The design constraints and parameters, i.e., rise time, settling time and overshoot ratio of this controller are given in Table 5.4.

Table 5.4 Design Parameters for Heading Angle Autopilot

Design Constraints / Parameters	Rise Time (s)	Settling Time (s)	Overshoot (%)
	2 / 0.405	6 / 0.612	5 / 1.55

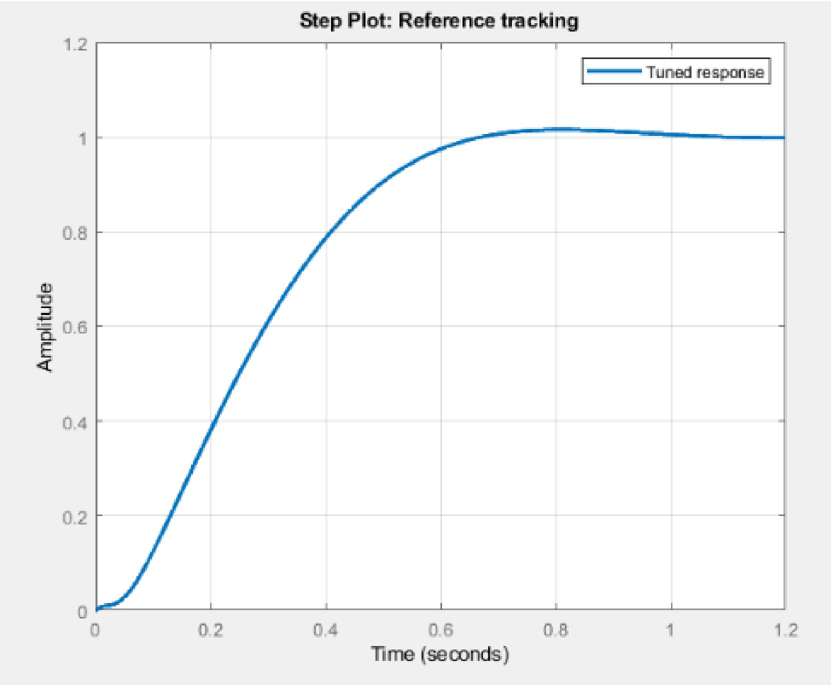

Figure 5.12. Step response of heading angle

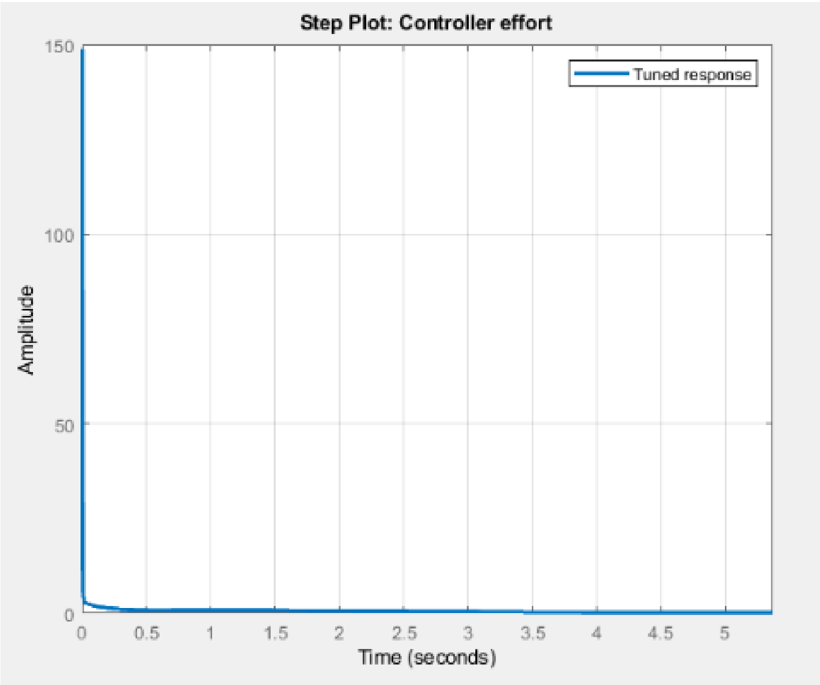

Figure 5.13. Controller effort for rudder

Resultant structure of the heading angle autopilot is shown.

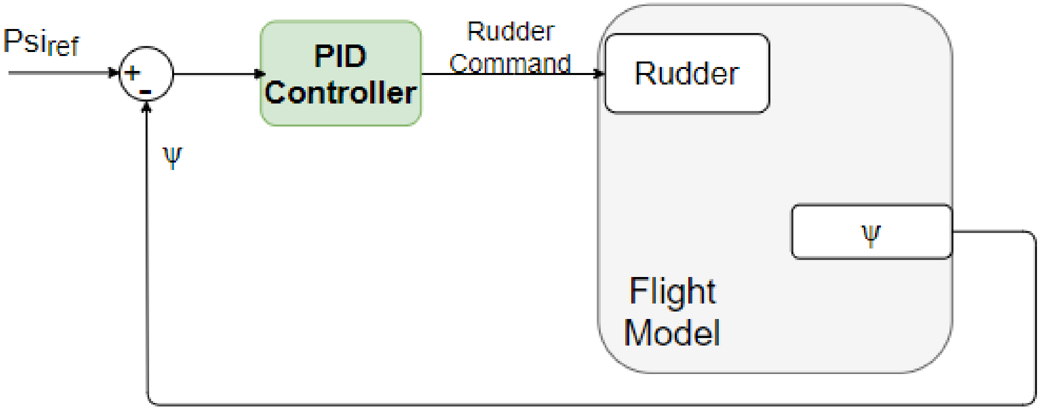

Figure 5.14. Heading angle autopilot structure

In bank angle autopilot, the roll angle of the aircraft is used as input of the PID controller [38]. The second control surface of lateral axis of the aircraft, i.e., aileron is controlled with the output of this structure. Aileron movement is limited to -40˚ to +40˚ with a nonlinear second order actuator to build the relationship between the desired deflection angle and the realized deflection angle [39]. The design parameters, i.e., rise time, settling time and overshoot ratio of this controller are given in Table 5.5.

Table 5.5 Design Parameters for Bank Angle Autopilot

Design Constraints / Parameters	Rise Time (s)	Settling Time (s)	Overshoot (%)
	2 / 0.0771	6 / 1.77	5 / 12.9

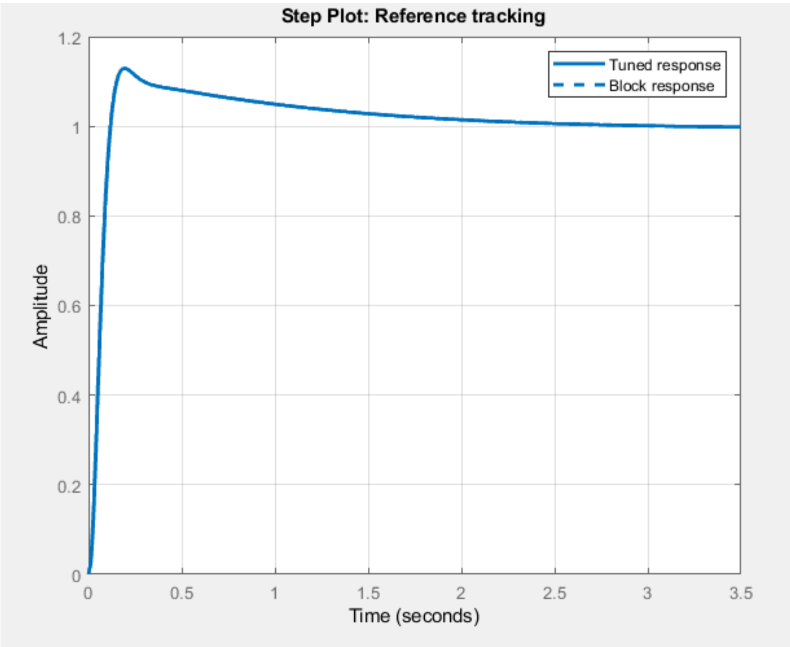

Figure 5.15. Step response of bank angle

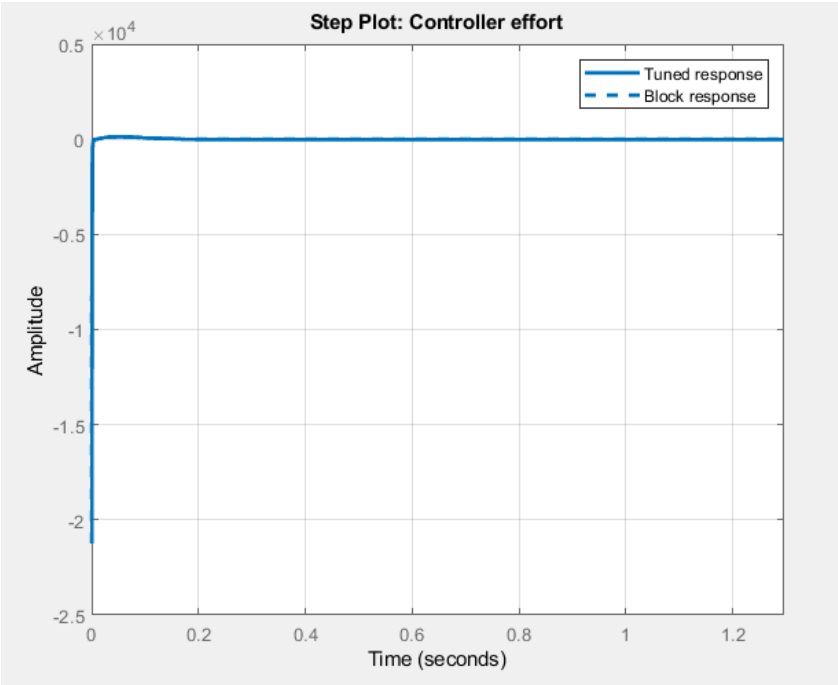

Figure 5.16. Controller effort for aileron

Resultant structure of the bank angle autopilot is shown in Figure 5.17.

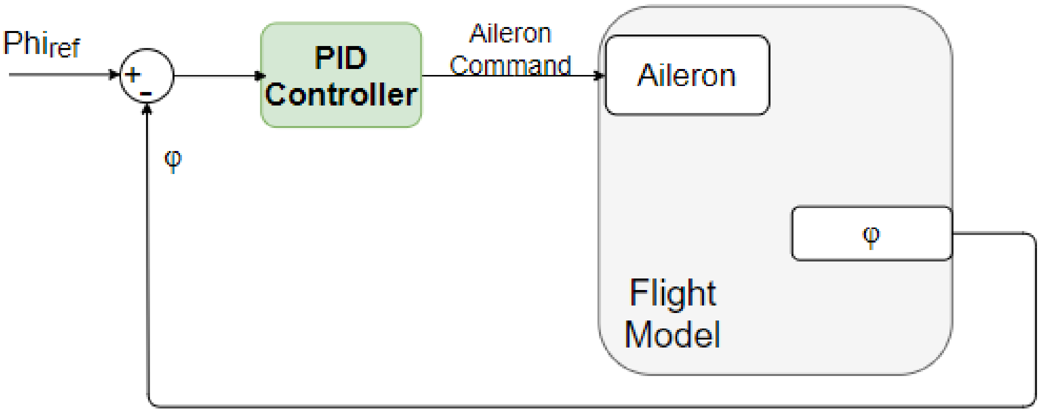

Figure 5.17. Bank angle autopilot structure

CHAPTER 6

GUIDANCE AND SIMULATION RESULTS

Guidance specifies to the defening of the desired path of movement from the aircraft's current location to a certain the target, as well as required changes in velocity, attitude and acceleration for desired path [40].

6.1 Guidance

Flight path contains an initial position, waypoints, final position and velocity [41]. Guidance part of the system calculates the required time to reach the final position with the given velocity [42]. According to the resultant yaw angle, this system decides whether to use agile heading angle maneuver autopilot system. Also, when the desired yaw angle is between -10˚ to -4˚ or 4˚ to 10˚, guidance system arranges the use of all lateral autopilots together. The outputs of guidance contain the path of x, y and z axes and the path of velocity. Block diagram of the guidance system is shown below.

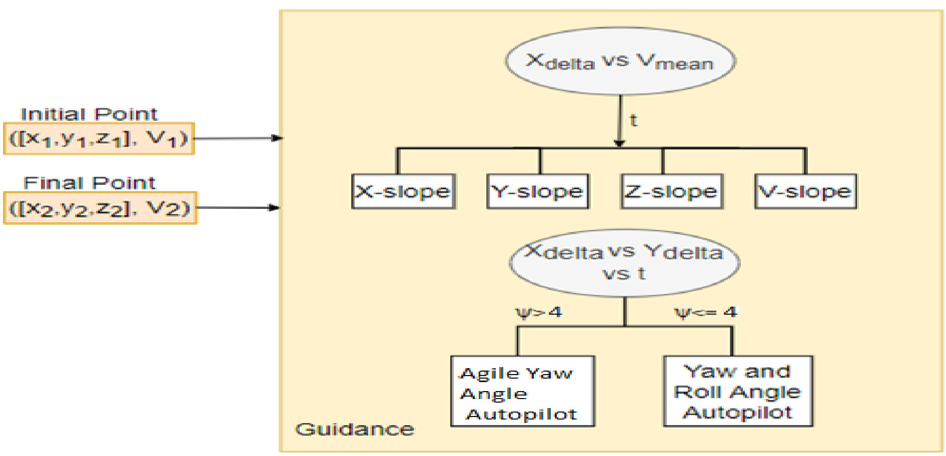

Figure 6.1. Block diagram of guidance system

6.2 Flight Management System

The outputs of guidance are the inputs of the flight management system [43]. This system creates the reference values for each autopilot's inputs. With the calculated slopes for position vectors that come from guidance system, flight management system creates ramp signals. Initial and final values for this referance signals are determined with given waypoints. Flight management system changes the attitude of the reference signals with the approach of waypoint approximation logic . According to the paths of inputs, agile heading angle autopilot is used in simulations when desired yaw angle is larger than +/- 4˚. For lower yaw angles, this autopilot is not used and rudder and aileron controls are used to reach the final position. This is achieved by coordinated turn algorithm, which means heading angle and bank angle are controlled together with the certain correlation.

Block diagram of the flight management system is given below.

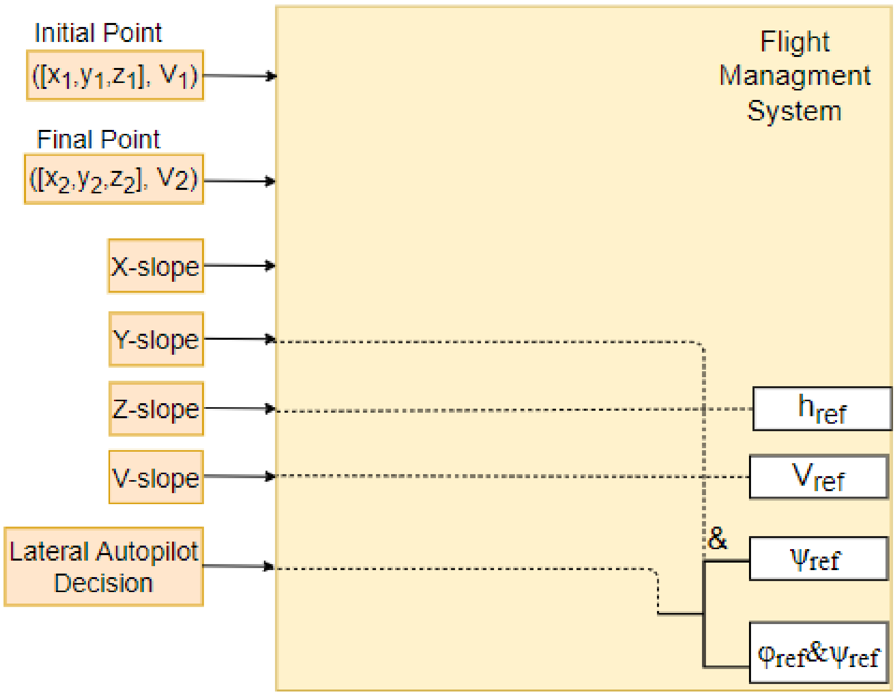

Figure 6.2. Block diagram of the flight management system

6.3 Simulation Results

In simulations, five different cases are conducted to show the autopilot designs follow the commands correctly. The paths are defined with five waypoints.

6.3.1 Case 1: Basic Flight Scenario

In this simulation, only climb, level flight and descent are covered. The waypoints are:

WP1: [0, 0, 1000, 400],

WP2: [4000, 0, 1000, 400],

WP3: [45000, 0, 2000, 400],

WP4: [50000, 0, 2000, 400],

WP5: [80000, 0, 1800, 400].

In this scenario, velocity and Y positions are constant and altitude change of the aircraft are observed. The waypoint tracking illustration is given in Figure 6.3.

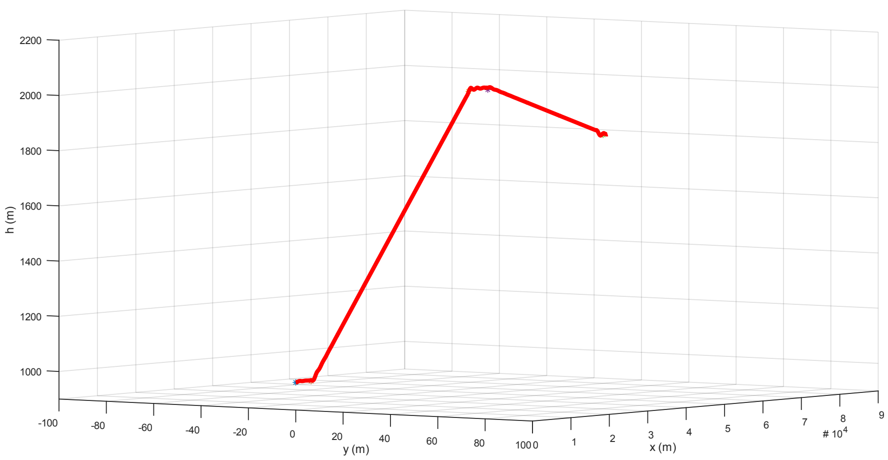

Figure 6.3. Waypoint tracking in case 1

The related results of the attitude of the aircraft are shown in Figures 6.4, 6.5, 6.6, 6.7 and 6.8.

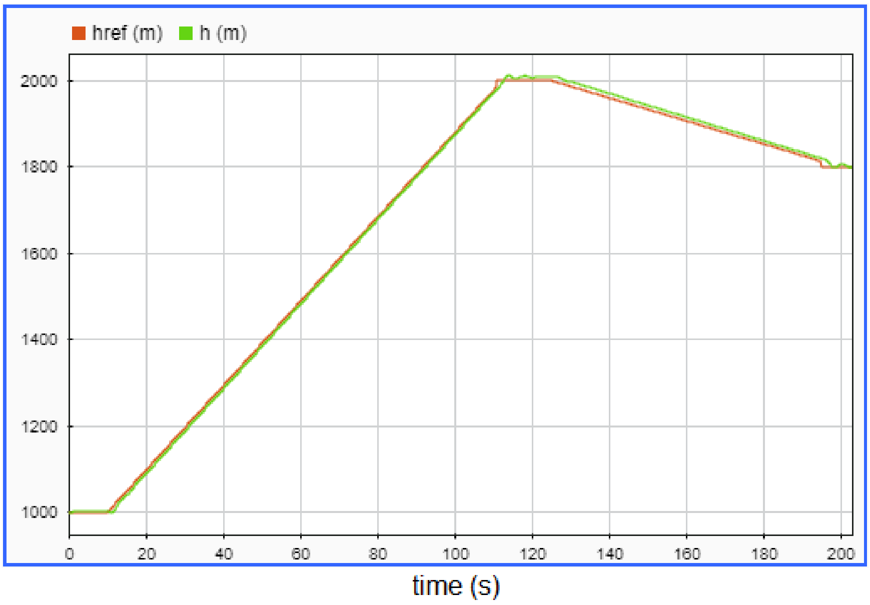

Figure 6.4. Altitude of the aircraft in case 1

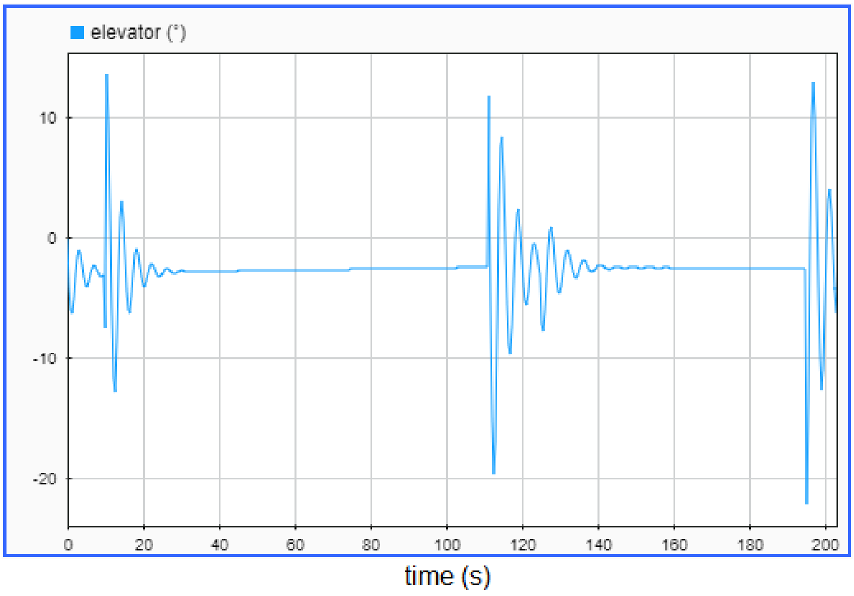

Figure 6.5. Elevator deflection of the aircraft in case 1

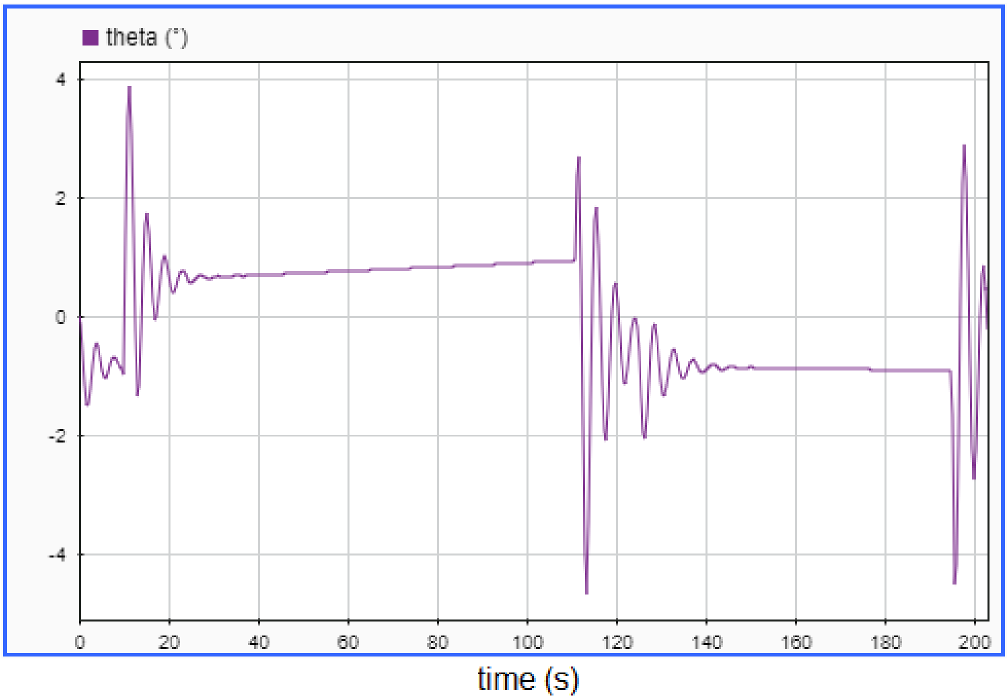

Figure 6.6. Pitch angle of the aircraft in case 1

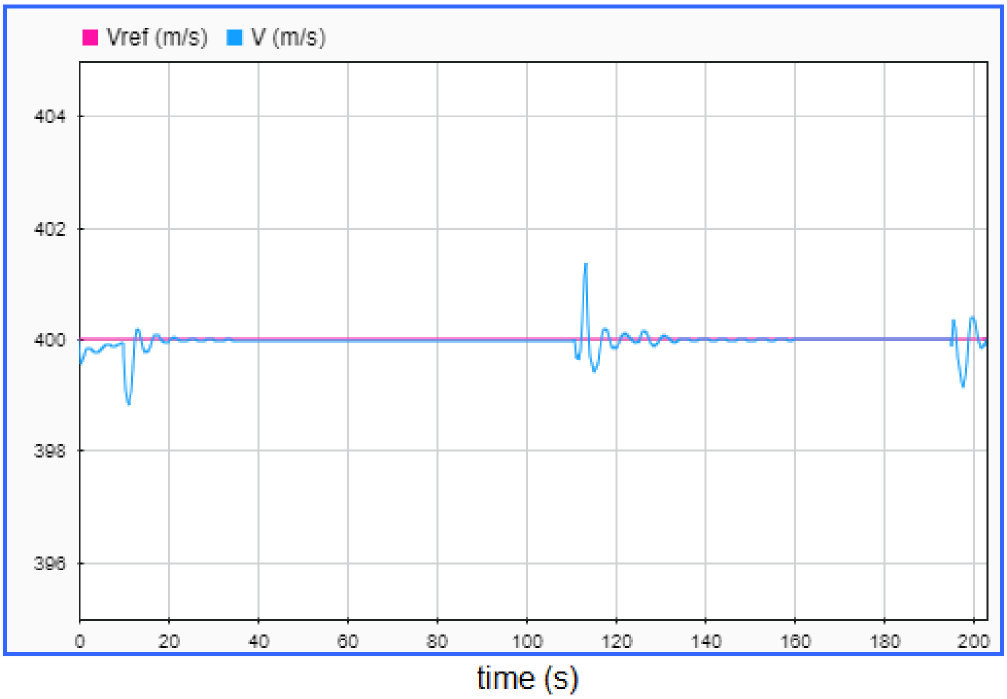

Figure 6.7. Velocity of the aircraft in case 1

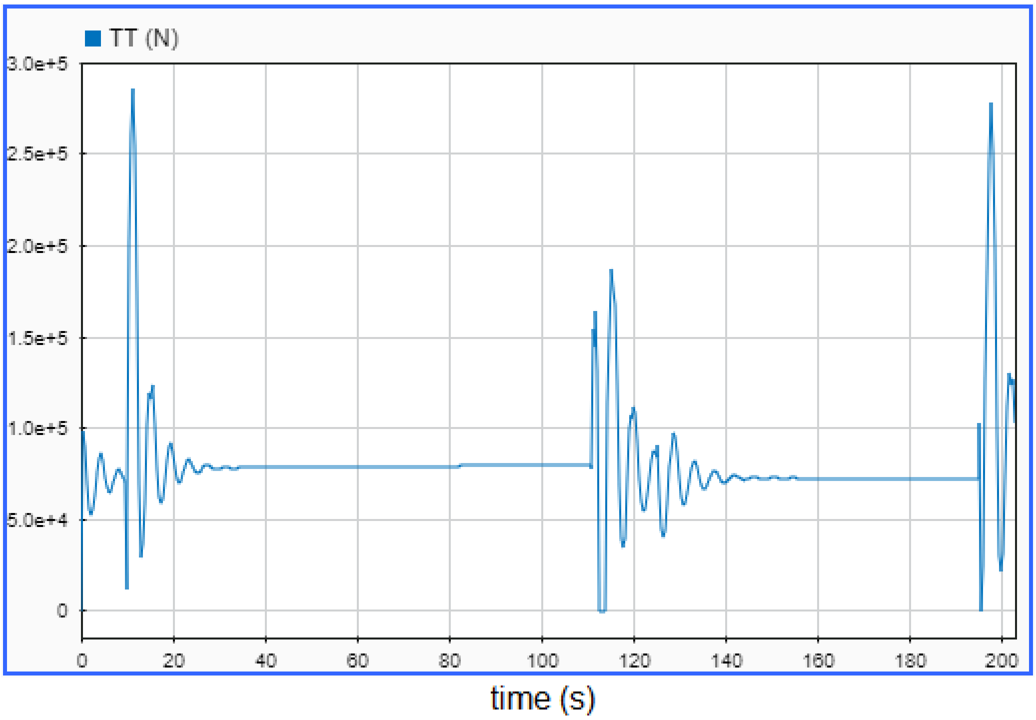

Figure 6.8. Total thrust of the aircraft in case 1

6.3.2 Case 2: Steady Acceleration Scenario

In this case, the path is defined such that the autopilot can control the velocity during climb, level flight and descent. The waypoints are:

WP1: [0, 0, 1000, 400],

WP2: [4000, 0, 1000, 400],

WP3: [45000, 0, 1800, 440],

WP4: [50000, 0, 1800, 440],

WP5: [80000, 0, 1500, 420].

In this path, there are different velocity commands during flight and Y position is constant. The waypoint tracking visualization can be found in Figure 6.9.

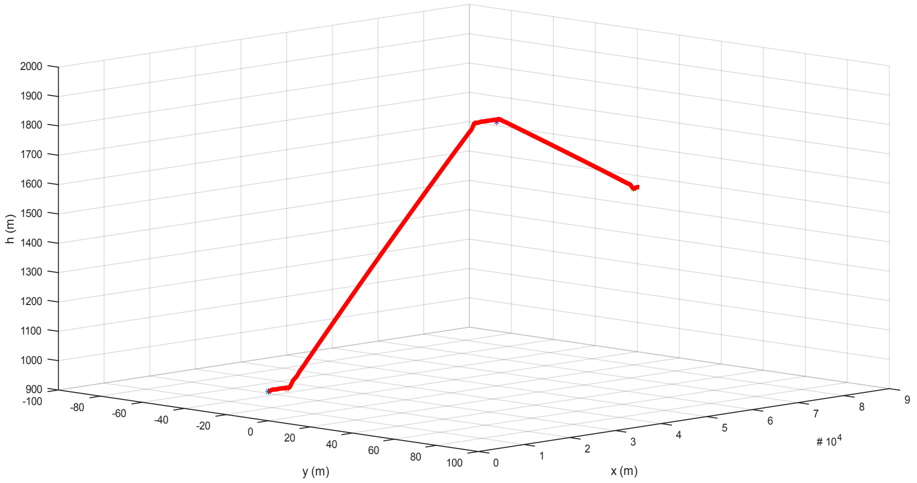

Figure 6.9. Waypoint tracking in case 2

The related results of the attitude of the aircraft are shown in Figures 6.10, 6.11, 6.12, 6.13 and 6.14.

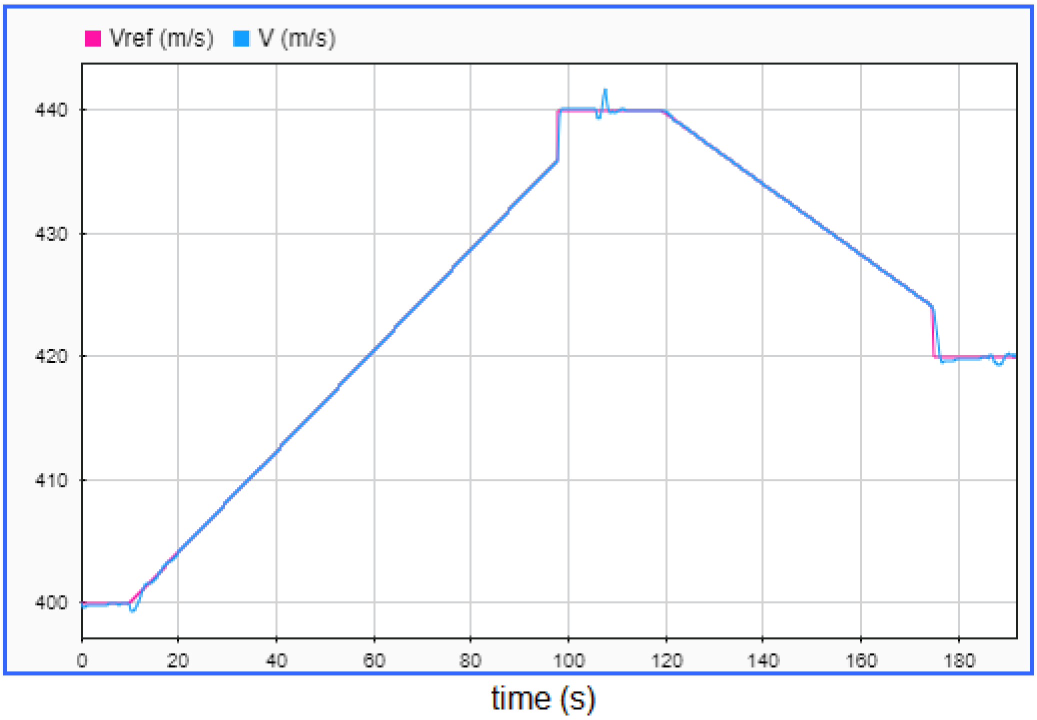

Figure 6.10. Velocity of the aircraft in case 2

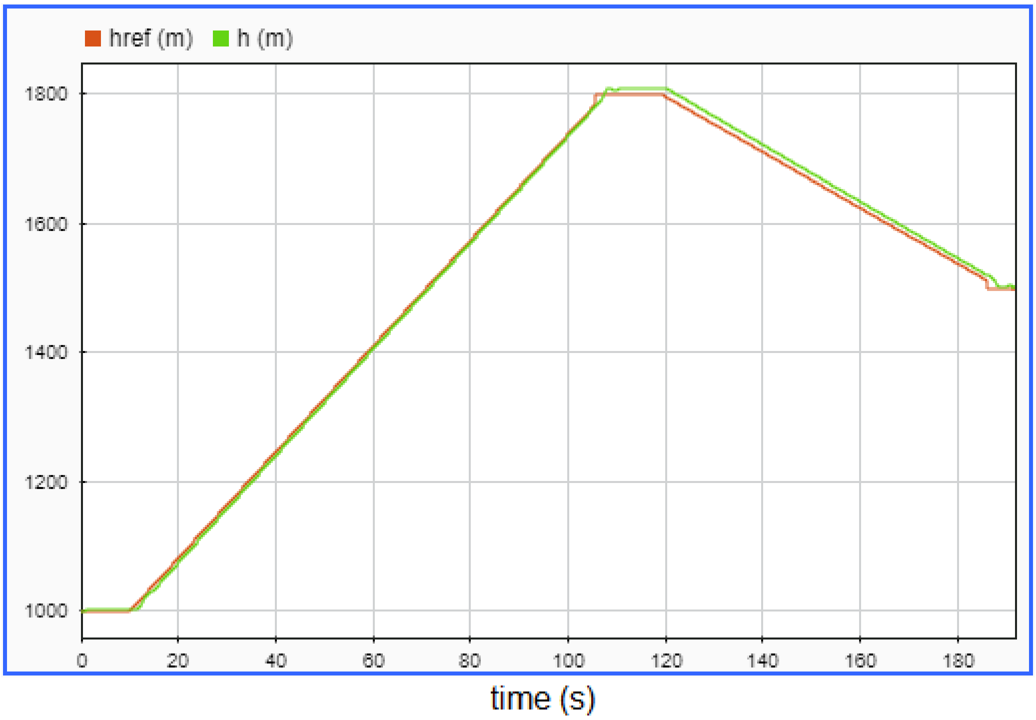

Figure 6.11. Altitude of the aircraft in case 2

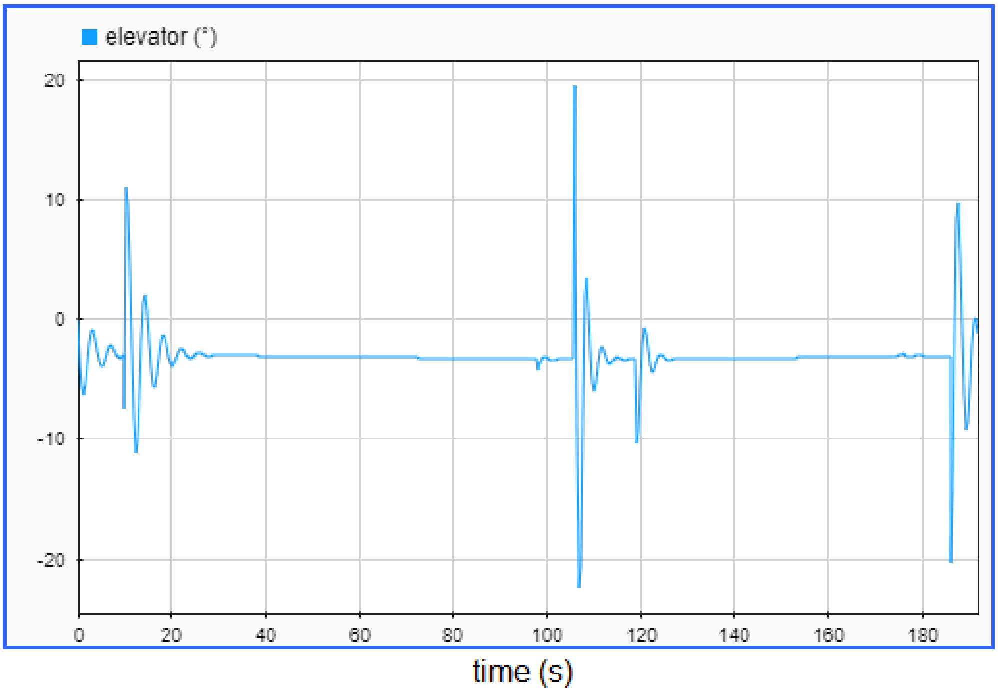

Figure 6.12. Elevator deflection of the aircraft in case 2

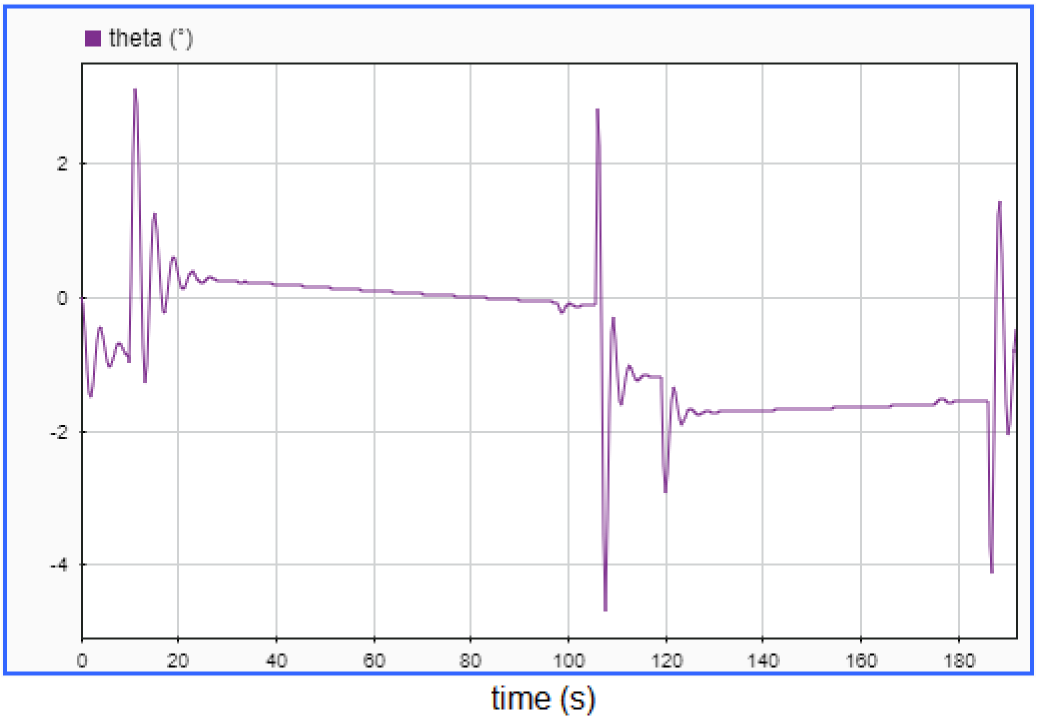

Figure 6.13. Pitch angle of the aircraft in case 2

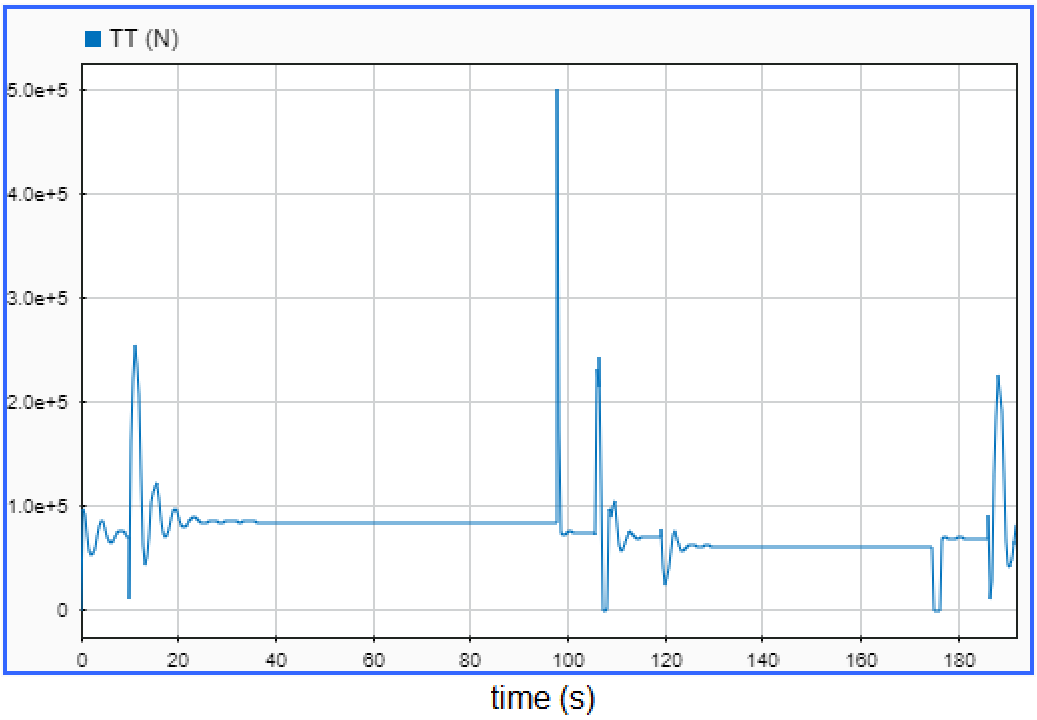

Figure 6.14. Total thrust of the aircraft in case 2

6.3.3 Case 3: Steep Turn Scenario

In this scenario, the path is defined such that the autopilot can simulate steep turn scenario at constant altitude. The waypoints are:

WP1: [0, 0, 1000, 400],

WP2: [4000, 0, 1000, 400],

WP3: [45000, -15000, 1000, 400],

WP4: [50000, -15000, 1000, 400],

WP5: [80000, -15000, 1000, 400].

In this path, agile heading maneuver is needed because the desired heading angle between waypoint 2 and 3 is appriximately 20˚. Velocity and altitude are constant during flight. The waypoint tracking illustration is given in Figure 6.15.

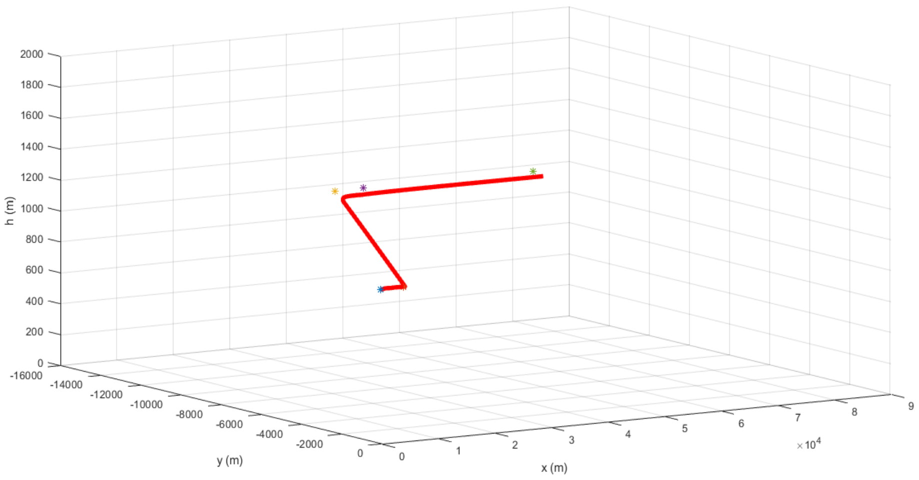

Figure 6.15. Waypoint tracking in case 3

The related results of the attitude of the aircraft are shown in Figures 6.16, 6.17, 6.18, 6.19, 6.20, 6.21, 6.22 and 6.23.

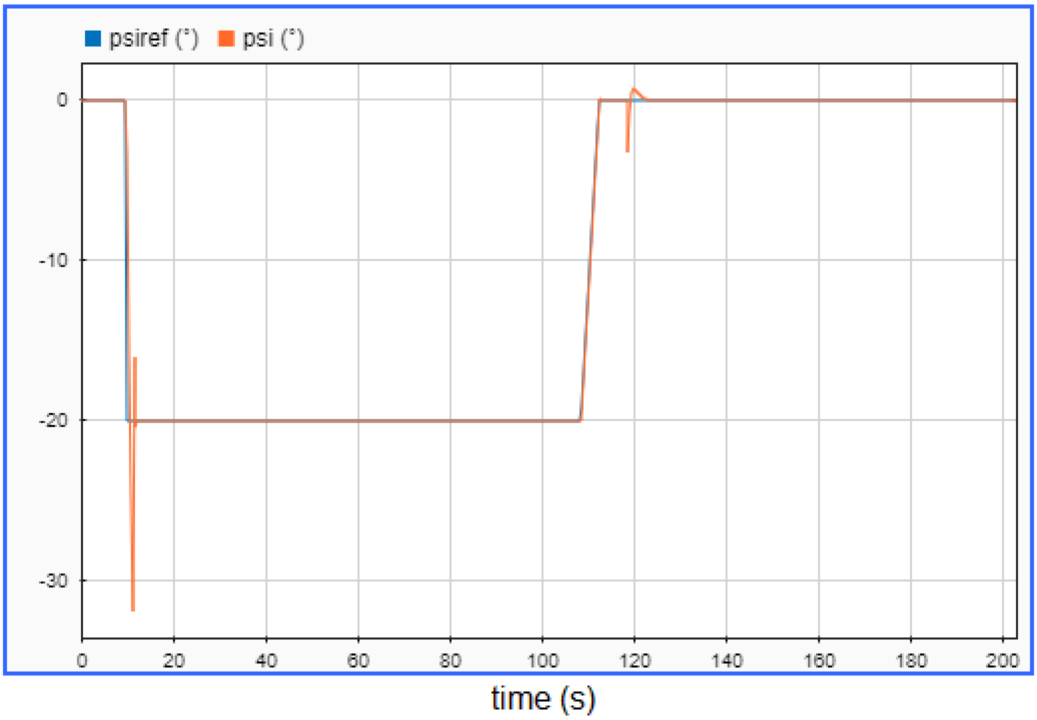

Figure 6.16. Yaw angle of the aircraft in case 3

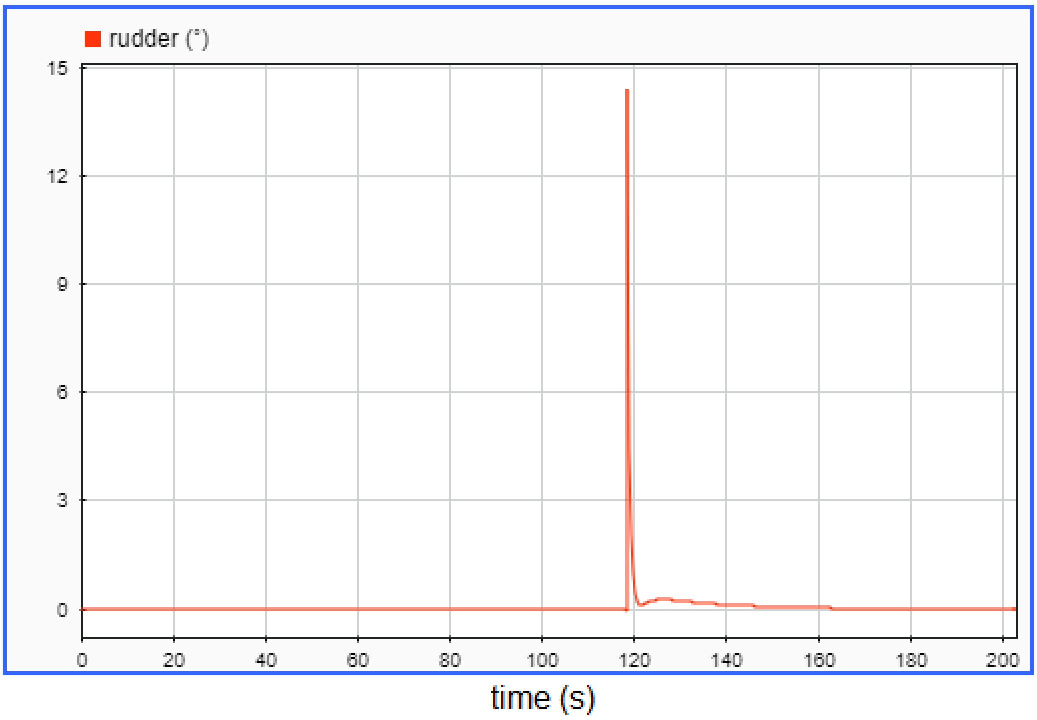

Figure 6.17. Rudder deflection of the aircraft in case 3

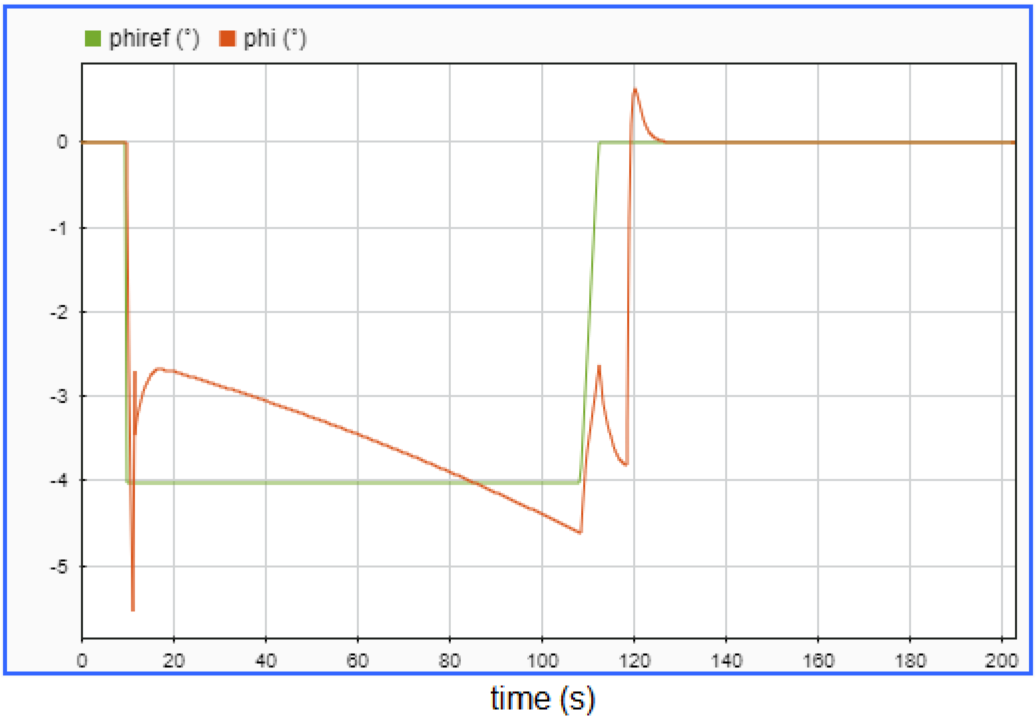

Figure 6.18. Bank angle of the aircraft in case 3

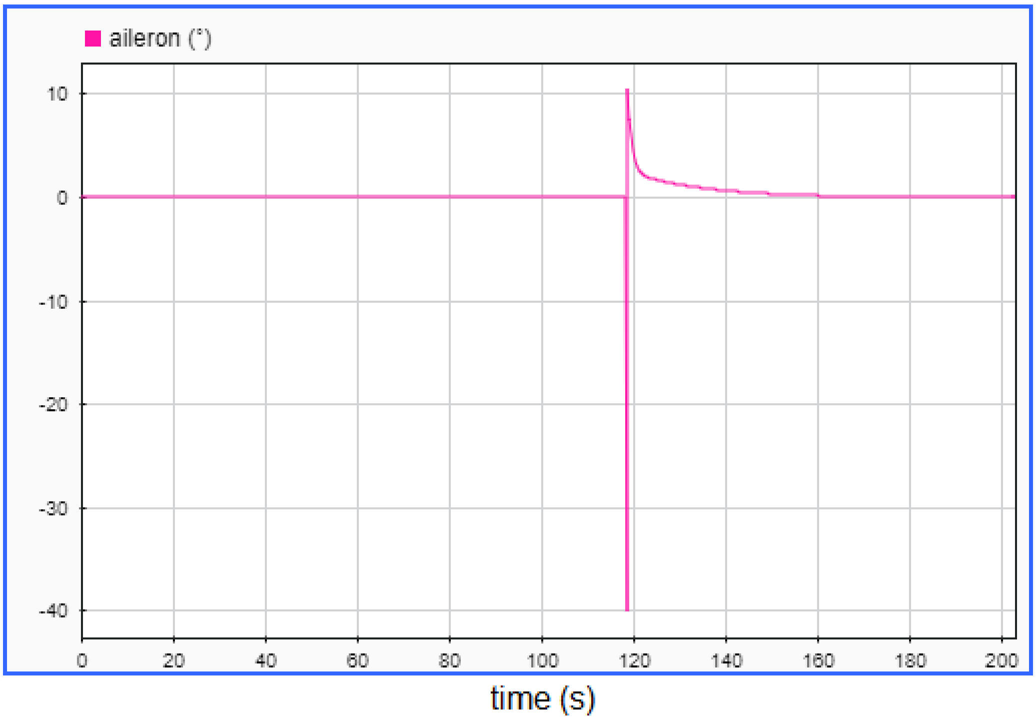

Figure 6.19. Aileron deflection of the aircraft in case 3

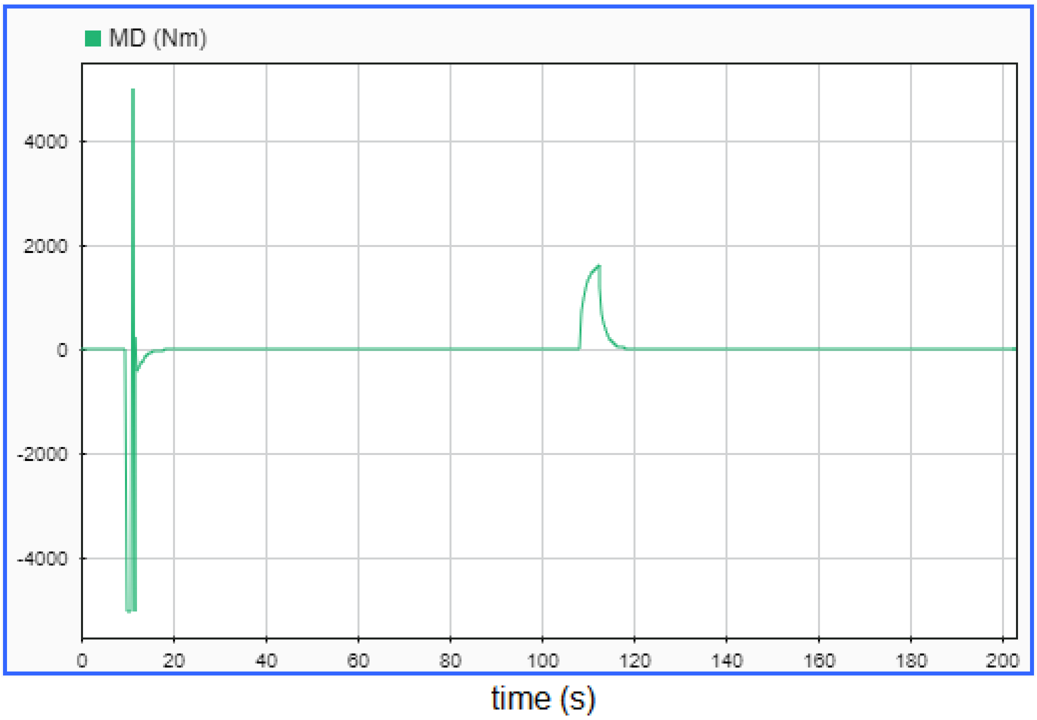

Figure 6.20. Moment difference of the aircraft in case 3

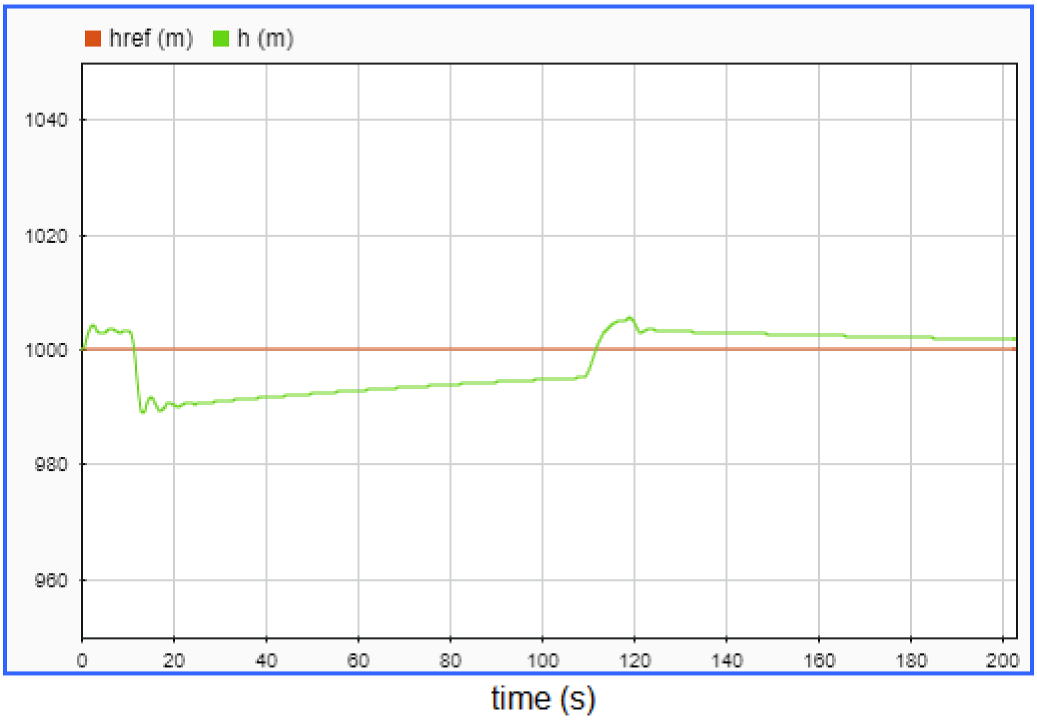

Figure 6.21. Altitude of the aircraft in case 3

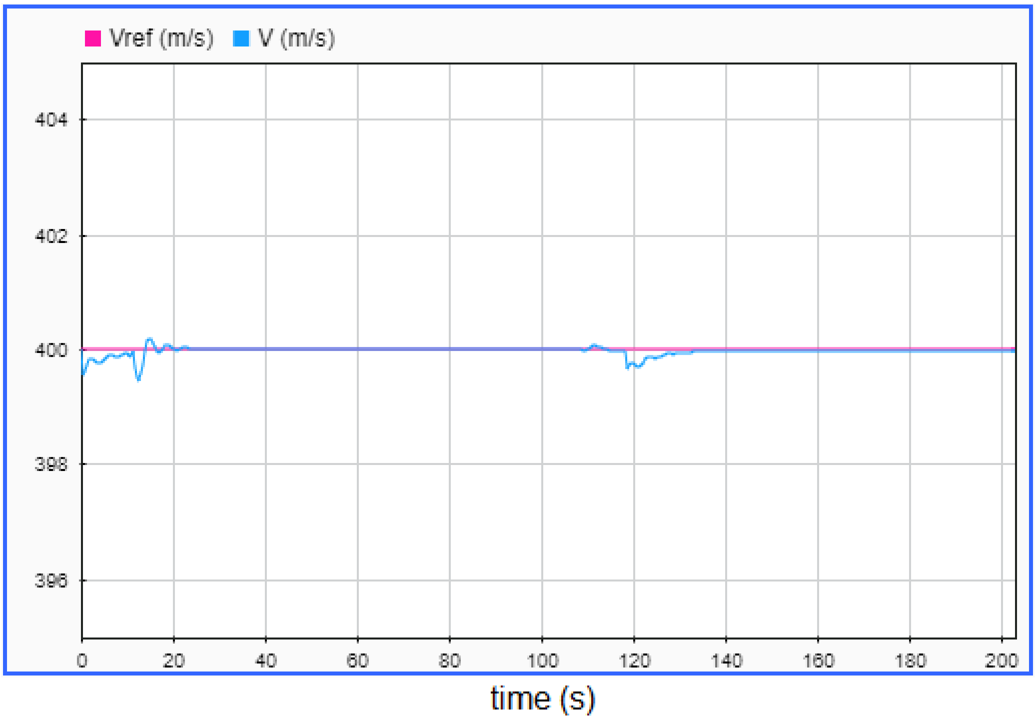

Figure 6.22. Velocity of the aircraft in case 3

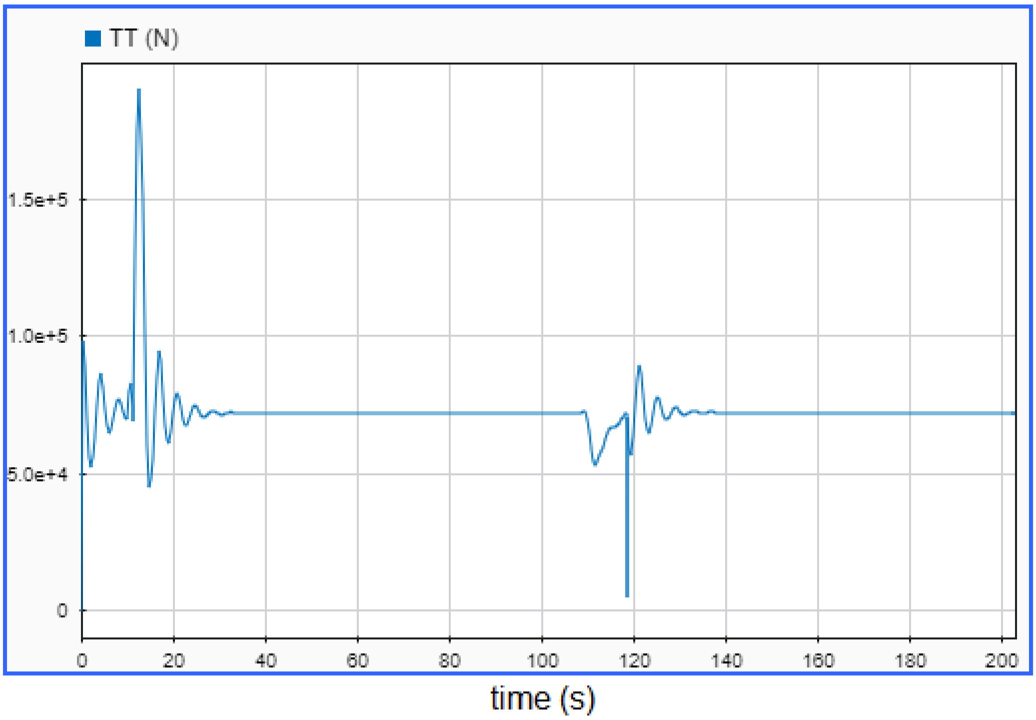

Figure 6.23. Total thrust of the aircraft in case 3

6.3.4 Case 4: Level Turn Scenario

In this case, level turn with low bank angle is simulated. The waypoints are:

WP1: [0, 0, 1000, 400],

WP2: [4000, 0, 1000, 400],

WP3: [45000, 2000, 1000, 400],

WP4: [50000, 2000, 1000, 400],

WP5: [80000, 1500, 1000, 400].

In this scenario, the aircraft makes coordinated turn with heading angle and bank angle autopilots with at velocity and altitude. The waypoint tracking illustration is given in Figure 6.24.

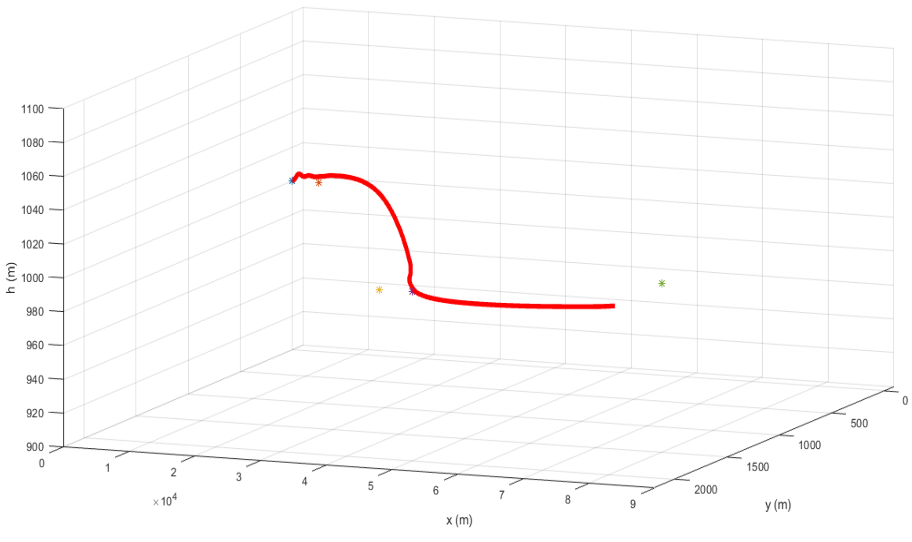

Figure 6.24. Waypoint tracking in case 4

The related results of the attitude of the aircraft are shown in Figures 6.25, 6.26, 6.27, 6.28, 6.29, 6.30, 6.31 and 6.32.

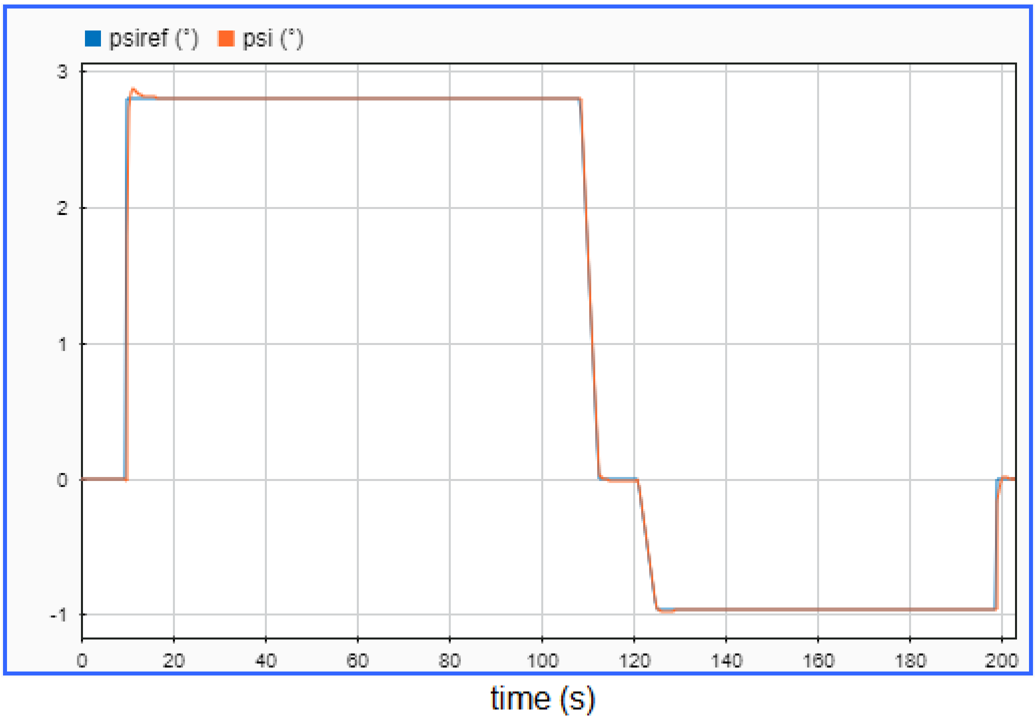

Figure 6.25. Heading angle of the aircraft in case 4

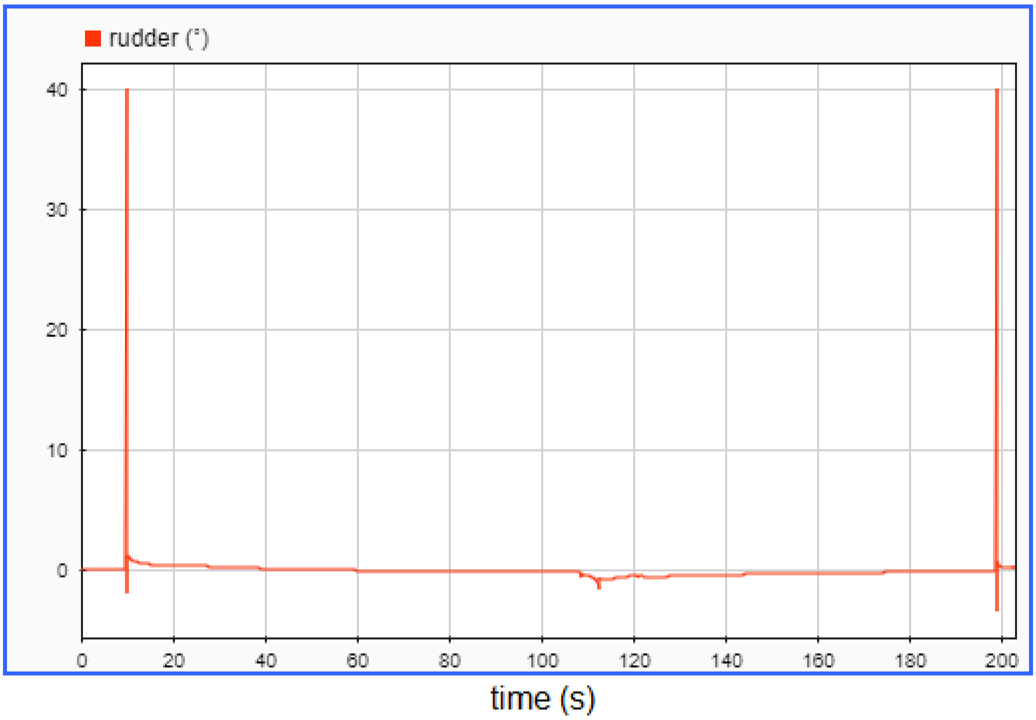

Figure 6.26. Rudder deflection of the aircraft in case 4

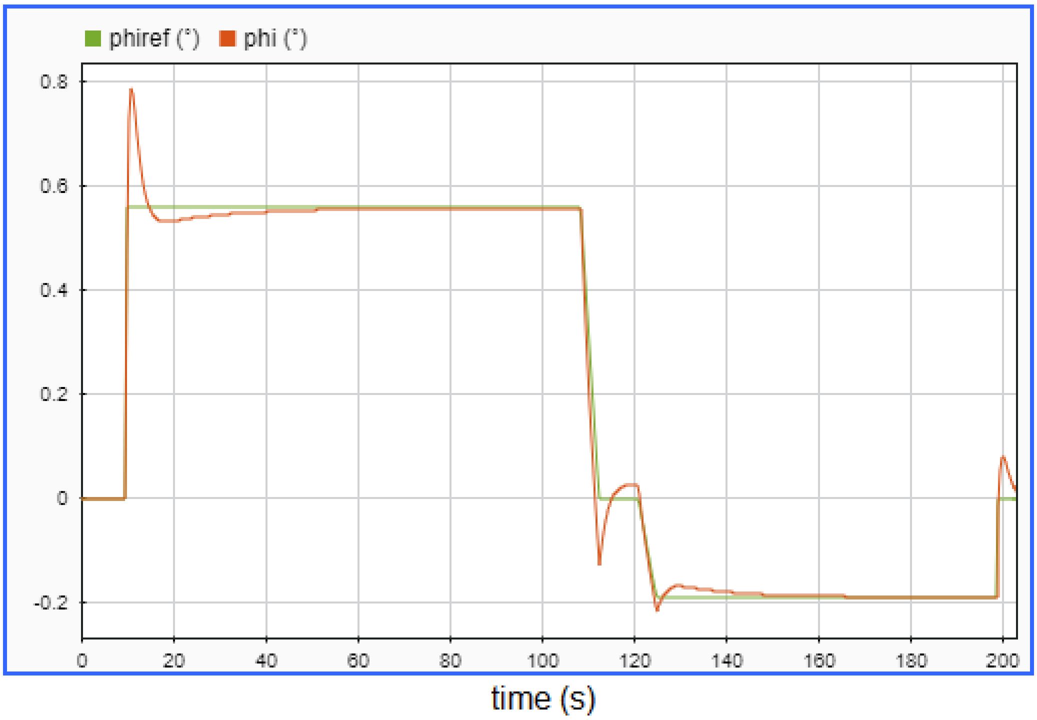

Figure 6.27. Bank angle of the aircraft in case 4

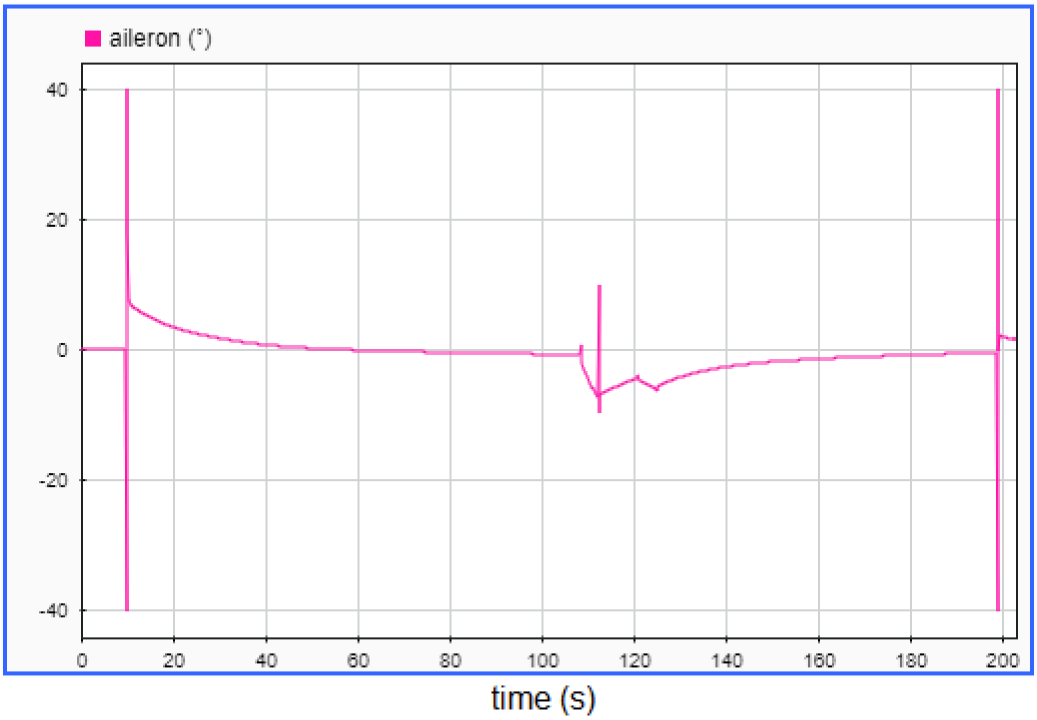

Figure 6.28. Aileron deflection of the aircraft in case 4

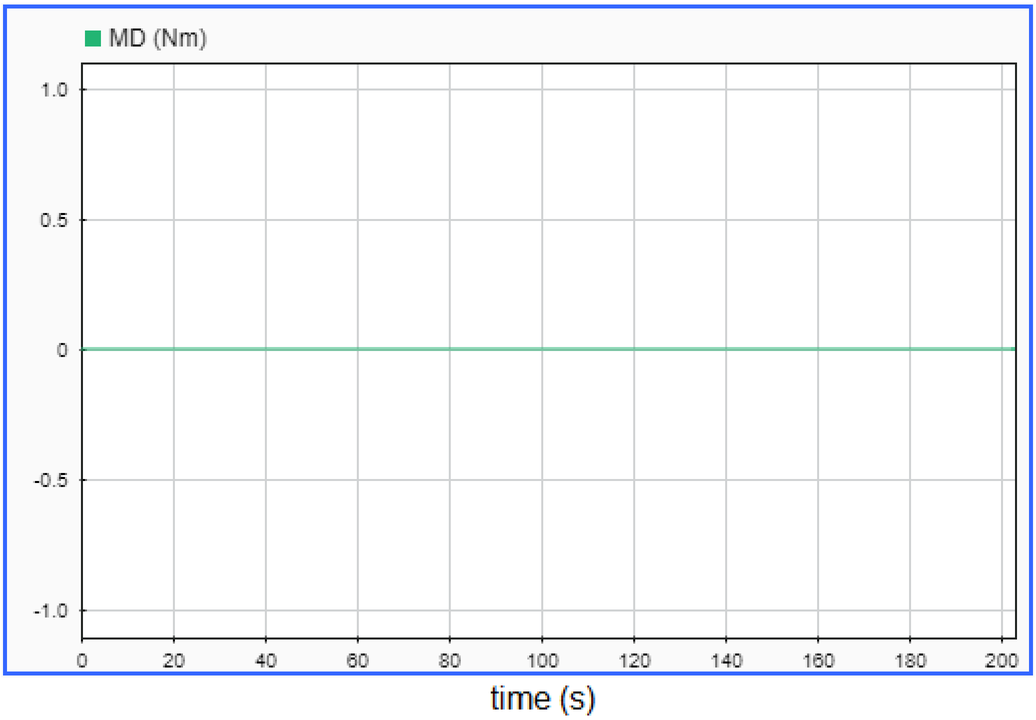

Figure 6.29. Moment difference of the aircraft in case 4

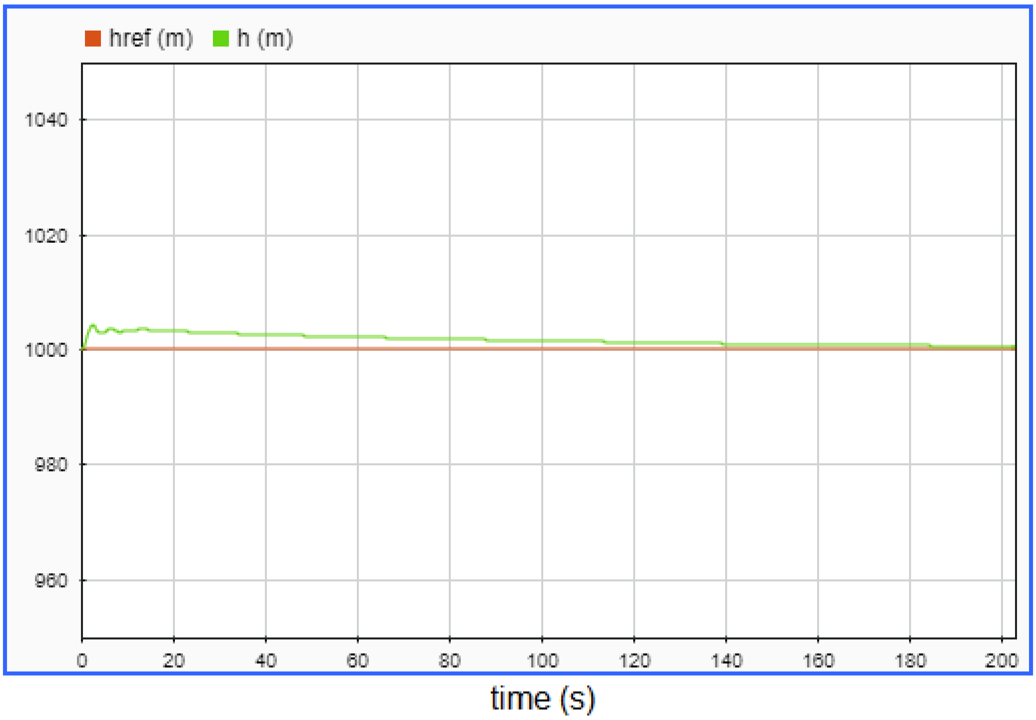

Figure 6.30. Altitude of the aircraft in case 4

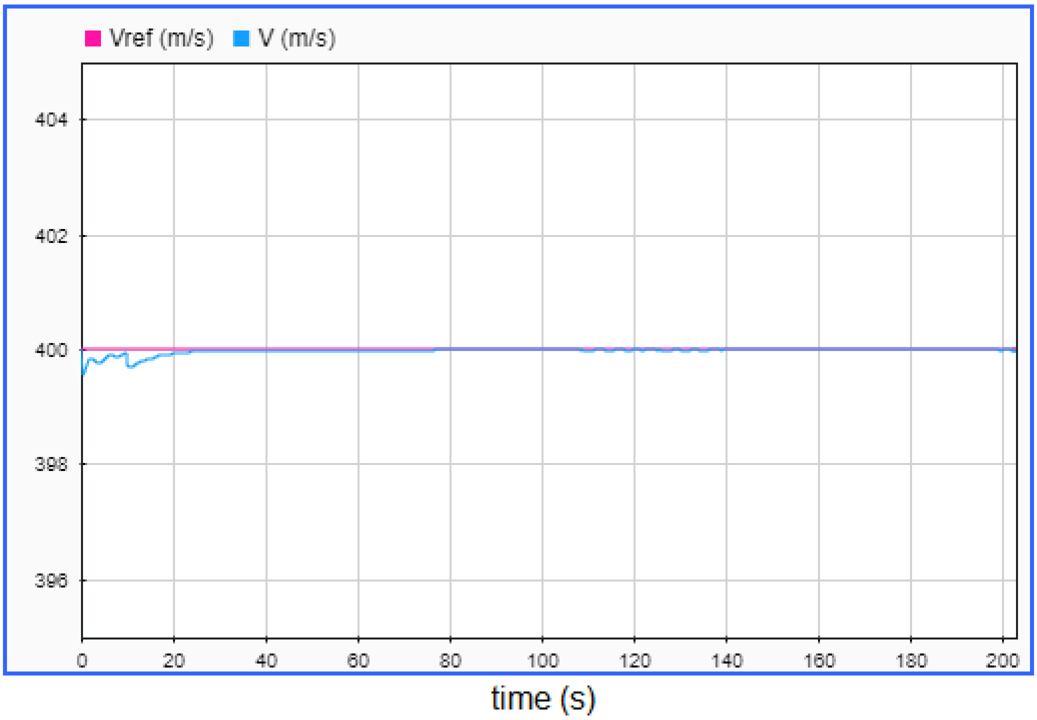

Figure 6.31. Velocity of the aircraft in case 4

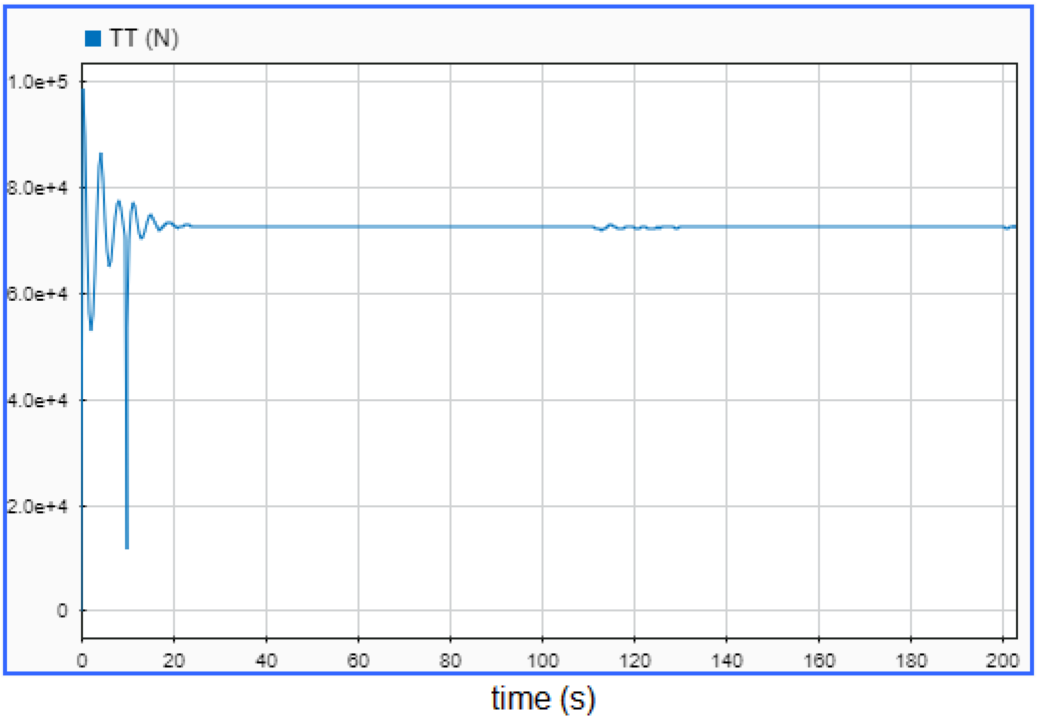

Figure 6.32. Total thrust of the aircraft in case 4

6.3.5 Case 5: Coordinated Turn Scenario

In this case, level turn with moderate bank angle is simulated. When the desired heading angle is between -10˚ to -4˚ or 4˚ to 10˚, guidance system activates the agile heading angle maneuver autopilot with heading and bank angles autopilots together. The waypoints are:

WP1: [0, 0, 1000, 400],

WP2: [4000, 0, 1000, 400],

WP3: [45000, 4000, 1000, 400],

WP4: [50000, 3700, 1000, 400],

WP5: [80000, 1000, 1000, 400].

In this case, between waypoint 3 and 4, only heading angle and bank angle autopilots are used and the rest of the flight, coordinated turn with agile heading angle maneuver autopilot in addition to the heading angle and bank angle autopilots is achieved while the altitude and the velocity of the aircraft stay constant. The waypoint tracking graph is shown in Figure 6.33.

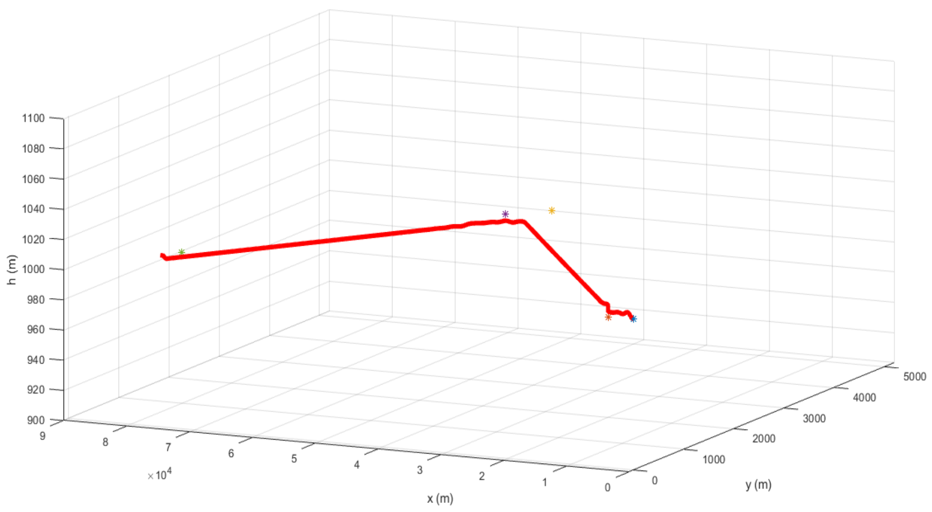

Figure 6.33. Waypoint tracking in case 5

The related results of the attitude of the aircraft are shown in Figures 6.34, 6.35, 6.36, 6.37, 6.38, 6.39, 6.40 and 6.41.

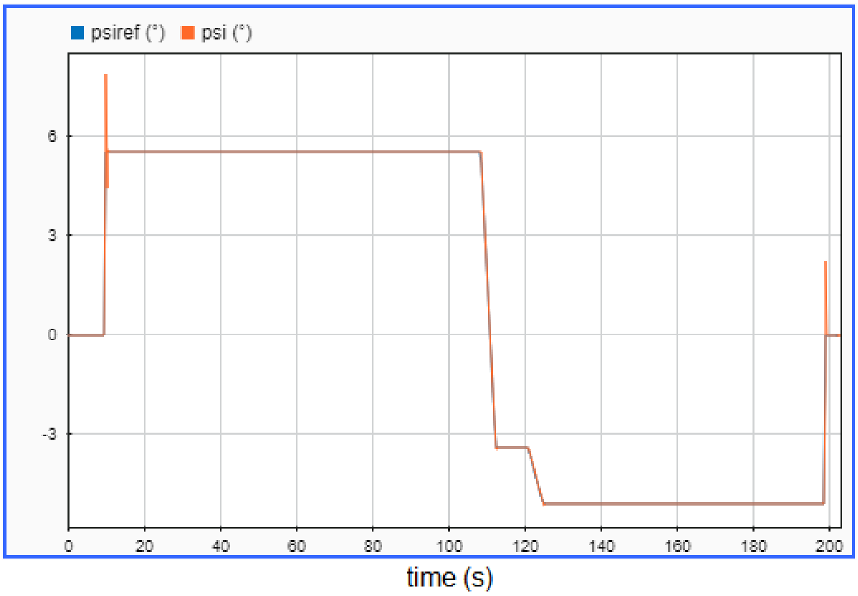

Figure 6.34. Heading angle of the aircraft in case 5

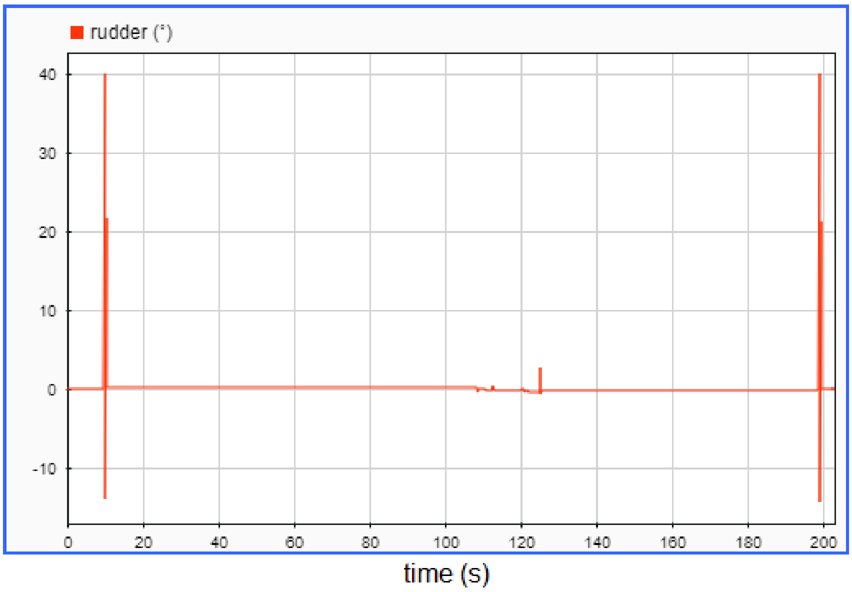

Figure 6.35. Rudder deflection of the aircraft in case 5

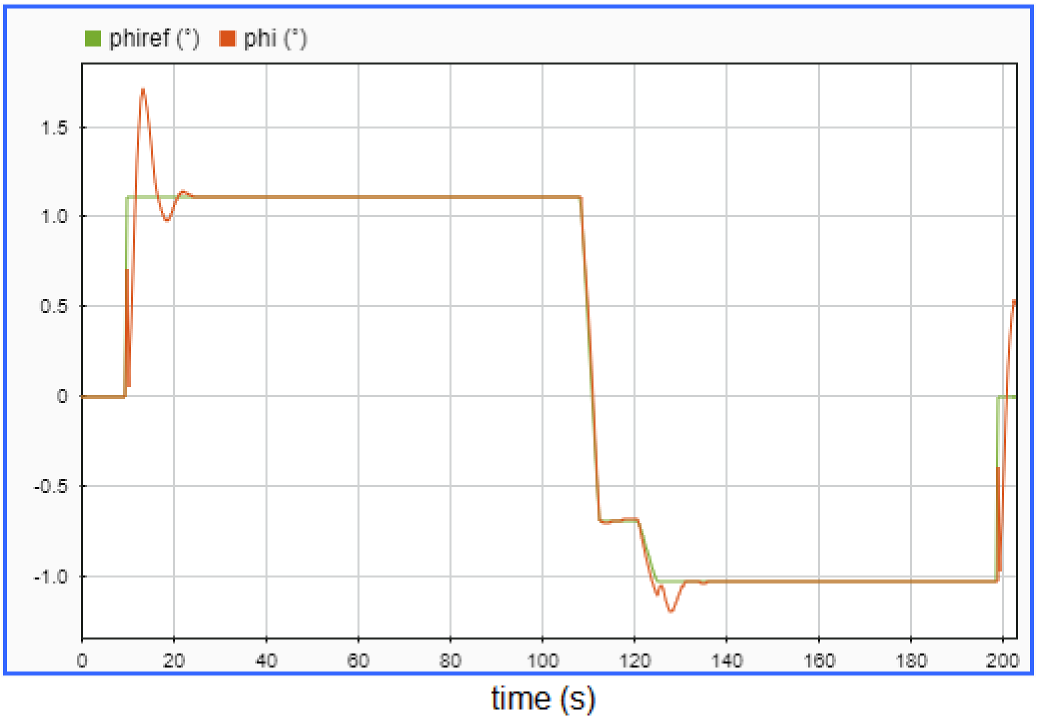

Figure 6.36. Bank angle of the aircraft in case 5

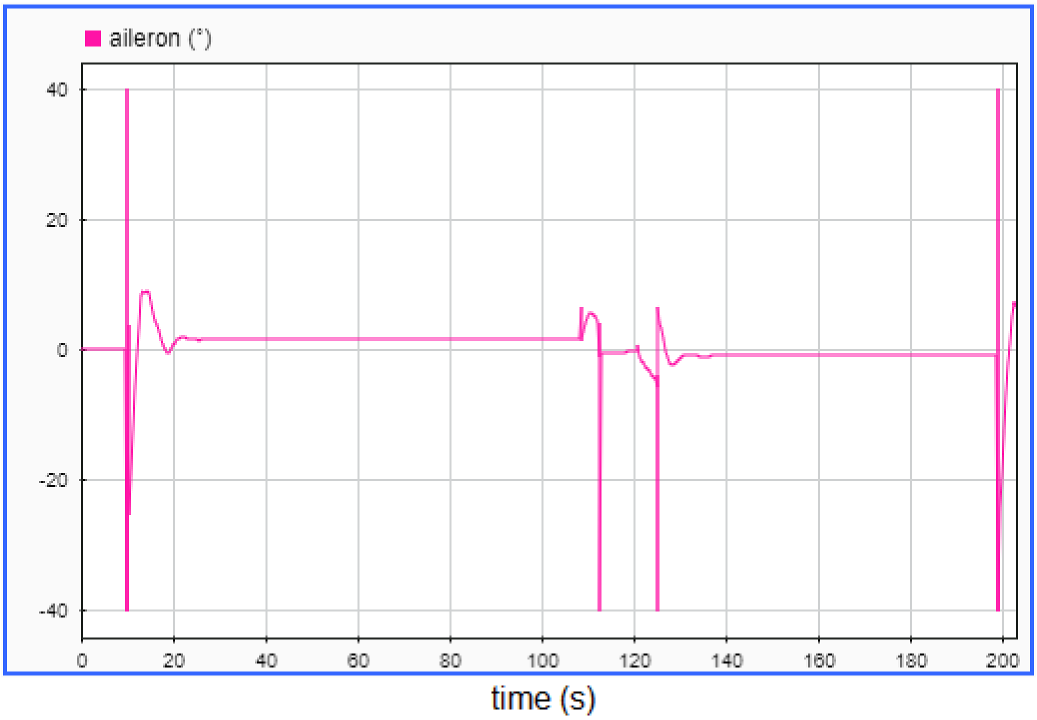

Figure 6.37. Aileron deflection of the aircraft in case 5

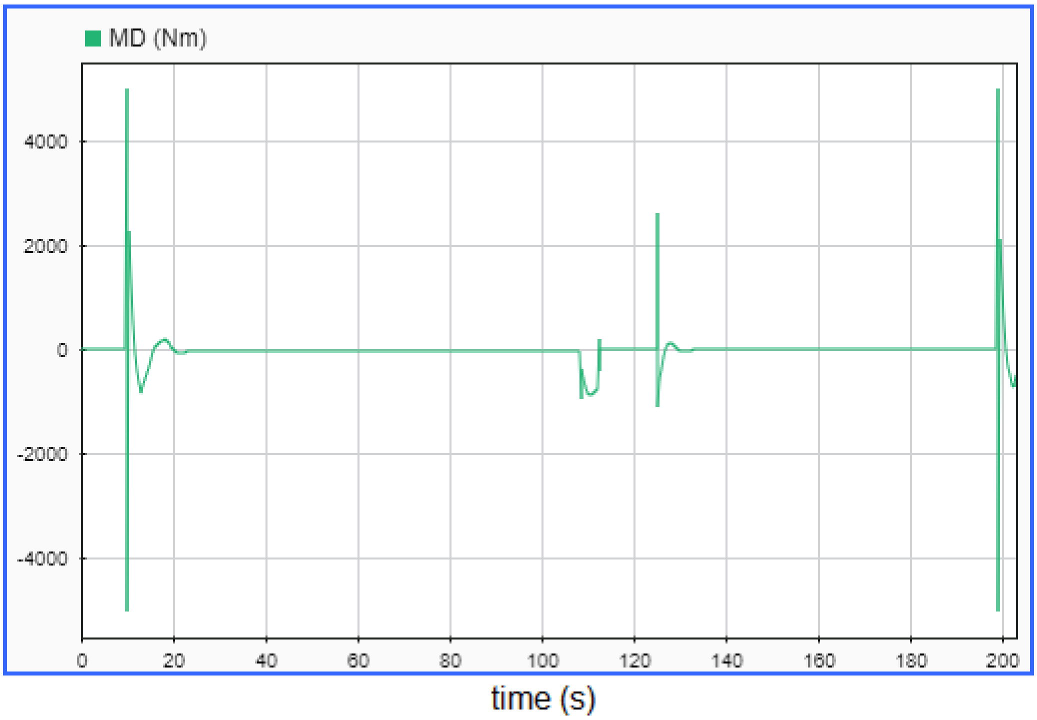

Figure 6.38. Moment difference of the aircraft in case 5

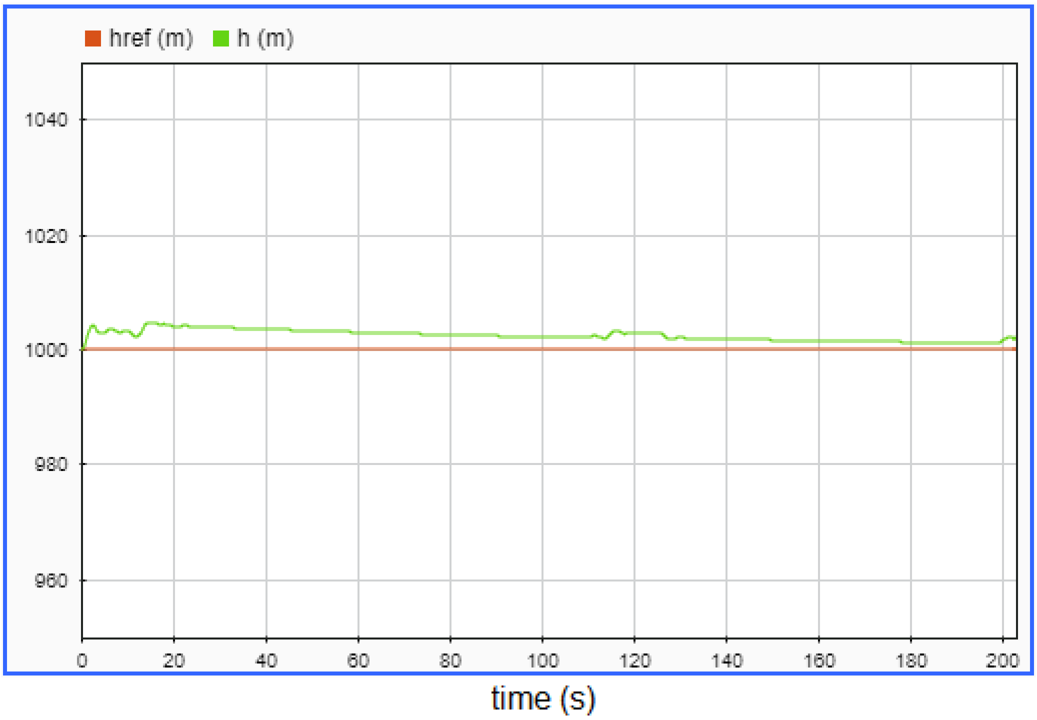

Figure 6.39. Altitude of the aircraft in case 5

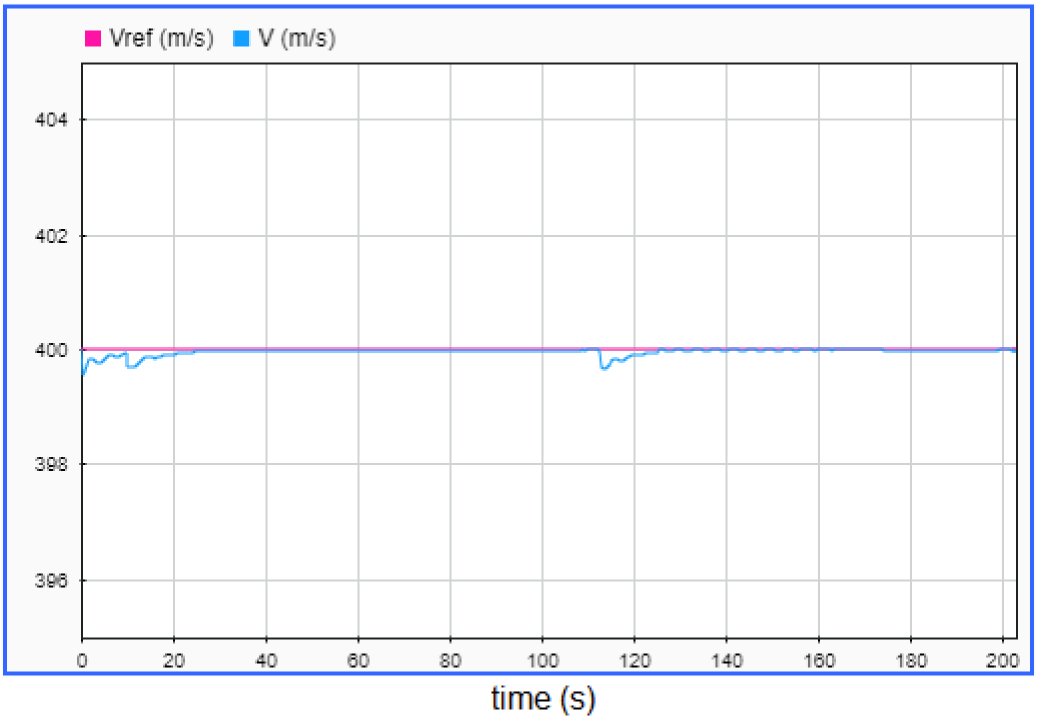

Figure 6.40. Velocity of the aircraft in case 5

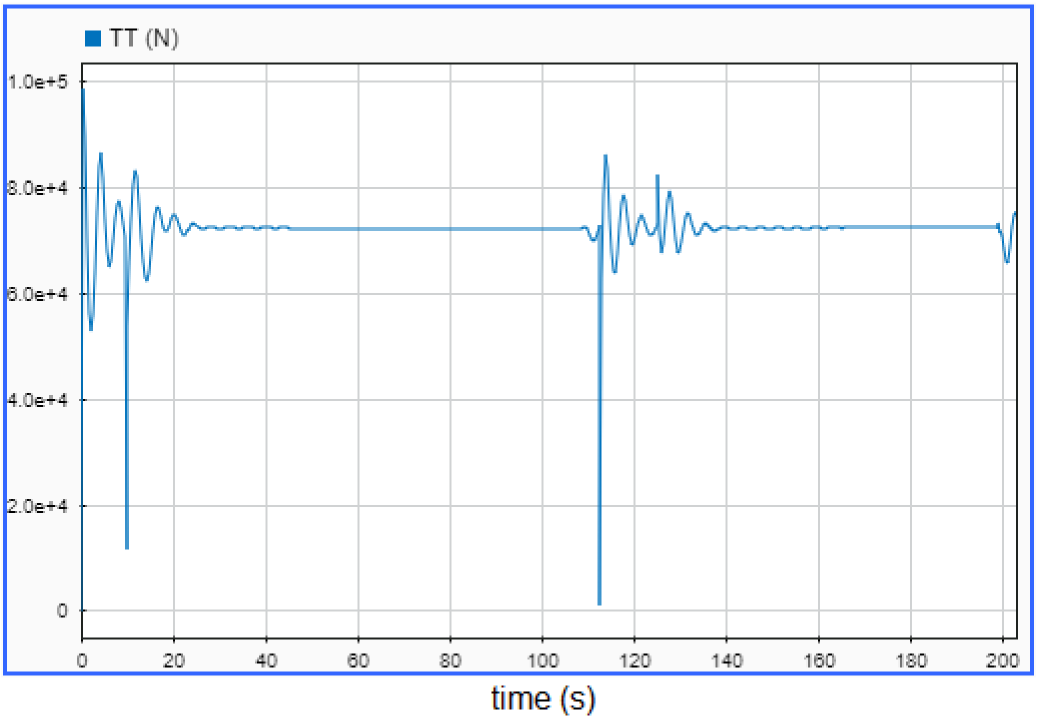

Figure 6.41. Total thrust of the aircraft in case 5

6.3.6 Case 6: Navigation Scenario

Navigation scenario covers basic flight maneuvers and operational concepts such as level flight, turning towards to the next waypoint including level turn, coordinated turn and steep turn, altitude change and acceleration. The waypoints are:

WP1: [0, 0, 1000, 400],

WP2: [4000, 0, 1000, 400],

WP3: [45000, -15000, 2200, 440],

WP4: [75000, -16000, 2200, 440],

WP5: [100000, -14000, 2100, 420].

In this case, between waypoint 2 and 3 agile heading maneuver autopilot is used and the rest of the flight coordinated turn are achieved while the altitude and the velocity of the aircraft changes. The waypoint tracking graph can be found in Figure 6.42.

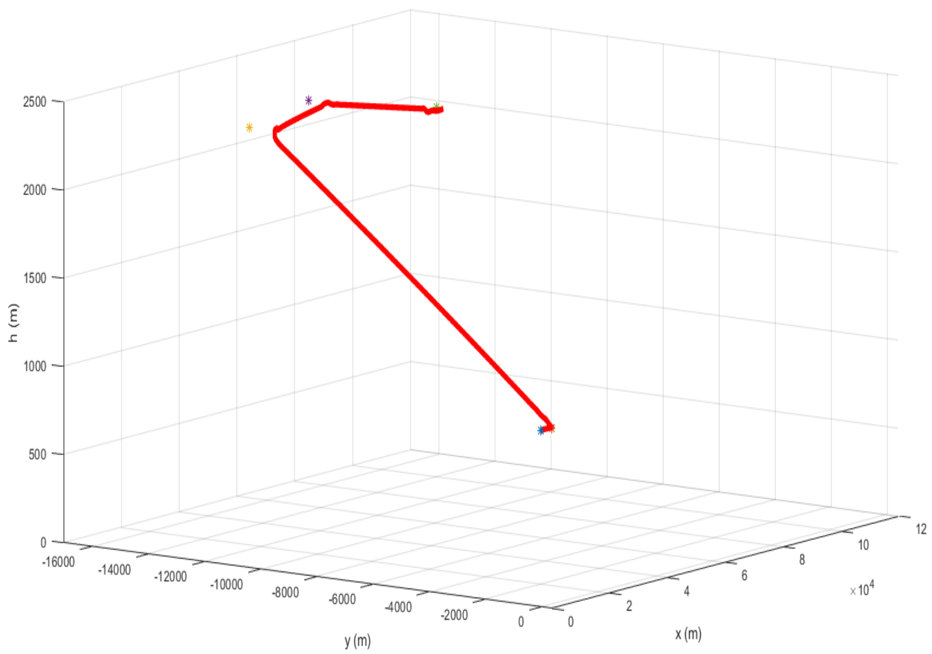

Figure 6.42. Waypoint tracking in case 6

The related results of the attitude of the aircraft are shown in Figures 6.43, 6.44, 6.45, 6.46, 6.47, 6.48, 6.49, 6.50, 6.51 and 6.52.

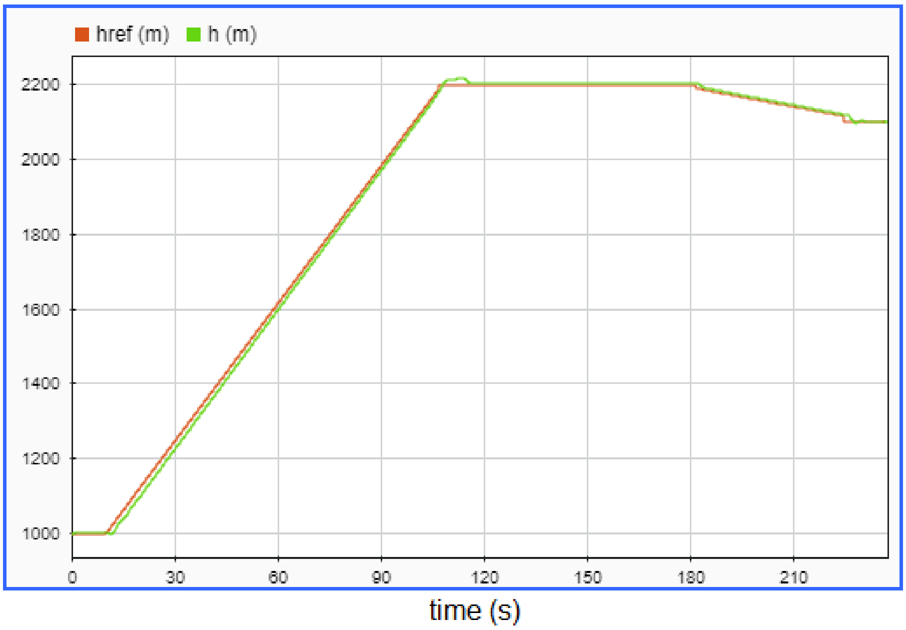

Figure 6.43. Altitude of the aircraft in case 6

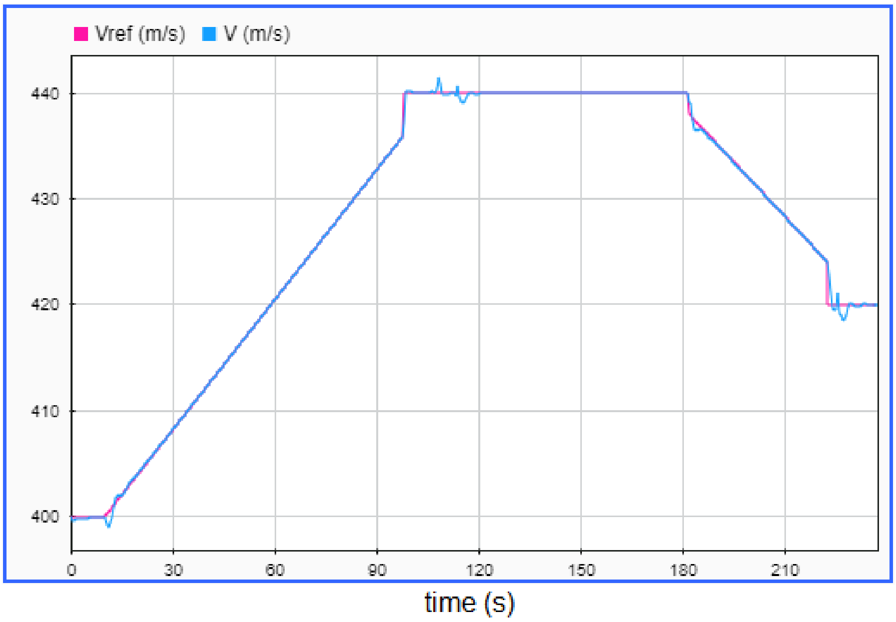

Figure 6.44. Velocity of the aircraft in case 6

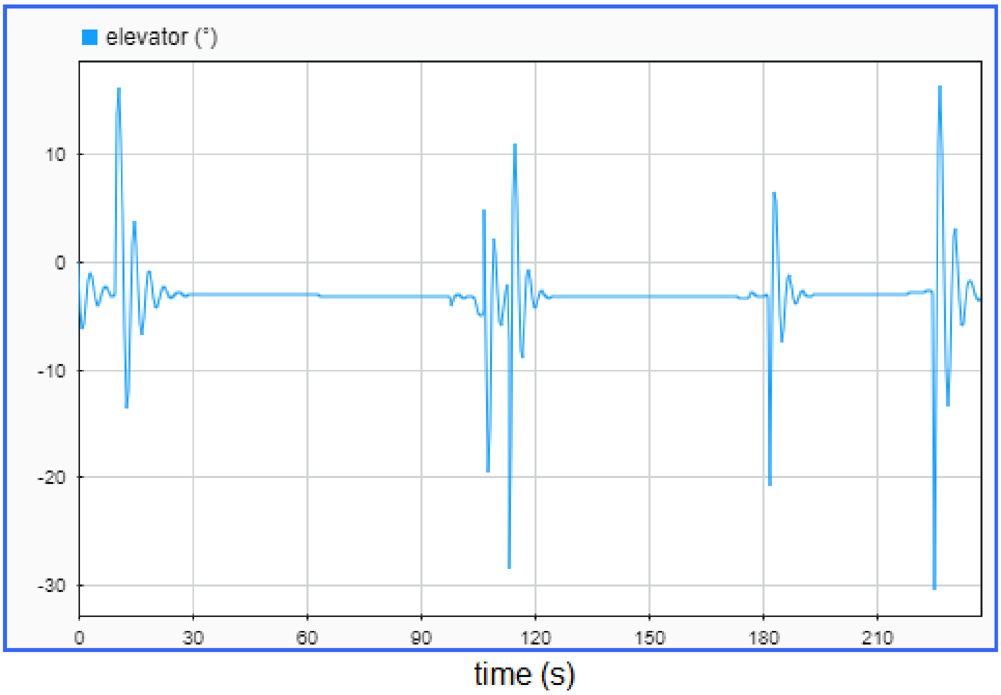

Figure 6.45. Elevator deflection of the aircraft in case 6

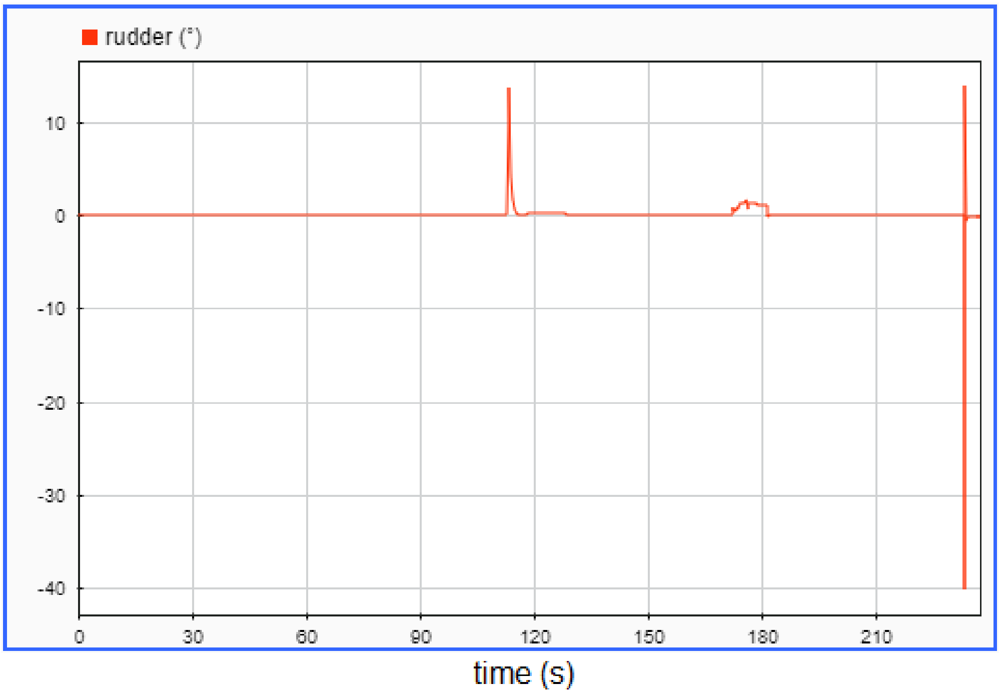

Figure 6.46. Rudder deflection of the aircraft in case 6

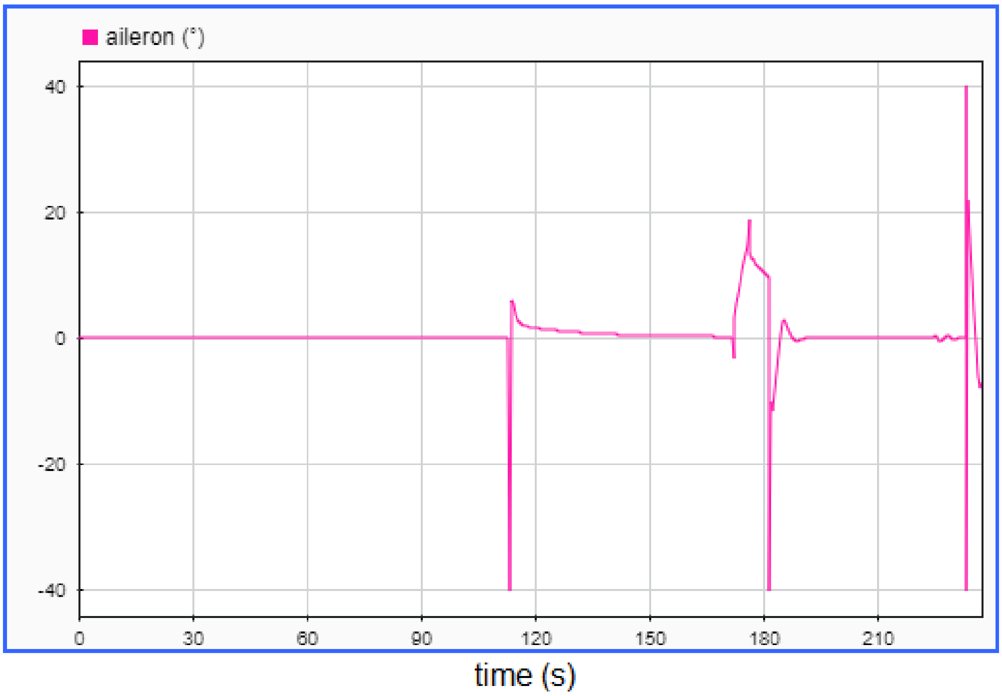

Figure 6.47. Aileron deflection of the aircraft in case 6

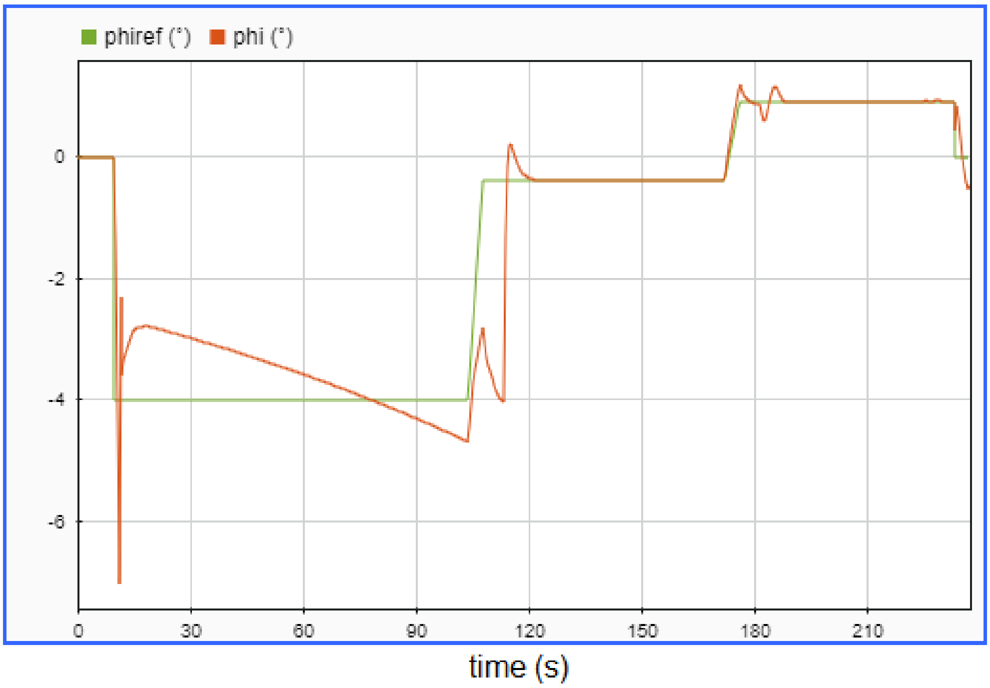

Figure 6.48. Bank angle of the aircraft in case 6

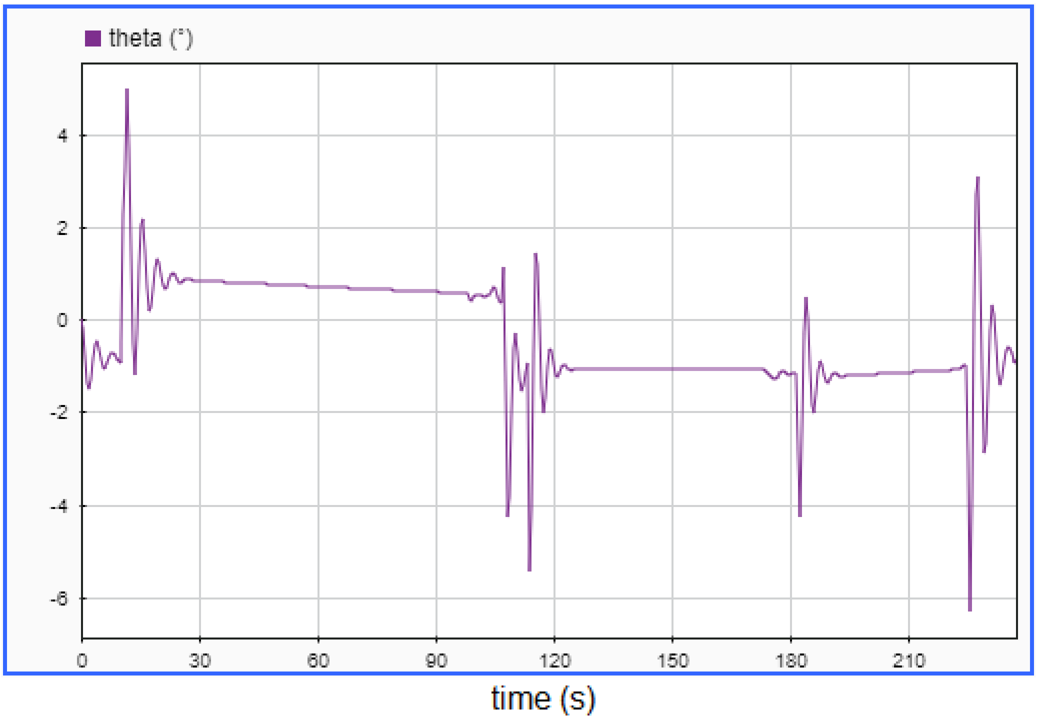

Figure 6.49. Pitch angle of the aircraft in case 6

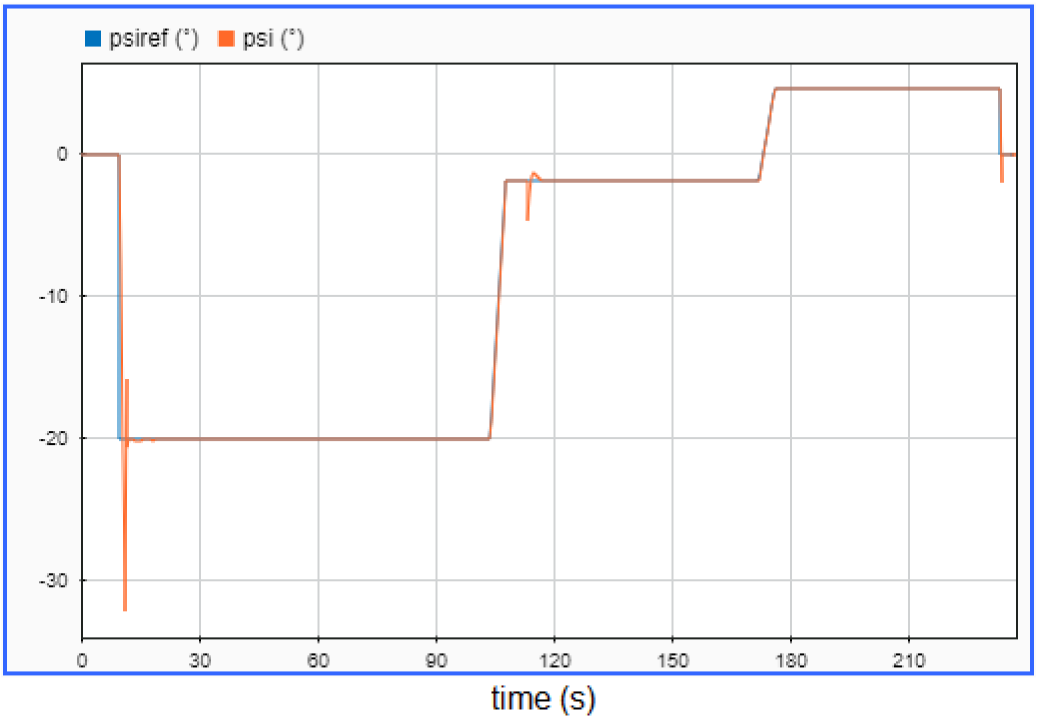

Figure 6.50. Heading angle of the aircraft in case 6

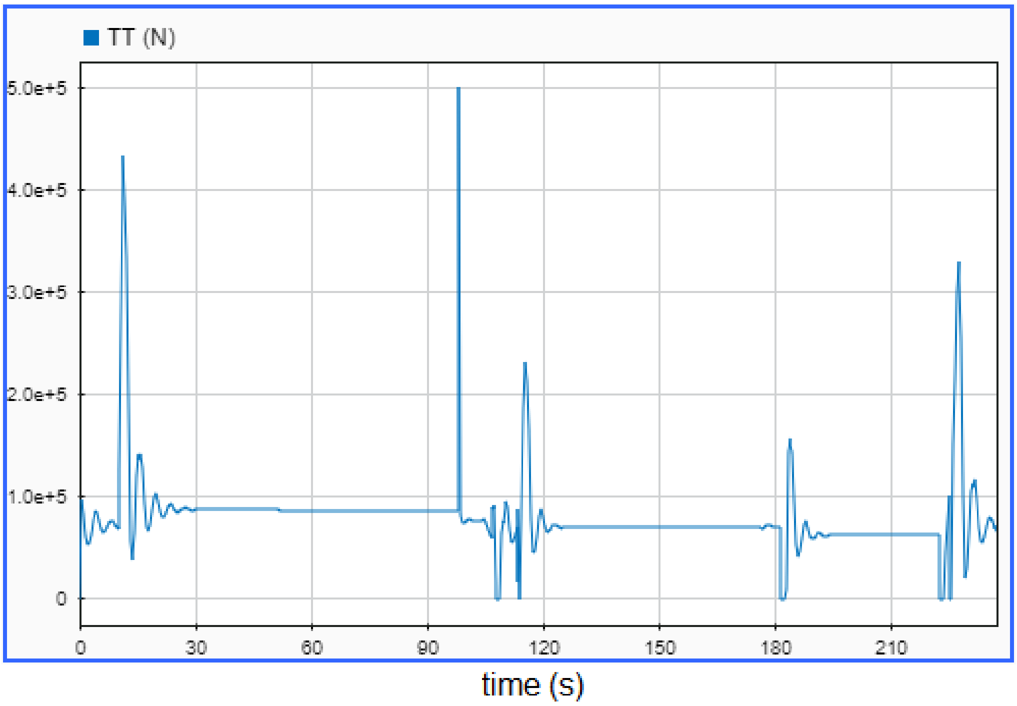

Figure 6.51. Total thrust of the aircraft in case 6

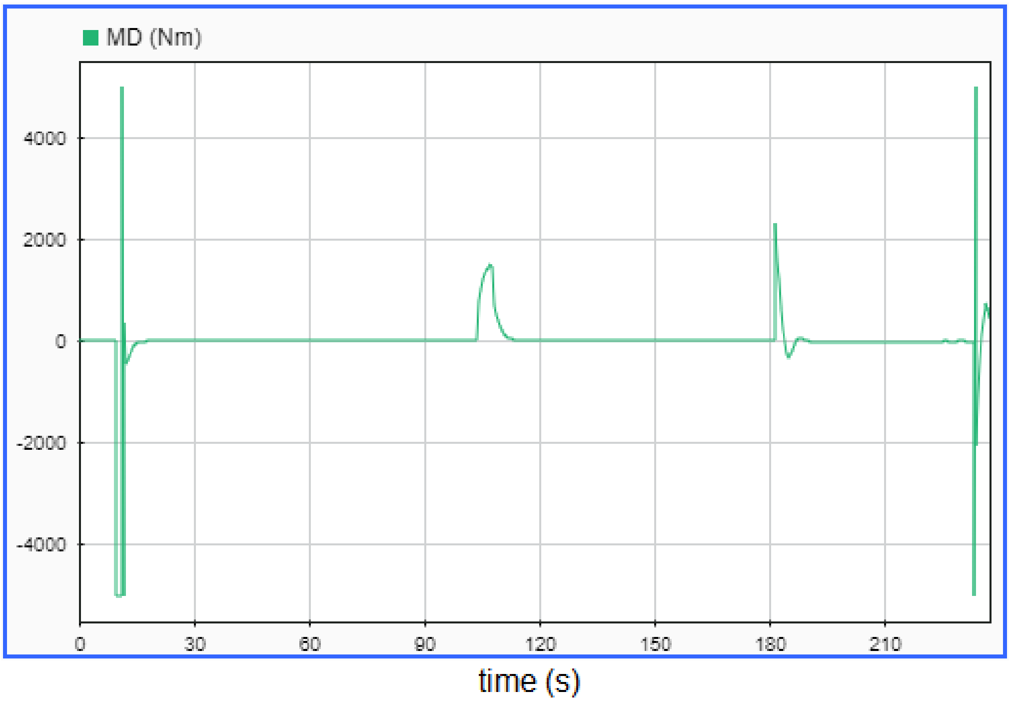

Figure 6.52. Moment difference of the aircraft in case 6

CHAPTER 7

CONCLUSION

In this thesis, first, a mathematical model of a twin-engine jet plane is constructed. Secondly, autopilot designs are studied with cascaded PID controllers.

This study has started with the task focusing on the defining geometry of the aircraft. Similar aircrafts are examined and the geometry is determined with the improvements of more payload capacity. To achieve this goal wingspan and wing area are increased and as a result heavier aircraft is obtained which requires slightly more powerfull engines. This design is conducted in XFLR5 program to calculate aerodynamic derivatives. Fixed wing, horizontal tail and vertical tail options are selected in the design stage. As the main airfoil, NACA 64-210 is selected due to its high lift-to-drag characteristics. This airfoil is used in wing design and a thinner custom version of it is used in horizontal and vertical tail designs. In addition, two more airfoils are generated whose neutral forms are used to simulate movements of control surfaces by changing the tip edge flap angle.

After the calculation of aerodynamic derivatives, a suitable turbojet engine is modeled in MATLAB / Simulink mathematically. The input limits of the turbojet engine are chosen by considering nominal flight conditions and the base thrust to stabilize the drag force that is produced from aerodynamic characteristics of the aircraft. Produced thrust of the turbojet engine for different velocities and throttle settings, is examined.

Next, mathematical model of the aircraft with 6-DOF equations of motion is constructed. All state variables to create flight model and the calculation of the attitude of the aircraft are studied. Aerodynamic forces and moments are calculated and propulsion forces and moments are studied with thrust vector control approach. Elevator, rudder, aileron and two throttle settings for each turbojet engine are defined as control parameters of the aircraft. Engines are controlled with two different settings: first, the total thrust that is a component of x-axis force. Second setting is the moment difference that is a component of yawing moment. In the autopilot design to control aircraft motion in z-axis with elevator control surface, pitch angle of the aircraft is used as the inner loop input and the altitude of the aircraft is used as the outer loop input. In velocity control part, total thrust is assigned as the output. For the motion in y-axis, two different settings are examined. Due to the limitation of the aerodynamic characteristics of the aircraft, rudder and aileron are assumed to work in small angles, to stabilize the system (up to +/- 4˚ yaw angle). Therefore, for the command of more than +/- 4 ˚ yaw angle, agile heading angle control is supposed to take place obtained with the output of moment difference that is produced with the thrust difference of turbojet engines. In this autopilot mode, yaw rate of the aircraft is used in the inner loop and the desired yaw angle is used in the outer loop. In the case of rudder and aileron limitations, yaw angle and roll angle are chosen as controller inputs, respectively.

Finally, as the final stage of this work, guidance and flight management system concepts are discussed to simulate overall system. Guidance is an important concept when controlling a complicated system because it is the part that generates actual reference commands that are given as inputs to the autopilots. In this part of work, the required time is calculated to reach the desired point with desired velocity and the decision of which lateral autopilot is used are made. Flight management system is created to determine reference signals to the autopilot with the outputs of the guidance system. To demonstrate the performance of the autopilot system, five simulations are conducted with different paths and it is observed that the system achieved the destination positions successfully.

Simulation studies have shown that this twin engine turbojet model is quite a useful idea to be employed especially in the design of national fighter/bomber aircrafts of Turkey. In particular, performing agile maneouvers with the help of thrust difference of engines is a very interesting idea particularly useful in dog-fight and avoiding missiles. We have planned to study on these concepts further to reveal the missile avoidance property of this chosen structure in the future.

REFERENCES

[1] A. F. Gabernet, “Controllers for systems with bounded actuators : modeling and control of an F-16 aircraft,” M.Sc. thesis, Dept. Mechanical and Aerospace Eng., Univ. California, Irvine, 2007.

[2] D. Dasgupta, D. K. Bhardwaj, J. K. Balu, J. U. K, and J. Kumar, “Design of rc aircraft,” Dept. Aerospace Eng., IITM, Madras, India, AS5210, May, 2013.

[3] S. Maurya, “Pressure distribution on an airfoil,” Aerodynamics Lab., Indian Institute of Space Science and Technology, Thiruvananthapuram, Kerala, India, Rep. 695547, 2012.

[4] S. I. Sakir and A. R. Laskar, “Design and optimization of a multi-role fighter aircraft,” *SEU J. Sci. Eng.*, vol. 11, no. 1, pp. 1999-1630, June 2017.

[5] J. C. Sivells, “Experimental and calculated characteristics of three wings of NACA 64-210 and 65-210 airfoil sections,” Langley Memorial Aeronautical Lab., Langley Field, VA, Washington, USA, Rep. 1422, Aug. 1947.

[6] M. H. Sadraey, “Tail design,” in *Aircraft Design: A Systems Engineering Approach*, New Jersey, USA: Wiley, ch. 6, pp. 274–352, 2012.

[7] A. S. Shohan, I. Khan, A. Shahriar, G. Captain, and A. Salam, “Design and optimization of a ground attack aircraft,” *IOSR Journal of Mechanical and Civil Engineering*, vol. 13, no. 3, pp. 104–110, 2016.

[8] M. H. Sadraey, “Wing design,” in *Aircraft Design: A Systems Engineering Approach*, New Jersey, USA: Wiley, ch. 5, pp. 167-275, 2012.

[9] D. Olinger, D. Bradway, and K. Miller, “Aircraft design,” Dept. Mech. Eng., Worcester Polytechnic Institute, Worcester, UK, ME4770, 2009.

[10] W. H. Mason. (2004). Transonic aerodynamics of airfoils and wings [Online]. Available: http://www.dept.aoe.vt.edu/~mason/Mason_f/ConfigAero.html

[11] F. M. Sobolic, “Agile flight control techniques for a fixed-wing aircraft,” M.S. thesis, Dept. Aeronautics and Astronautics, MIT, Massachusetts, USA, 2009.

[12] J. Mattingly, *Elements of Gas Turbine Propulsion*. New York, USA: McGraw Hill, 1996.

[13] G. P. Sutton and O. Biblarz, *Rocket Propulsion Elements*. New Jersey, USA: John Wiley & Sons, 2016.

[14] M. Klimko, “Mathematical model of the jet engine fuel system,” in *EPJ Web Conf.*, 2015, pp. 1–4, doi: 10.1051/epjconf/20159202034.

[15] A. F. El-Sayed, *Fundamentals of Aircraft and Rocket Propulsion*, Berlin,

Germany: Springer, 2016.

[16] M. V. Cook, *Flight Dynamics Principles: A Linear Systems Approach to Aircraft Stability and Control*, Oxford, UK: Butterworth-Heinemann, 2007.

[17] R. Khan, P. Williams, P. Riseborough, A. Rao, and R. Hill, “Active fault tolerant flight control system design," 2016, *arXiv: 1610.02139v1*.

[18] Y. Jing, J. Xu, G. M. Dimirovski, and Y. Zhou, “Optimal nonlinear estimation for aircraft flight control in wind shear,” presented at the American Control Conf., ST. Louis, MO, USA, June 10-12, 2009, Paper ThC17.3.

[19] R. C. Nelson, *Flight Stability & Automatic Control*, New York, USA: McGraw Hill, 1998.

[20] J. L. Boiffier, *The dynamics of Flight*, New Jersey, USA: Wiley, 1998.

[21] P. H. Zipfel, *Modeling and Simulation of Aerospace Vehicle Dynamics*, Virginia, USA: American Institute of Aeronautics and Astronautics, 2007.

[22] B. Etkin and L. D. Reid, *Dynamics of Flight: Stability and Control*, New York, USA: Wiley, 1997.

[23] K. Ogata and Y. Yang, *Modern Control Engineering*, New Jersey, USA: Prentice-Hall, 2002.

[24] M. Seok and B. Jung, “Speed and surge control for an unmanned aircraft vehicle with turbojet engine," *Computer Science and Convergence*. Berlin, Germany: Springer, 2012, pp.735-743.

[25] A. Gupta, “Modeling and control of an aircraft system,” Ph.D. dissertation, Dept. Elect. Eng., National Institute of Technology Rourkela, Odisha, India, 2015.

[26] T. I. Fossen, *Mathematical Models for Control of Aircraft and Satellites*, Trondheim, Norway: NTNU, 2011.

[27] D. McRuer and I. Ashkenas, *Aircraft Dynamics and Automatic Control*, New Jersey, USA: Princeton University Press, 1973.

[28] J. Roskam, *Airplane Flight Dynamics and Automatic Flight Controls*, Lawrence, USA: Darcorporation, 1998.

[29] J. W. Roberts, R. Cory, and R. Tedrake, “On the controllability of fixed-wing perching,” in *Proc. American Control Conference*, 2009, pp. 2018–2023.

[30] J. B. Hoagg and D.S. Bernstein, "Nonminimum-Phase Zeros," *IEEE Control Systems Magazine*, pp. 45-57, June, 2007.

[31] F. Haugen, “Experimental tuning of PID controllers,” in *PID Control*, Norway: Tapir Academic Press, 2004.

[32] A. Visioli, *Practical PID control*, Berlin, Germany: Springer Science & Business Media, 2006.

[33] G. Zhang and J. Furusho, “Speed control of two-inertia system,” IEEE Trans. on Ind. Elect., vol. 47, no. 3, pp. 603-609, June, 2000.

[34] W. S. Levine, *The Control Handbook*, Boca Raton, Florida, USA: CRC Press, Inc., 1999.

[35] D. Allerton, *Principles of Flight Simulation*, New Jersey, USA: John Wiley and Sons Ltd., 2009.

[36] M. F. Ahmed and H. T. Dorrah, “Design of gain schedule fractional pid control for nonlinear thrust vector control missile with uncertainty,” Presented at Journal for Control, Measurement, Electronics, Computing and Communications [Online]. Available: https://doi.org/10.1080/00051144.2018.1549696

[37] Y. V. P. Kumar, A. Rajesh, S. Yugandhar, and V. Srikanth, “Cascaded PID Controller Design for Heating Furnace Temperature Control,” in *IOSR J. Electron. Commun. Eng.*, vol. 5, no. 3, pp. 76–83, 2013.

[38] W. S. Levine, *The Control Systems Handbook: Control System Advanced Methods*, Boca Raton, Florida, USA: CRC press, 2010.

[39] Y. Lee, M. Skliar, and M. Lee, “Analytical method of PID controller design for parallel cascade control,” in *J. Process Control*, vol. 16, no. 8, pp. 809–818, 2006.

[40] M. Jensen, "Waypoint-following guidance based on feasibility algorithms," M.S. thesis, Dept. of Cybernetics Eng., NTNU, Trondheim, Norway, 2011.

[41] F. A. Faruqi, “State space model for autopilot design of aerospace vehicles,” Weapons Systems Division Defence Science and Technology Org., Edinburgh, Australia, Rep. DSTO-TR-1990, 1990.

[42] S. Park, J. Deyst, and J. P. How, "A new nonlinear guidance logic for trajectory tracking," presented at the AIAA Guidance, Navigation, and Control Conference and Exhibit, Rhode Island, USA, Aug. 16-19, 2004, Paper AIAA 2004-4900.

[43] I.K. Peddle, "Acceleration based maneuver flight control system for unmanned aerial vehicles," Ph.D. dissertation, Dept. of Aeronautics, Stellenbosch Univ., Stellenbosch, South Africa, 2008.